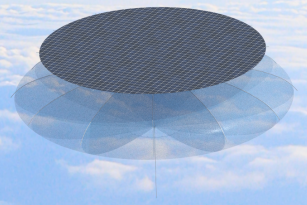
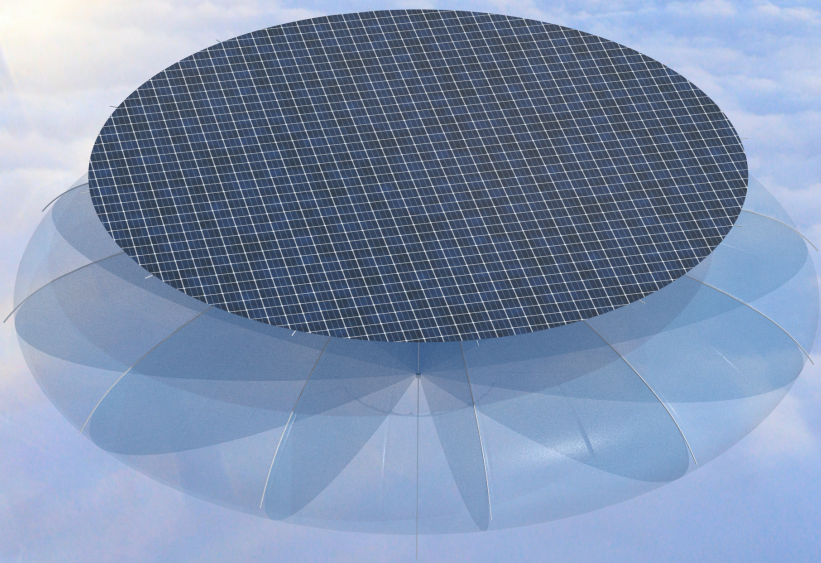


Skydancer

Stratospheric Solar Farm

AE3200: Design Synthesis Exercise
Group 3

Delft University of Technology



This page is intentionally left blank

Skydancer

Stratospheric Solar Farm

by

Group 3

Student Name	Student Number
Digna Jonikaitė	4838564
Jelte Bijlsma	5075599
Joep Stuyfzand	5109272
Matthijs van Lent	5105862
Niek Meijering	5071585
Niels Donners	5048761
Sahir Sujahudeen	5013801
Stella Wessels	4653688
Wouter Offringa	5078032

Project Tutor:	Dr. ir. J.M. (Hans) Kuiper
Coaches:	R. Pasolari and V. Poorte
Teaching Assistant:	C. Mihalache
Date:	Tuesday 31 st January, 2023
Version:	1.0
Project Duration:	November, 2022 - February, 2023
Faculty:	Faculty of Aerospace Engineering, Delft

Acknowledgements

Prof. Dr. De Vreede, Department of Microelectronics at Delft University of Technology, consulted on 1 December 2022

Prof. Dransfeld, Department of Aerospace Structures and Materials at Delft University of Technology, consulted on 1 December 2022

Dr. Ir. R. Saathof, Department of Space Systems Engineering at Delft University of Technology, consulted on 5 December 2022

C. S. Engelbrecht, Faculty of Electrical Engineering, Mathematics and Computer Science at TU Delft, consulted on 23 December 2022

Prof. Ir. Vaessen, Faculty of Electrical Engineering, Mathematics and Computer Science at TU Delft, consulted on 23 December 2022

Cover: Made by Group 3.

Summary

This report outlines the design process of a stratospheric solar farm. Lifting solar arrays into the stratosphere leads to a higher power output, as the solar irradiance is significantly higher. The Mission Need Statement for the system is given as:

"Supply Earth with solar energy utilising a sustainable stratospheric balloon system design."

The Project Objective Statement for this design project, incorporating the main requirements and constraints, is the following:

"Design a stratospheric balloon system that provides 100 MW solar energy at market compliance, by 9 students in 10 weeks."

To obtain a power output of 100 MW, a balloon constellation is designed, consisting of 100 stratospheric balloon designs (SBD) each generating 1 MW with a lifetime of 25 years. The final product, which is named 'Skydancer', is shown in Figure 1. It consists of a singular balloon with a plain solar array lifted on top and it is connected to ground by means of a tether, which takes care of the power delivery and station keeping.

Technical Characteristics

The design has the following technical characteristics. The total mass of the structure is 5735 kg and the balloon is 18 m high and 73 m wide. The solar array area is sized at around 2700 m² and the required internal balloon volume is around 50 600 m³. The balloon is filled with hydrogen as this is cheaper, has better lifting capacity and is more sustainable when compared to helium.

The solar array is placed on top of the balloon and incorporates space-grade 3G30C triple junction cells due to high efficiency and good temperature performance. The full array is modelled for thermal cycles and degradation is expected and designed for. The tether is 18 km long and consists of aluminium and ultra-high-molecular-weight polyethylene (UHMWPE) in a coaxial design. The aluminium takes care of the electricity flow, while the UHMWPE is the load carrying part and also functions as an insulator. The load carrying capabilities of the tether have been optimized with the use of a wind profile which has the maximum absolute wind speed of 30 m/s. The radius of the tether is 5.6 mm and it has a mass of 1800 kg.

The balloon has a pumpkin shape and has 12 gasbags, allowing the SBD to stay afloat should one gas bag fail. Moreover, ballonets are used within these gas bags to allow the balloon to maintain its shape under fluctuations in altitude and in balloon temperature. These ballonets are also used for control of altitude and roll and pitch angles. The skin consists of a layer of PVDC, which boasts very good permeability characteristics, and UHMWPE for keeping shape. A central rod through which the wire runs, connects the bottom payload, where the transformer and potential ridesharing payloads are located, to the top payload: the solar panels.

Performance and Sensitivity Analysis

The performance of the Skydancer in terms of power generation is summarized using I-V and P-V curves of the solar cells and using a Sankey diagram, showing the in and outflow of the power. Furthermore, a dynamic analysis is performed on the stability of the Skydancer under worst-case wind conditions.

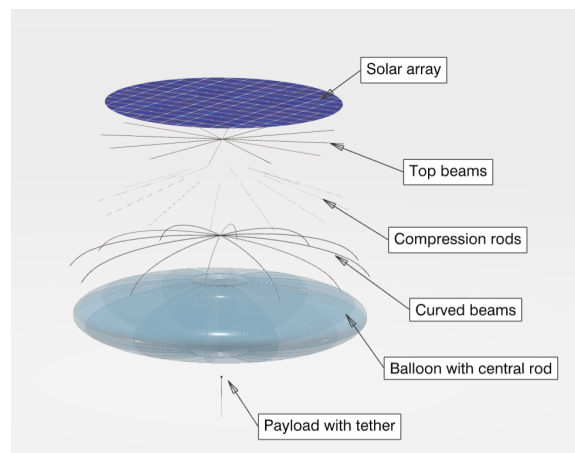


Figure 1: Exploded view of the Skydancer

Based on this analysis and the solar flux model, the design altitude of 18 km was chosen, as this limits the horizontal displacement to 5 km, which should be limited as the airspace occupied by the tether needs to be regulated or restricted, and minimises the tether weight, while still achieving a worst case height of 16 km and a maximum internal stress of 250 MPa in the tether. Lastly, the temperature response and power generation during one full day are plotted, showing a maximum temperature of 43°C, which is achieved by lifting the solar array above the balloon, to allow radiative and conductive cooling at both sides of this solar array.

Moreover, a sensitivity analysis was performed on the final design, which investigated the change of certain input parameters on the SBD. As the design was not strictly limited in mass or power budget, this sensitivity analysis focused on the impact of two possible customer requirements and on the possibility of scaling the product. Scaling up the Skydancer would be a possibility, as the main scaling is limited by the solar array, which scales linearly with power output. Regarding a change of customer requirements, both decreasing the airspace to be restricted as well as changing the lifting gas to helium are possibilities for the product and no fundamental issues arise. However, both changes lead to a change in dimensions, requiring structural re-design, and a 4-5% increased system costs.

Sustainability

Skydancer contributes to a multitude of the United Nation's Sustainable Development Goals. The most favorable aspects of Skydancer with respect to conventional renewable energy sources are the low impact on local ecosystems when compared to conventional renewables and Skydancer's negligible visual pollution. Furthermore, the Skydancer has a low carbon footprint of 5.4 g CO₂/kWh which is due to the extended lifetime and high, predictable power output and low material usage compared to ground based solar. Lastly, the system is designed with ridesharing in mind, as it always covers a certain range and is located close to Earth when compared to LEO satellites. Ridesharing payloads can target both Earth observation, for example regarding sea water quality or illegal fishing, as well as stratospheric research.

Technical Risk Assessment

With the final design concept a risk assessment has been performed. The most significant risk was that of extreme weather conditions, such as lightning storms and hurricanes, threatening the system's successful operation. This was mitigated using an extreme weather response protocol, allowing the system to land within 24 hours, in addition to minimizing the prevalence of lightning with a location trade-off. After mitigation all risk are located in an acceptable range.

Market Review

For the market analysis a location trade-off was performed. Equatorial coastal regions provided the largest potential, especially in comparison to other low-carbon energy sources. These regions have low potential for hydropower and wind energy, as well as great cloud coverage, lowering potential for ground based solar. Additional, non-tangible benefits were identified such as the reduction in pollutants, carbon emissions and the added economical benefits of a stable electricity grid. This is especially relevant for smaller islands, which are often not connected to the current grid. Through analysis of the solar patterns and design parameters the production of the system over its lifetime was analyzed and the revenue was determined. Cost estimates of all subsystems were made in addition to operating costs, which combined with the revenue analysis led to levelized cost of electricity of 0.60 €/kWh and a return on investment of 0.6% per year, not taking into account market inefficiencies. Should governmental policies be implemented in order to reduce inefficiencies in the electricity market the profit margins will further increase and the Skydancer system will become an even more attractive investment.

Conclusion and Recommendations

The design and research in this pre-phase A study indicate that the Skydancer boasts significant advantages compared to conventional renewables and has a high potential for equatorial coastal regions. Further research is needed to comply to all requirements, to further define TBD requirements and to reduce parametric uncertainties. In addition to a higher design fidelity, the scope of the research should also be increased to include the grid connection and integration. However, with current knowledge it is clear that the Skydancer concept can be priced competitively and comes with benefits regarding sustainability, ground use, grid stability & ridesharing.

Executive Overview

This executive overview serves as a summary of the most important contents of this report.

Design approach

This report aims to develop a system that collects solar energy in the stratosphere where the sunlight has for a large part not yet been absorbed by the atmosphere. The Mission Need Statement for this design is as follows:

"Supply Earth with solar energy utilising a sustainable stratospheric balloon system design."

The Project Objective Statement for the design project is the following:

"Design a stratospheric balloon system that provides 100 MW solar energy at market compliance, by 9 students in 10 weeks."

In the previous stage of the design, it was decided to design a system consisting of 100 balloons each generating 1 MW, adding to a total of 100 MW. Four initial conceptual designs were created using a Design Option Tree, a zeppelin concept, a doughnut concept, a flying wing concept and a kite concept. By researching the concepts more, a primary intuitive trade-off was done eliminating the zeppelin and flying wing concept. Four more detailed design options were created using different options for the photovoltaic implementation, inclusion of tandem balloons and attitude control. These were traded off in a trade-off table, where the weights were power efficiency, mass, design complexity, verifiability, sustainability, net costs and long-term performance. The eventual winner of this trade-off was a singular balloon with regular photovoltaics, passive ADCS and the possibility of using tandem balloons.

Sustainable Development Strategy

Sustainability is evaluated on three aspects: environmental, social and economic sustainability. It was found that Skydancer contributes to the following United Nation's Sustainable Development Goals (SDGs):

- Affordable & Clean Energy (SDG 7)
- Decent Work & Economic Growth (SDG 8)
- Industry, Innovation and Infrastructure (SDG 9)
- Communities & Cities (SDG 11)
- Climate Action (SDG 13)
- Life at Sea (SDG 14)
- Life on Land (SDG 15)
- Partnership for the Goals (SDG 17)

The most favourable aspects of Skydancer with respect to conventional renewable energy sources are the following: lower carbon footprint, lower impact on the ecosystems, Skydancer's negligible visual pollution and the grid stability. A comparison between the Skydancer concept and six main competitors based on six different metrics was performed.

Functional Overview

Before starting the detailed design, a functional overview of the system is provided. This is presented in a Functional Flow Diagram (FFD) and a Functional Breakdown Structure (FBS). The FFD also shows the design and manufacturing stages, but has significant changes from the Midterm Report[1] for the commission, perform operations and decommissioning phases. The FBS shows the hierarchical structure of the functions of these last phases.

Photovoltaics

Arguably the most driving design aspect is the solar array design. A choice is made to define a triple junction cell based on the existing 3G30C from Azurspace. This cell with its high efficiency and good temperature performance is re-sized in accordance with current and near-future developments to suit the mission requirements. For the panel design, a bypass diode is used per 12 cells as to not exceed its maximum rated voltage of 30 V. Panels are combined in series as much as possible to obtain a high

voltage, while ensuring the total DC voltage in the panels stays below 1500 V, compliant with regulations. The final array is divided into 478 parallel chains each consisting of 46 panels to achieve the required power output. The array is sized based on the modelling of the thermal cycles experienced due to solar incidence. With the array on a backplane raised above the balloon structure, a peak efficiency loss of about 3.9% can be achieved for low wind speeds.

Due to the required mission lifetime, degradation of the cells is expected and consequently designed for. A degradation of 5% after 25 years due to thermal cycling degradation is deemed achievable, as well as 7.5% after 25 years due to UV radiation. It was deemed that effectively no degradation will take place from particle radiation. Other aspects are included in the design in regard to the long lifetime requirement. The diodes, bypass and blocking, are included in a redundant capacity.

Solar Flux Modelling

There are numerous steps to achieve the flux at a given time, including the orientation and location of the solar array, the local time and Earth's position relative to the Sun, and Earth's atmospheric composition at the selected altitude. The irradiance can then be used to size the solar array accordingly to meet the power generation and thermal requirements. A parametric flux model that incorporates celestial solar mechanics and light transfer were created to analyse these effects. A custom algorithm was adopted for evaluating solar angles on Earth between 2000 BC and 6000 AD with an error of 0.0003° .

These angles can be used to calculate the net flux on a discrete element by splitting it into direct, diffuse, and reflected solar fluxes. These are dependent on solar and geometric planar angles, orbit true anomaly and eccentricity, ambient-to-sea-level pressure ratio, and atmospheric transmittance. The entire model was validated by comparing the solar model results with real solar data for similar input conditions, and flux outputs with research papers that have also simulated flux distributions on high-altitude bodies.

Tether Electrical Design

The design of the tether in an electrical sense is done before the structural aspect is considered. A first look is taken into the different types of losses in a high-voltage cable, inductive losses, Ohmic losses, and corona losses.

Inductive losses come from the opposition to change of current. They increase for thinner wires and higher AC frequencies. To avoid these losses, the rectification of the AC signal is necessary.

Ohmic losses come from the basic resistance of a conductor. Using high voltages can greatly reduce this loss, for which the wire needs to be designed.

Corona losses occur due to corona discharge, which happens when the electric field exceeds the breakdown voltage of the air, resulting in the air becoming conductive. This type of loss can be avoided by reducing the strength of the electric field. A coaxial cable is used to avoid these losses. In this type of cable, the electric field ideally only exists between the core and outer sheath, reducing the electric field outside of the cable to under the corona inception voltage. The higher breakdown voltage of the chosen insulator and load carrier UHMWPE allows the voltage to be higher than for regular cables, about 130 kV. A safety factor of two then requires a minimum insulator thickness of 0.289 cm and a conductor cross-sectional area of 1.9 mm^2 for both the plus and minus of the tether.

The total power produced per Stratospheric Balloon Design (SBD) (1 MW) requires a transformer weighing 100 kg which takes up a volume of 0.04 m^3 . Lastly, a switch mode power supply is used to increase the DC voltage.

Tether Structural Design

The structural design of the tether now simply consists of determining the required cross-sectional area of UHMWPE to be able to withstand the loads encountered by the tether over its lifetime. These consist of the lift and drag of the balloon, the weight of the tether, and the drag of the tether due to winds.

The wind speed versus altitude, and wind profile, will change a lot over the full system life, hence the tether is designed for a worst-case design where the wind blows in the same direction everywhere over the tether length. The maximum wind speed is about 30 m/s at a 10 km altitude.

A dynamic simulation model is set up which models the tether as a number of nodes connected by springs. The aerodynamic forces, weight and tether tension are calculated for each node which is used

to numerically integrate Newton's Second Law. The area of UHMWPE is updated throughout the simulation to make sure the maximum stress in the tether will be equal to 250 MPa. This value is chosen using a safety factor of 4, standard for similar balloon tethers, while also checking that this stress is acceptable to limit the creep of the material. Simulating the tether this way eventually converges to a solution where the full tether is in equilibrium.

This simulation ran with various values for design altitude (equal to the unstretched tether length) and total lift applied. The minimum operational altitude of the system is 15 km, with higher altitudes yielding slightly more solar energy production. Designing for very high altitudes requires a very large balloon size and longer tether and thus more materials and costs. Designing for altitudes close to 15 km altitude requires very high tension in the tether to keep the vertical displacement low, and thus very thick and heavy tethers. The design point chosen from the ran simulations is 18 km, with the applied lift being 6 kN higher than the tether weight. Further optimisation can be performed in the future to this design point. This results in a final altitude (before the iteration of design processes) of 16.8 km, displacing 5 km horizontally. The radius of the tether will be 5.59 mm, weighing 17.66 kN. The final result after design iterations is shown in Figure 2.

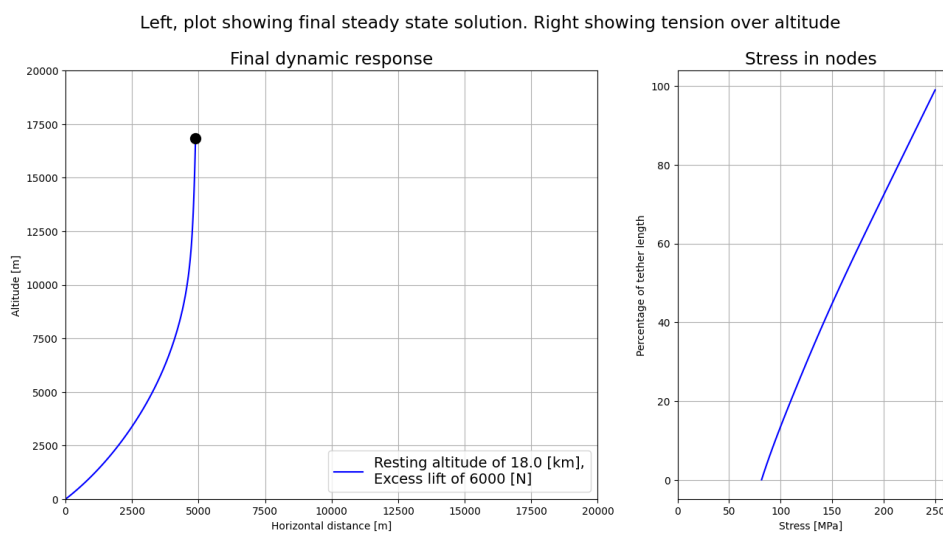


Figure 2: Dynamic response of the final design to incident wind profile

Aerostatics and Aerodynamics

Aerostatic lift is quantified to attain the desired altitude, in addition to design load carrying elements. The balloon uses hydrogen, at an excess amount - an additional 6 kN of lifting force - to reduce horizontal displacement and increase altitude stability. A differential pressure of twice the dynamic pressure at 30 m/s and at a design altitude of 18 km is set for increasing balloon rigidity given wind loads. With a target altitude of 18 km a balloon internal volume of 50 600 m³ is required.

Ballonets are used to mitigate pressure differential and structural rigidity. Given a 10-fold increase in hydrogen volume at 18 km, the ballonets occupy 90.1% of the balloon volume on the ground. Ambient air can then be pumped in as residual to increase the weight of the balloon, leading to a new altitude equilibrium.

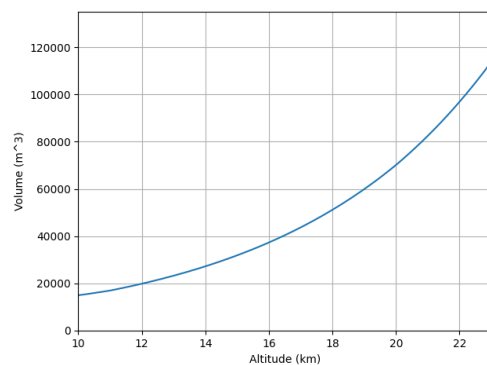


Figure 3: Differing volume of the balloon for changes in height

The balloon's aerodynamic drag is also essential to quantify given that it will drift due to winds and attribute to the design of the tether, as well as abiding by regulations. As empirical models for an oblate

spheroid are not available at a Reynolds number greater than 10^5 , a Computational Fluid Dynamics model in Ansys FLUENT was made to evaluate the C_D at a Reynolds number of $O(10^6)$. This uses a $k-\epsilon$ turbulence model in a wind-tunnel like setup, for a steady velocity inflow of 30 m s^{-1} . The result for C_D , with boundary layer modelling, was found to be 0.117. Validation is performed by similarity.

Balloon Structural Design

The design of the balloon structure consists of designing the configuration in terms of balloon shape and solar panel and payload positioning, next to the design of important structural elements.

A render of the full balloon is shown in Figure 4. The balloon will have a pumpkin shape, consisting of 12 gas bags in 24 legs. The solar array will be placed on top of the balloon, supported by 12 aluminium I-beams. It is suspended by a carbon fibre composite central rod, which goes through the balloon, and by 12 compression rods which are attached to 12 curved aluminium beams laying on the top side of the balloon.

The shape of the balloon is taken to be equal to the initially assumed shape of an ellipsoid with a slenderness ratio of about one to four. The balloon skin will be made of UHMWPE. The volume of the balloon follows the design altitude and required generated lift.

The dimensions of the structural elements are shown in Table 1. The final dimensions of the design are shown in Table 2.

Table 1: Parameters of the beams

	Top beam	Bottom beam
Web thickness [mm]	1.63	1.77
Area [cm ²]	5.36	6.26
Weight [kg]	42.1	49.2

Stability & Control

The stability of the system is largely dependent on the tether as it restrains the movement and rotation of the balloon. Ballonnets can be used for control of altitude and roll and pitch angles (although to a limited amount) by changing the weight and weight distribution. Rotation in the yaw axis is free, which is deemed acceptable as the balloon is fully circularly symmetric.

Payload

The last part of the detailed design is the design of the payload, consisting of a number of sensors, wireless communication and data handling constituents and supporting components like the battery. These have been sized to a total mass of 200 kg. The volume of the lower payload bay is not limiting and thus not considered yet.

Logistics and Operations

The first part of the design realisation is defining the logistics and operations of the system. This considers the ground segment, (de)commissioning and operations phases and the maintenance and emergency procedures. The ground segment shall be placed at sea and will be a tension leg platform. The deployment will be done using modular sea platforms to carry the balloon skin before inflation. After inflation, ballonnets are slowly emptied to regulate pressure and floatation equilibrium. The operations are solely split in how data will be handled during day and night, and the decommission is similar to commissioning except reversed. Scheduled maintenance is required less and less often further in the lifetime. Due to safety reasons a restricted airspace is needed of a certain radius. The size of the restricted area will be investigated in the future.

Production Plan

The created production plan is split into manufacturing, assembly and integration. Components and parts are produced with key materials and then assembled into the balloon, sea platform and tether. The tether is connected to the balloon at land and the whole is integrated at sea before deployment. A flow diagram was generated to visualise the production plan.

Resource Allocation

The resource allocation shows how the mass of the system is divided between subsystems or parts and where the total received power flows, which is done in a Sankey diagram. The total efficiency of the system is furthermore estimated to be 32.2% at BOL and 28.2% at EOL. A margin of 10% is added to the mass and power budgets due to the possibility of changes in further design, possibly required by the customer.

Design & Development Logic

The last part of design realization is the plan for the future development of the system. This will start with the validation of the initial design presented in this report. Next, the SBD should be designed in more detail. Afterwards, the SBD can be verified, validated and certified. The construction is split into procuring and manufacturing components, after which the system can be assembled and delivered to customers. These activities and their sub-activities are presented in a flow diagram and a Gantt chart, showing also the time planning.

Performance Analysis

The performance of the SBD in terms of power generation is summarized using I-V and P-V curves of the solar cells and a Sankey diagram of one SBD. Furthermore, a plot is provided showing that under worst-case wind conditions, the balloon does not drift more than 5 km to the side and stays well above 16 km, while remaining internal stress of 250 MPa or less. Lastly, the temperature response and power generation during one full day are plotted.

Configuration and Layout

The configuration and layout of the SBD are shown by means of a hardware diagram, a software diagram and a number of renders of a generated CAD model. The final dimensions of the balloon are shown in Table 2. An isometric view of the balloon is included in Figure 4

Table 2: Final dimensions of a number of structural elements

Part	Length	Width	Height
Balloon	73 m	73 m	18 m
Central rod	14 cm	14 cm	21.2 m
Curved beam	38.6 m	5.7 cm	12.2 cm
Compression rod	2cm	2cm	22.8 m
Top beam	29.1 m	4 cm	8cm
Solar Array	58.2 m	58.2 m	-

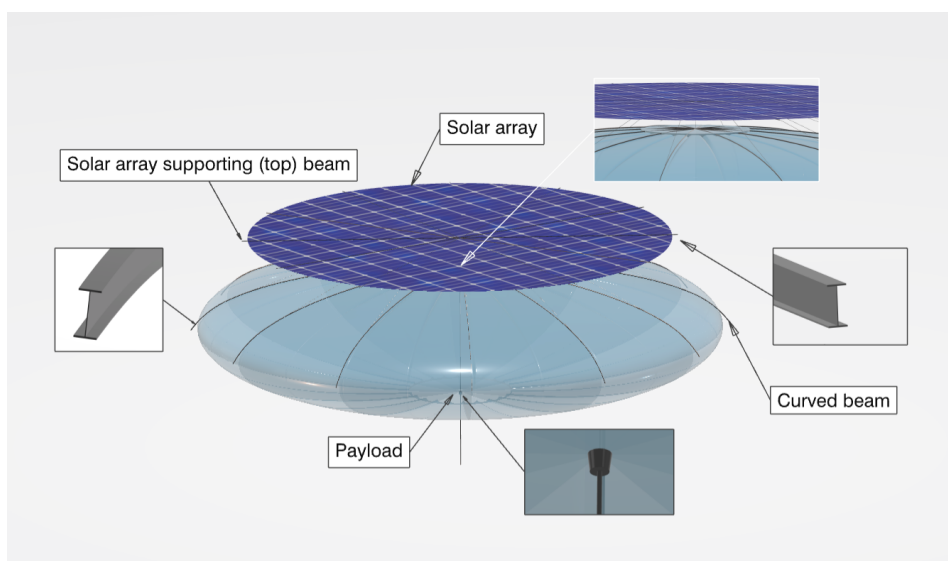


Figure 4: Isometric view. Cross sections of top and curved beams are shown. The payload is hidden behind the balloon skin.

Carbon footprint

As part of the overview of the design and in light of the focus on sustainability, the carbon footprint of the full system is calculated. The total CO₂ emitted by material production is 14 200 kg. Other CO₂ emissions from manufacturing, transportation, maintenance, decommissioning and the ground segment bring the total emitted CO₂ to 267 000 kg. Over a 25 year lifespan producing about 52 GWh, the carbon footprint equals 5.4 g CO₂/kWh.

Verification and Validation

To aid in verifying the system requirements, a verification matrix is used to allocate means of establishing being able to meet the requirements. These can be done in the form of testing, various analyses and simulations, or reviewing documents and procedures. For product validation, the key is to assert being able to meet the mission goals. A viable proposition is to construct a series of tests that are similar to the final design, but with increasing scale. This has the added benefit of improving product release rates and workforce efficiency in the long-run

Reliability, Availability, Maintainability, and Safety (RAMS)

The RAMS analysis is used to indicate the utility and life-cycle considerations of the system. The photovoltaic diode network has a success probability of 0.999 751 , with the array at 0.999 832 Recommendations on structural and material reliability in light of the operating environment are also given. Maintainability is conserved due to the long-lasting and failsafe architecture of the subsystems, thus also increasing availability. Safety design principles with regard to hydrogen and its containment & stability are presented.

Sensitivity Analysis

A sensitivity analysis was performed on the final design, which investigated the change of certain input parameters on the SBD. It was concluded that a change or limit in the operational altitude and vertical displacement would lead to a stronger required tether, but that this would pose no fundamental problems. Furthermore, filling the balloon with helium instead of hydrogen would also lead to alterations in the volume and structural department, but it would still provide a manufacturable design, albeit at a less strong market position because of the increased costs of helium compared to hydrogen, which differs by a factor 70. Finally, the upscaling of the SBD was investigated, which resulted in the conclusion that a 2 MW SBD would be a realistic possibility, providing benefits regarding material usage and airspace restrictions. The design of a 5 MW SBD would need further research, as the structure of this larger design will require a complete overhaul. In general, expanding the catalogue from one Skydancer to Skydancers in multiple sizes can prove beneficial for the market position and can tailor to specific locations.

Risk Assessment

With the final design, the technical risks were re-assessed. These cover risks regarding requirements, performance, resources, complexity & quality. The worst risks were those regarding not being able to meet driving, top-level requirements, the failure of the main systems for adequate performance and extreme weather conditions. For all identified risks a mitigation strategy was set up, lowering the severity, impact or both of each individual risk. The mitigation of the worst risks was achieved by designing for end of life conditions, setting up a maintenance and inspection strategy every five years and setting up an emergency protocol, which can bring the SBD back to the sea platform within a 24 hour notice.

Market Review

First of all, for a more accurate market analysis, the location is determined. There are multiple drawbacks when it comes to deploying Skydancer at northern and southern latitudes, including high wind potential due to polar vortex and/or hydropower potential due to elevation differences. Around the equator, a business case can be made since conventional renewable energy methods are more disruptive to the local environment. Only limited area is available due to large valuable rain forests, the space that is available would rather be used for food production and livable areas. Hence it is determined upon that Skydancer is set up around the equator at places such as Pacific Asia and the Gulf of Guinea.

Skydancer has a multitude of benefits with respect to conventional energy sources, such as a reduction in pollutants, low ground usage, enabling ridesharing to the stratosphere, an increase in energy

independence, and encouraging grid stability and weather independence. The cost of the different system components and the full SBD are depicted in Table 3.

Table 3: The cost breakdown of the system per component and total cost

Category	Value
Tether	€ 200,000
Balloon	€ 69,790
Structure	€ 12,250
Solar Array	€ 2,257,600
Electronics	€ 20,000
C&M&D Factor	1.2
Total:	€ 3,071,580

The expected revenue is €143 000 annually, for 25 years of lifetime. An additional source of income is expected by rideshare payloads, as the system provides a great and easy-to-reach platform for both Earth observation as stratospheric research.

The profit margin is €9.8 MWh assuming an electricity price of €70 per MWh, which is applicable for Pacific Asia and the Gulf of Guinea. This yields a return on investment of 17.2% at the end of the twenty five years, or €528 000. Over 25 years, taking into account compound interest, this results in a yearly Return on Investment of 0.64%. Potential subsidies could greatly improve profitability.

These numbers do not necessarily make it a positive business case, as is historically proven, a Return on Investment of 0.64 % does not outperform inflation. Compared to other investments, such as real estate or even other renewables, the return is low and dissuading to potential investors. A local government plays an important role in creating an attractive environment to stimulate a sustainable, secure and clean energy supply, once this happens, opportunities are created.

Requirements & Compliance

Lastly, it is checked whether all requirements are met. This is done in the compliance matrix, which shows each requirement and lists where compliance with it is proven. Some requirements are not met yet. These are mostly dependent on unknown payloads to be carried in the future besides the power generation, such as positioning, communication and subsystem temperature requirements. Requirements due to regulations have not been examined yet due to the uncertainty of the exact operational area. The required RoI is dependent on subsidies and government policies, which also differ per operational area.

Recommendations

The Skydancer concept has potential within the energy market but does require more research to move beyond the conceptual design stage. One major field of future development is the response of a tethered balloon to a complex environment. Investigating the scaling of the design could also prove useful, as it comes with both benefits and drawbacks. Lastly, it is necessary to look at regulations applicable to the utilisation of Skydancer and to further verification and validation of the product.

Contents

Summary	i	5.3 Resource Allocation	66
Executive Overview	iii	5.4 Project Design & Development Logic	68
List of Figures	xii	5.5 Project Gantt Chart	69
List of Tables	xiii	6 Design Overview	71
Nomenclature	xiv	6.1 Configuration & Lay-out: H/W and S/W diagrams	71
1 Introduction	1	6.2 Configuration & Lay-out: Structure of the SBD	72
2 Design Approach	2	6.3 Carbon footprint	75
2.1 Design Process	2	6.4 Verification & Validation	76
2.2 Sustainable Development Strategy . .	5	6.5 Performance Analysis	79
3 Functional Overview	8	6.6 Reliability, Availability, Maintain- ability, and Safety	81
3.1 Functional Flow Diagram	8	6.7 Sensitivity Analysis	84
3.2 Functional Breakdown Structure . .	8	7 Technical Risk Assessment	87
4 Detailed Design	12	7.1 Risk Identification	87
4.1 Solar Array Design	12	7.2 Risk Map and Mitigation	89
4.2 Solar Flux Modelling	21	8 Market Review	93
4.3 Tether Electrical Design	27	8.1 Market Analysis	93
4.4 Tether Structural Design	31	8.2 Cost Break-Down Structure	98
4.5 Aerostatics & Aerodynamics	37	8.3 Market Compliance	101
4.6 Balloon Structural & Material Design	45	9 Requirement Compliance	106
4.7 Stability & Control	55	9.1 Requirements Review	106
4.8 Payload Design	56	9.2 Compliance Matrix	107
5 Design Realisation	61	9.3 Feasibility Analysis	109
5.1 Logistics & Operations	61	10 Conclusions	111
5.2 Manufacturing, Assembly and Inte- gration Plan	64	References	114

List of Figures

1	Exploded view of the Skydancer . . .	i	4.9	Variation of solar flux with heights for January 18, 2023, over Delft, The Netherlands (52.01° N, 4.36° E). Note that Julian Day is used to demonstrate the use of absolute time scales.	24
2	Dynamic response of the final design to incident wind profile	v	4.10	Case study used to validate solar position model	25
3	Differing volume of the balloon for changes in height	v	4.11	Li et al.'s flux distribution for the mentioned parameters [20]	26
4	Isometric view. Cross sections of top and curved beams are shown. The payload is hidden behind the balloon skin.	vii	4.12	Plot of irradiance versus panel slope, with the slope in degrees on the x-axis and irradiance in W/m ² on the y-axis	27
2.1	Design options, generated from design option trees	2	4.13	Graphs showing the effect of varying voltage on different loss types.	28
2.2	Conceptual Designs used in the trade-off table	3	4.14	Graphs showing the total losses and effects of the varying frequency.	29
2.3	Sustainable Development Goals	5	4.15	Cross section of the tether.	29
2.4	Carbon footprint of SBD compared to other renewables	6	4.16	A high level overview of the stages of a SMPS.	31
2.5	Size comparison between Skydancer and the Sun	7	4.17	Profile of the wind speed versus altitude and accompanying dynamic pressure	32
3.1	Functional Flow Diagram	9	4.18	Sketch of how the tether was simulated [31]	33
3.2	Functional Flow Diagram (cont.)	10	4.19	Best solutions for altitudes. The left figure shows the final steady state converged solution. The right figure shows the stress in the tether.	35
3.3	Functional Breakdown Structure	11	4.20	Zoomed in versions of the steady state solutions for 50, 100, 150, 200 and 1000 nodes. The left figure shows the final steady state converged solution. The right figure shows the stress in the tether.	36
4.1	Semiconductor lattice constant versus bandgap [7]	13	4.21	Radius update over iterations amount for 50, 100, 150, 200 and 1000 nodes	37
4.2	Performance curves for the V1.0 cell design for standard conditions	14	4.22	Differing volume of the balloon for changes in altitude	38
4.3	Electrical diagrams for the defined panel configurations.	16	4.23	Lifting capabilities of the balloon varying over positive differential temperature from its ambient temperature	39
4.4	Simple thermal model setup and response for 20 km altitude and 5 m/s wind speed.	17	4.24	Sketch of the altitude adjustment mechanism of the balloon [37].	40
4.5	Backplane thermal model setup and response for 20 km altitude and 5 m/s wind speed.	18	4.25	Sizing of the ballonet for a specific design altitude	40
4.6	Performance curves for the V1.0 cell design for operational conditions (44.6 °C) compared to standard (28 °C).	19			
4.7	Illustration of the coordinate system and notable angles used in describing incoming radiation. Note that the astronomer's definition of azimuth γ , South moving Westward, is used here.	21			
4.8	Variation of Sun zenith angle θ_z for February 2, 2023 at 11:45 AM UTC on an equirectangular projection of Earth. Colours represent isosurfaces.	22			

4.26	Variation of Reynolds number with length scale, at different altitudes and at 50 m s^{-1}	41	6.3	Isometric view. Cross sections of top and curved beams are shown. The payload is hidden behind the balloon skin.	73
4.27	CAD model used for CFD analysis	42	6.4	Cross-section view. The cutting plane is located at the middle section, and is twisted under an angle that allows to inspect internal structure of the gasbags.	73
4.28	Enclosure geometry used for creating fluid domain	42	6.5	Top view. At the outer balloon edges, longer supporting rods would be needed to enable flat layout of the solar panels, so the radius of solar panel plate is smaller than the radius of the balloon.	74
4.29	Transparent view of domain with colours indicating different boundary conditions	42	6.6	Side view. Note that the solar panels are not shown in this picture, which allows to have a better look at the configuration of the top structure	74
4.30	Isometric visualisation of the mesh used. A visual cutting plane has been added for section detail	43	6.7	Exploded view. Top beams, compression rods and curved beams compose "Top structure". Central rod is inside of the balloon.	75
4.31	Magnified view of the same mesh, with focus on the boundary layer inflation mesh	43	6.8	End-of-life power distribution for peak operating conditions (in Watts).	79
4.32	Static pressure plots over the simulation domain	44	6.9	Dynamic response of the final design to incident wind profile	80
4.33	Velocity contour plot comparison	44	6.10	Temperature and power generation response at design parameters (wind speed of 5 m s^{-1}).	80
4.34	Dependency of normalised drag coefficient of freely falling particles on normalised Reynolds number [42]. The shape dataset is provided in the reference.	45	6.11	Performance curves for the V1.0 cell design for peak operational conditions versus standard.	81
4.35	Sketch of the Skydancer	46	7.1	Technical risks before mitigation	92
4.36	Free body diagrams	47	7.2	Technical risks after mitigation	92
4.37	Top view and side view of top structure	48	8.1	Estimated average EU external costs for electricity generation technologies [65]	96
4.38	Free body diagram of top beam	49	8.2	Estimated levelized full system cost of electricity for multiple energy sources. [67]	98
4.39	Free body diagram of bottom beam	50	8.3	Direct manufacturing cost breakdown for 3J III-V solar cells [69].	100
4.40	General lay-out and nomenclature for an I-beam	50	8.4	Revenue and costs over time, steeper lines have higher subsidies - which are based on energy produced.	102
4.41	Pumpkin balloon shape [48]	53	8.5	External Effects Skydancer.	103
4.42	Data handling block diagram for a singular balloon	58	8.6	Competitiveness Skydancer	105
4.43	Electrical block diagram for the complete system	60			
5.1	Visualisation ground segment	62			
5.2	Modular sea platform	63			
5.3	Production plan for Skydancer	65			
5.4	Power breakdown in Watts	68			
5.5	Project design and development flow diagram	69			
5.6	Gantt chart for the activities to be performed after the DSE	70			
6.1	Hardware block diagram	71			
6.2	Software block diagram	72			

List of Tables

1	Parameters of the beams	vi	4.12	Technical parameters of the data transmission system.	58
2	Final dimensions of a number of structural elements	vii	5.1	Maintenance and emergency procedures	64
3	The cost breakdown of the system per component and total cost	ix	5.2	Engineering mass budget	67
2.1	Overview of trade-off criteria weights	4	5.3	Updated power budget with margins	68
2.2	Design option trade-off scoring, higher is better	4	6.1	Final dimensions of the SBD	72
4.1	Solar cell design parameters for 3G30C and 'V1.0'	13	6.2	Carbon footprint SBD materials	76
4.2	Heat transfer contribution for backplane design (wind speed of 5 m/s, altitude of 20 km and plane spacing of 1 m)	18	6.3	Carbon footprint SBD	76
4.4	Transformer characteristics	30	6.4	Verification Matrix. Requirement statements can be found in chapter 9	77
4.5	Simulation results for different excess lift values for 18 km and the excess lift for all considered altitudes giving the best results	34	6.5	Mass budget for SBD sizing, all values are in kg	85
4.6	Parameters of the beams	51	6.6	Size budget for SBD sizing	86
4.7	Material selection	55	7.1	Risk mitigation and rankings	90
4.8	Axial stability control methods	56	8.1	Location selection for different regions	94
4.9	Rotational stability control methods	56	8.2	The cost breakdown of the system per component.	101
4.10	All sensors and meters to be present in the payload.	57	9.4	Compliance Matrix	107
4.11	Downlink budget at 18 km with a transmission power of 15 W.	58	10.1	Dimensions of the final design	112
			10.2	Mass breakdown of the final design	112
			10.3	Work Division for Final Report	113

Nomenclature

Abbreviations

Abbreviation	Definition
ADCS	Attitude Determination and Control System
BOL	Beginning Of Life
CFRP	Carbon Fibre Reinforced Polymers
CPU	Central Processing Unit
DOT	Design Option Tree
DSE	Design Synthesis Exercise
EOL	End Of Life
FBD	Free Body Diagram
FBS	Functional Breakdown Structure
FEM	Finite Element Method
FFD	Functional Flow Diagram
FPV	Floating Photovoltaics
GPU	Graphics Processing Unit
HCPV	High Concentrated Photovoltaics
ISA	International Standard Atmosphere
LCOE	Levelized Cost Of Electricity
LCPV	Low Concentrated Photovoltaics
LEO	Low Earth Orbit
LFSCOE	Levelized Full System Cost Of Electricity
MPPT	Maximum Power Point Tracking
MNS	Mission Need Statement
NOAA	National Oceanic Atmospheric Administration
OSW	Offshore Wind
PDM	Power Distribution Module
POS	Project Objective Statement
PV	Photovoltaics
PVDC	Polyvinylidene Chloride
RAMS	Reliability, Availability, Maintainability and Safety
ROI	Return Of Investment
SBD	Stratosphere Balloon Design
SDG	Sustainable Development Goal
UHMWPE	Ultra High Molecular Weight Polyethylene

1 | Introduction

Modern developments have made it clear that a response to climate change is vital. A powerful step towards climate change mitigation is the use of renewable energy instead of fossil fuels. Amongst the leading techniques for renewable energy generation is the concept of solar energy, which is a concept which has been practised broadly. Ranging from solar panels on homes to solar powered flying vehicles. The output from solar arrays can be increased significantly by placing them higher in the atmosphere, where the solar irradiance is higher and weather conditions do not effect their output.

This increased efficiency combined with the lack of suitable ground locations for solar farms leads to a novel business case of retrieving solar energy using a stratospheric balloon design (SBD), which is branded as Skydancer. This SBD is designed to deliver 1 MW of power to ground, with the full system consisting of 100 of these SBDs. The main requirements are power delivery at market compliance, with a 25 year mission lifetime and at least 10% return on investment within 5 years of operation. Special focus is given to the creation of a sustainable design by using cradle-to-cradle materials and assessing the life-cycle greenhouse emissions. Furthermore, the system is targeted to contribute towards the sustainability development goals of the United Nations.

This report showcases the final design and performance characteristics of this SBD. The report is structured as follows. First, the design process up to the detailed design phase is summarized and the sustainable development strategy is explained in chapter 2. Afterwards, the functional analysis of the product is performed in chapter 3. The detailed design of the different subsystems is explained in chapter 4, whereas the realisation of this design is covered in chapter 5. With these results, chapter 6 covers the overview and analysis of the final design, which also explores whether upscaling the design is a possibility. The final design also allows for an updated risk assessment and mitigation, shown in chapter 7, and an updated market analysis, covering the requirement on market compliance in chapter 8. Finally, the design is shown to comply with the most important requirements in chapter 9.

2 | Design Approach

This chapter will provide an overview of the design process so far, up until the Midterm Report [1] in section 2.1. Furthermore, the sustainable development strategy is laid out in section 2.2, which connects the Skydancer concept to the United Nations Sustainable Development Goals (SDGs).

2.1. Design Process

The aim of the design originates from the Mission Need Statement, where special focus is given to the sustainability aspect. It is as follows:

"Supply Earth with solar energy utilising a sustainable stratospheric balloon system design."

The constraints of the project are captured in The Project Objective Statement:

"Design a stratospheric balloon system that provides 100 MW solar energy at market compliance, by 9 students in 10 weeks."

The first stage of the design process was the generation of concepts based on a Design Option Tree. This tree was converted into four different designs based on an intuitive trade-off. The concepts can be seen in Figure 2.1.

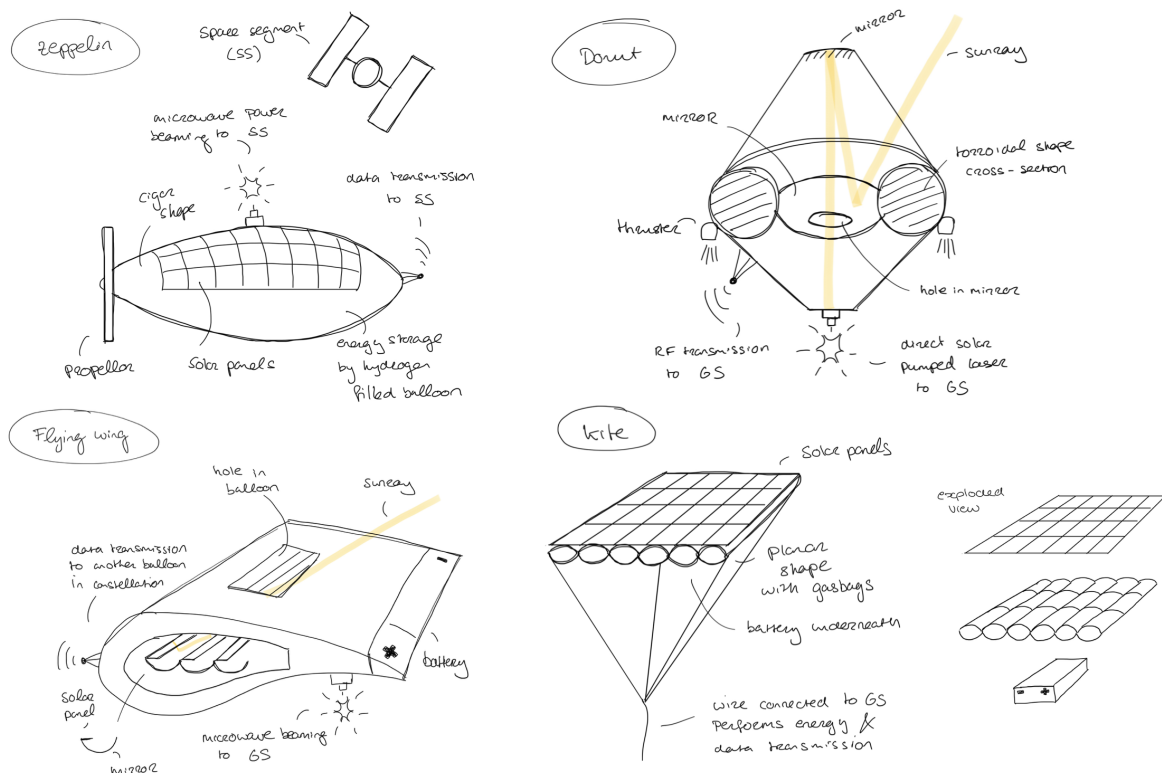


Figure 2.1: Design options, generated from design option trees

In the next design stage, the four design concepts were evaluated on the differing subsystems. In

particular, the power beaming versus tethered solutions were properly assessed. It was determined that wireless energy transfer is not a feasible solution for the given five year time frame. Meanwhile, the tether turned into a reasonable design option. This tethered design option was taken forward with various photovoltaic and balloon compositions. For the specifics behind this decision, the Midterm Report should be consulted [1].

The four generated options varied in photovoltaic implementation, tandem balloon inclusion and attitude control. In the midterm report, research on these other subsystems was also done. These concepts were selected to enter the trade-off for choosing the final design. They are visualised in Figure 2.2.

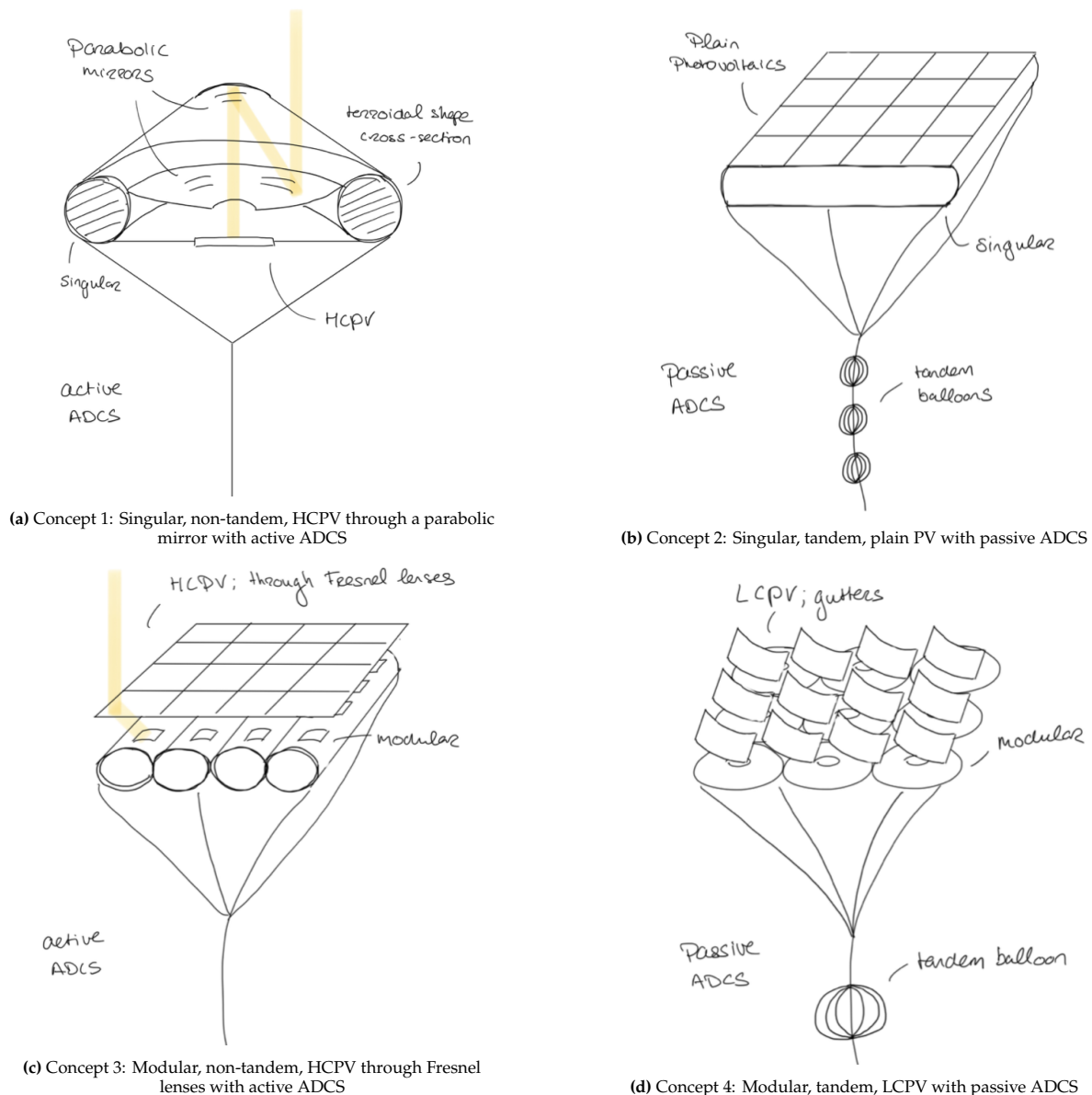


Figure 2.2: Conceptual Designs used in the trade-off table

To perform the trade-off, the following rationale has been used for the weights. The chosen trade-off criteria are power efficiency, mass, design complexity, variability, sustainability, net costs and long-term performance. Each of these criteria has a certain weight assigned, where power efficiency has the highest weight.

Table 2.1: Overview of trade-off criteria weights

Criterion	Weight	Weight Rationale
Power Efficiency	8	Power efficiency is a project-driving property. It is crucial for a project's success, and having insufficient efficiency (e.g. too many energy losses in the transmission) can result in a project failure, as the proposed system shall outperform existing solutions on the ground.
Mass	4	Mass is relevant for the project's success. Minimising the mass can minimise waste in terms of materials, energy-demanding transportation and labour. Specifically, the hydrogen required and consequently balloon size scale rapidly with increased mass.
Design Complexity	5	Having a complex design brings direct development risks by making it difficult to evaluate design drawbacks, or to find clever ways to solve complexity related problems. Problems that might arise include the need for pointing accuracy and stability as well as the need for thermal control systems.
Verifiability	4	Having a verifiable design reduces risks of system malfunctions and unpredicted events during operation. Verifiability closely relates to design complexity and directly follows from it.
Sustainability	5	Sustainability is a driving aspect of this project and it shall not be ignored. The project goal is providing green energy, and not considering sustainable design aspects would result in double-edgedness of design purpose.
Net Costs	3	Overspending at the development stages might have little added value. However, the cost shall not be the main measure of a successful project, because even if the return is too little or negative, the development and operation of such a system can be a basis for future opportunities.
Long-term performance	4	Longevity is directly related to a challenging system requirement of operating for 25 years. However, it is not as critical as minimising design complexity, because as long as degradation is not related to complexity, can be predicted and mitigated, and results in a market competitive design, the long-time performance itself should not be a limitation.

This trade-off resulted in two design options coming out on top with a marginal difference between them in the scoring as can be seen in Table 2.2. These options were concept 2 and concept 4, see Figure 2.2. A sensitivity analysis was performed and it was decided to continue with option 1, while considering design options from option 2. Specifically, the use of ultra-low mass low concentrated photovoltaic gutters, which required more research into specific integration effects for this mission. The final decision on photovoltaic integration is presented in Table 2.1. From here on uncomplicated concept 2 is taken as a baseline for detailed design.

Table 2.2: Design option trade-off scoring, higher is better

	Concept 1	Concept 2	Concept 3	Concept 4
Power efficiency	3	4	3	4
Mass	2	4	2	5
Design complexity	2	4	2	3
Verifiability	3	4	2	3
Sustainability	4	3	4	4
Net Costs	2	4	3	3
Long-term performance	2	4	2	3
Total score	2.67	3.85	2.63	3.64

Ultra-low Mass LCPV Considerations

The photovoltaic implementation of design concept 4 was taken forward into the detailed design due to the fact it offers unrivalled specific power (W kg^{-1}) over plain cells. It is a complex system to integrate into the design with various consequences, thus requiring more research. The idea is based on the ultralight concentrator photovoltaic system designed for Space Solar Power (SPS) systems by CalTech [2]. Here the authors present a design that integrates lightweight solar cells that receive concentrated light. The rest of the structure consists of even lighter mirrors that also act as a support structure to

achieve a quadrupling of specific power compared to plain cells.

Important factors to consider in the photovoltaics implementation are costs and long term performance. The cost of the solar array presents the largest contributor to costs and long term performance is important to present a solid business case. First off, the CalTech design features 15x concentration, meaning fewer cells are required to be manufactured. However, the cells used to achieve this feat are SolAero IMM- α 's. Without going into much detail, these thin cells require state-of-the-art production techniques in which the substrate is inverted and each layer must be electronically and mechanically matched. The costs of manufacturing would increase drastically.

The other aspect to consider is the environment these were designed for. The atmosphere is much less kind to such slim, flimsy fins than the vacuum of space. To cope with atmospheric aspects such as wind and precipitation, the fins would need to be more rigid. This would negate most of the gain in specific power. A concentrator cell also runs hotter, and consequently more inefficient, than plain cells, an aspect most unfavourable to long term performance. Factors that affect long term performance are thermal cycling, radiation flux and UV absorption. All of these effects scale with the concentration of the cell. With these considerations combined it was determined to not use concentrated photovoltaics in the design.

2.2. Sustainable Development Strategy

Sustainability is evaluated on three aspects in this project: environmental, social, and economic sustainability, treated in subsection 2.2.1, subsection 2.2.2 and subsection 2.2.3 respectively. Moreover, aspects are linked to the United Nation's Sustainable Development Goals (SDGs), shown in Figure 2.3¹. These goals have been set up to achieve a better and more sustainable future for all, specifically focusing on the biggest challenges to tackle by 2030. The United Nations also emphasises that there must be a balance between environmental, social and economical sustainability and that one can affect the other. Skydancer can play a part in this initiative. In the following subsection, references will be made to the SDGs.



Figure 2.3: Sustainable Development Goals

2.2.1. Environmental Sustainability

The four SDGs goals that Skydancer contributes to when it comes to environmental sustainability are: Affordable & clean energy (SDG 7), Climate action (SDG 13), Life below water (SDG 14) and Life on land (SDG 15).

¹'Sustainable Development Goals'. United Nations. Last accessed on 24-01-2023. <https://www.un.org/en/sustainable-development-goals>

First of all, considering the affordability and cleanliness of the energy provided by the SBD. The product has the same order of magnitude of pricing as conventional renewable energies such as wind and solar, though it is often not necessarily the most affordable option.

Though when it comes to clean energy, Skydancer performs extremely well, thereby contributing to mitigating climate change. The measurable impact on the environment is parameterized by means of the life-cycle carbon footprint. The carbon emissions from manufacturing, commission and decommission, operations and maintenance are taken into account as these are the driving factors for emissions coming from existing renewable energy sources [3]. The carbon footprint of one balloon providing the 1 MW is provided in section 6.3 and equals $5.4 \text{ gCO}_2/\text{kWh}$. This is half as much as the one for wind, and a fourth of the emissions of solar, as depicted in Figure 2.4 [4]. Hence, the SBD is favourable when it comes to carbon emissions. Moreover, Skydancer is deployable in areas where conventional renewable energies are less likely to be adopted, as described in section 5.1, therefore increasing accessibility of renewable energy in general. And lastly, the SBD does not require a form of active propulsion. The only form of emission during the operational lifetime is the emissions created by maintenance.

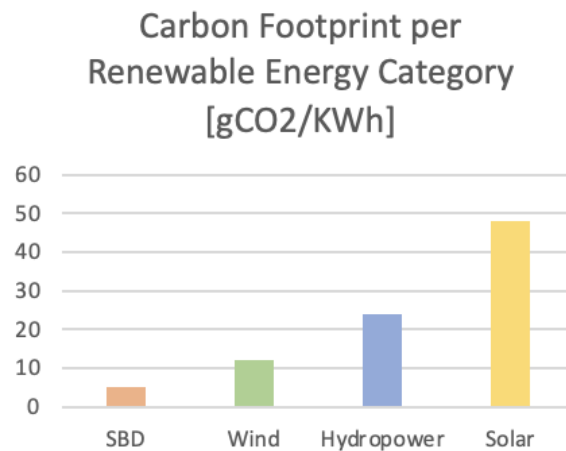


Figure 2.4: Carbon footprint of SBD compared to other renewables

Considering the effect of Skydancer on the local environment, an important consideration is the way wildlife is affected, both at sea and on land. Conventional renewable energies such as solar and wind have multiple drawbacks. Solar takes up a considerable area on land or sea, resulting in a habit loss for plants and animals. For a 1 MW providing solar farm, using Silicon type S 32 solar cells, an area of 7300 m^2 is needed at equatorial latitude. Moreover, the local heat profile changes, causing prolonged effects on the surroundings. Wind energy farms are affecting local habitats for animals by means of their noise emission, also in the ultrasonic spectrum. Moreover, their extensive size has an effect on the profile of the environment and induces periodic shadows.

The impact of Skydancer on the environment is mainly due to the configuration of the ground system. Since the tether of one centimetre thick does not interrupt the ecosystem in a considerable manner. Something to note is the effect of the electromagnetic fields that might occur due to the electricity flow through the wire, beneficially, it has been researched that exposure to these low-level electromagnetic fields is not harmful ². Skydancer is to be deployed at sea around the equator as described in section 5.1. Sea life needs to be taken into consideration when determining on the exact location. Coral reefs and frequented areas by certain species (such as gulf streams) should be avoided for placing the sea platform. When looking at the sample location of Indonesia, multiple locations are feasible taking into account these considerations. Moreover, the blocks at the bottom of the sea platform can be used as a basis for an artificial reef, concrete is often used as a building material ³. The impact of having a large body with

²Radiation: Electromagnetic fields'. Last accessed on 24-01-2022. <https://www.who.int/news-room/questions-and-answers/item/radiation-electromagnetic-fields>

³Artificial Reefs'. Last accessed on 24-01-2023. <https://www.ecoshape.org/en/knowledge-articles/artificial-reefs/design-of-reefs>

solar panels on top in the stratosphere, with an aerostatic behaviour, is negligible, since only certain microbes are present at this height.

2.2.2. Social Sustainability

The two goals that are contributed to when it comes to social sustainability are Communities & Cities (SDG 11) and Partnership for the Goals (SDG 17).

The system contributes to sustainable cities and communities as it can connect villages & small cities to a sustainable energy source. Visual pollution of one's product is also relevant when it comes to communities and cities of the future, aiming for green public spaces and improving urban planning. Public resistance has been expressed to wind energy farms and solar technologies for example. Skydancer's tether going up with a diameter of one centimetre will induce no considerable visual pollution, one can spot the wire on stark one colour backgrounds, such as a cloud base, though it will remain difficult to spot. The balloon could be spotted and will also induce a shadow on the ground. When using the design configuration from this report, where 1 MW is provided per balloon, the following analysis is done. When using 100 balloons with a diameter of approximately 70 m, an angular diameter of 0.2° is determined. This magnitude is visible to the human eye and is equal to an apparent area of about 1/6th of the Sun. A visual representation is provided in Figure 2.5. The shadow of the balloon will not reach Earth's surface due to the ratio of the great distance from Earth and the size of the sun.

While designing Skydancer, we have always kept both current and future generations in mind. Hence, the system was required to be upgradeable with any future technological developments. This requirement will be reached an easy retrieval method, where the system is able to land for inspection & maintenance, but also for replacement of parts. If higher grade solar panels would become available for example, the solar array can be replaced to further increase the power output. And lastly, considering global partnerships, Skydancer can be a platform for promoting international sustainable growth. Considering this concept is developed in the Netherlands and to be deployed around the equator in areas that are able to significantly grow in their renewable energy usage, opportunities will present themselves.

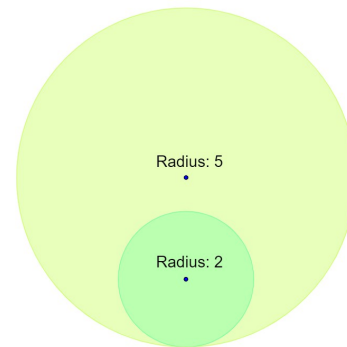


Figure 2.5: Size comparison between Skydancer and the Sun

2.2.3. Economical Sustainability

The two goals that are contributed to when it comes to economics are Decent Work & Economic Growth (SDG 8) and Industry, Innovation and Infrastructure (SDG 9).

Skydancer has a positive impact on work opportunities and innovation. It provides a research platform for future renewable energy sources. Moreover, with the deployment of the SBD opportunities arise such as further stratospheric research and Earth observation. To this day long-duration continuous measurements and observations are often limited to LEO satellites, no stratospheric balloon has been in operation for longer than NASA's Ultra-Long Duration Balloon, which had a stratospheric lifetime of approximately 100 days.

Furthermore, Skydancer is promoting independence when it comes to energy acquisition. Self-reliance has become an even more relevant topic after Europe has recently seen the effect of the energy crisis that followed the war in Ukraine. Moreover, the fact that the SBD is operating at sea means that innovative solutions are applied in order to realise this, also allowing more flexibility for infrastructure on land. Other economical benefits of the system are mentioned in subsection 8.1.2.

3 | Functional Overview

This chapter presents a functional overview of the SBD, in the form of a Functional Flow Diagram (FFD) and a Functional Breakdown Structure (FBS). The combination of the two provides the functions to be performed by the system in a logical order. It serves as an overview of the design and design approach. The Functional Flow Diagram is shown in section 3.1 and the Functional Breakdown Structure is shown in section 3.2.

3.1. Functional Flow Diagram

The FFD, updated from the FFD presented in the baseline report, is shown in Figure 3.1 and Figure 3.2. It presents five stages, being the design, manufacture, commission, perform operations and decommission. The design and manufacturing stages have not changed since the baseline report, as the design method remains the same and more specific manufacturing aspects are outlined in section 5.2. The changes are in the last three stages. The commission, perform operations and decommission stages have changed due to a different final design to what was presumed before. It should be noted that the REF above certain blocks means reference to the same earlier mentioned block.

3.2. Functional Breakdown Structure

The FBS with the hierarchical structure of all the functions from the FFD is shown in Figure 3.3. It only contains the three updated phases in commission, perform operations and decommission. It contains functions one level lower than the FFD.

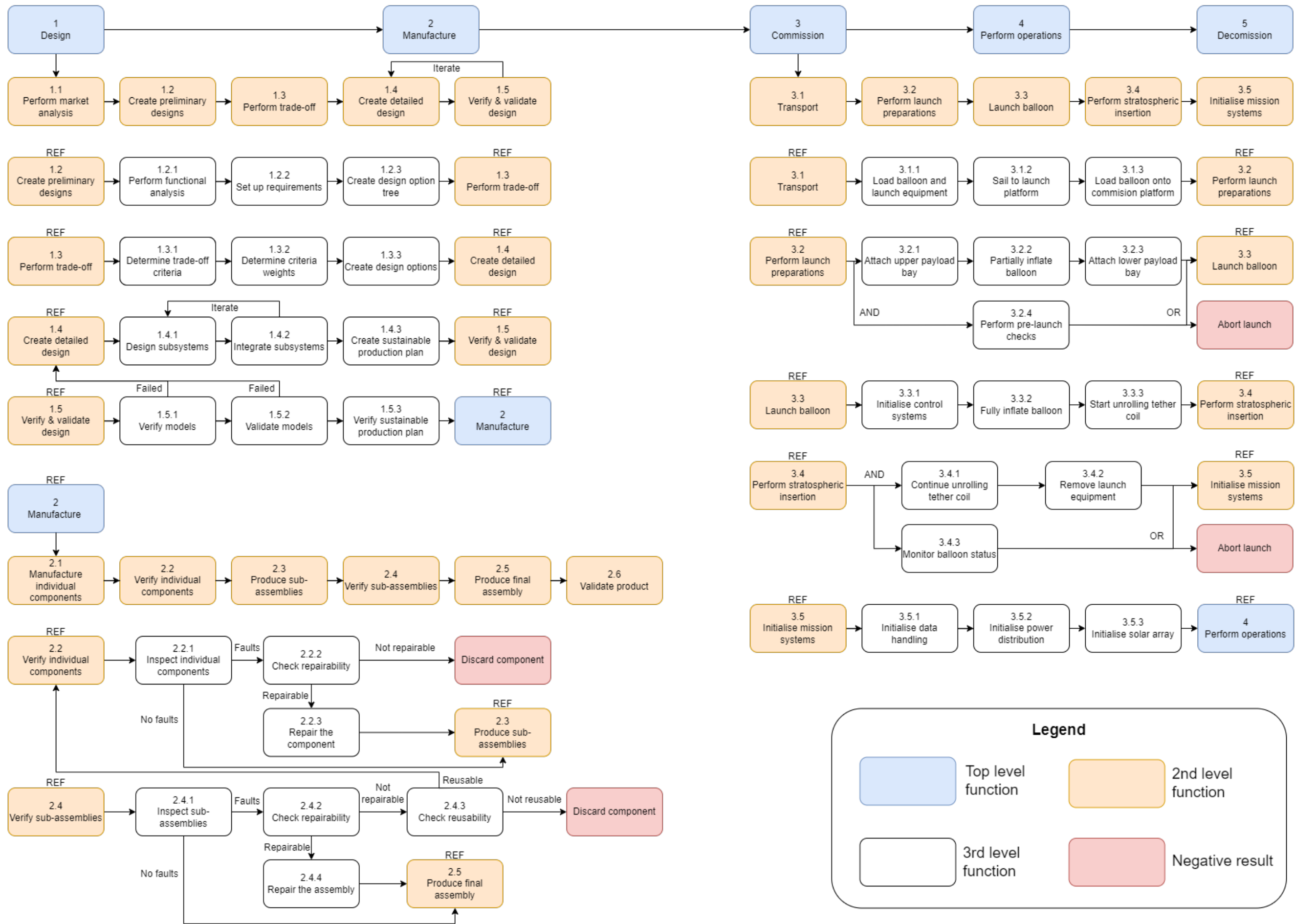


Figure 3.1: Functional Flow Diagram

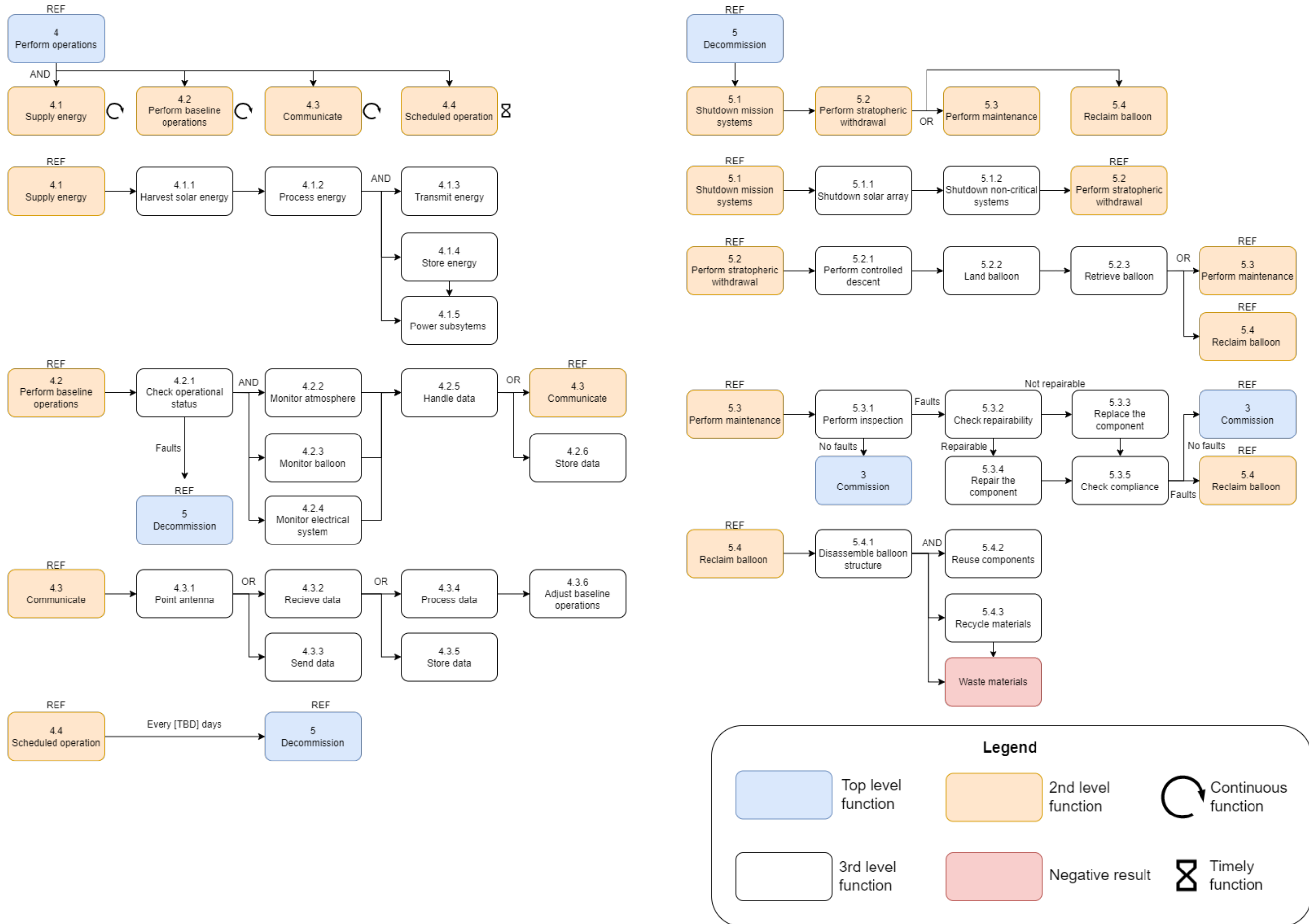


Figure 3.2: Functional Flow Diagram (cont.)

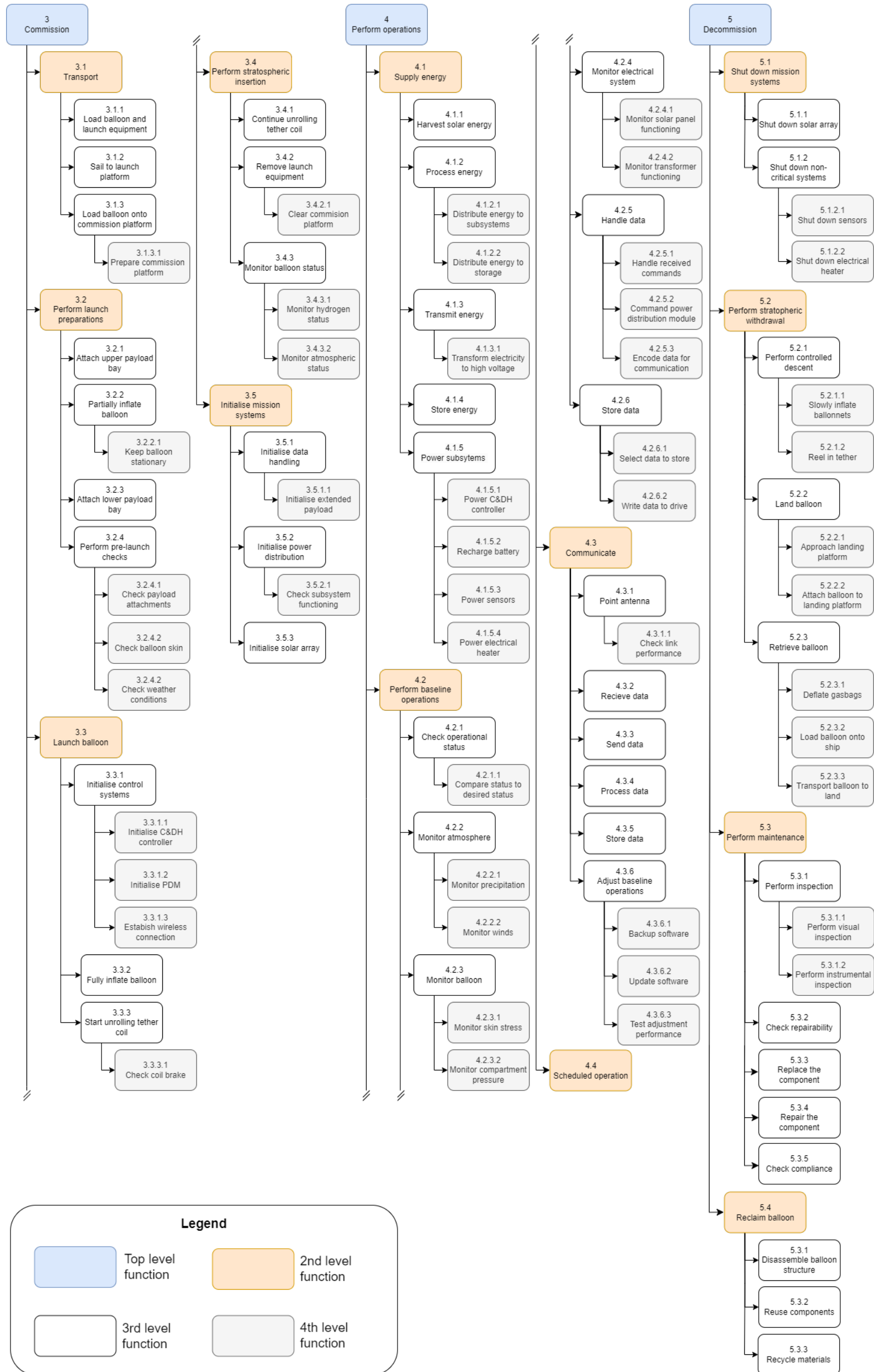


Figure 3.3: Functional Breakdown Structure

4 | Detailed Design

The design of such a complex system cannot be performed in one go, but it requires an iterative process. This chapter aims to explain the sizing of the individual subsystems and the relations between these. The starting point for all subsystems was the preliminary sizing and budget, originating from the Midterm Report [1]. When specific subsystems have been sized or other parameters changed, these changes were taken into account for the consequent subsystems.

The starting point of the detailed design process is the sizing of the solar array, which is done in section 4.1. The top level input for this sizing is the required power delivery of the SBD, which is set at 1 MW per SBD. Furthermore, the sizing of the solar array is dependent on the solar flux. A model to determine the solar flux based on the height and location of the SBD is presented in section 4.2. The second subsystem covered is the tether, for which the electrical and structural aspects are covered in section 4.3 and section 4.4 respectively. Since the material providing strength doubles as an insulator, these two sections are directly linked. For the structural aspects of the tether, a dynamic model is set up, which calculates the displacement of the SBD taking into account the winds. For this, the aerodynamic and aerostatic aspects have to be known. These are covered in section 4.5. These aerostatic aspects also provide a relation between the mass and volume of the structure, which is the starting point of the structural balloon design, covered in section 4.6. This structural analysis allows for the sizing of the structure, which further refines the mass budget and the balloon sizing. Based on this, the stability & control characteristics are covered in section 4.7. Finally, the payload is designed in section 4.8.

4.1. Solar Array Design

The detailed design starts by sizing the photovoltaics, as this relates to the main requirement regarding energy harvesting capabilities. For photovoltaics, the starting point is the cell design, which is based on commercially available models. This is presented in subsection 4.1.1. Electrical considerations accompanying full array design are discussed in subsection 4.1.2, as well as thermal considerations in subsection 4.1.3. Based on models, the array is sized in subsection 4.1.4 as a first estimate. Finally, the array is sized according to all system requirements in subsection 4.1.5, which includes degradation and redundancy considerations.

4.1.1. Photovoltaic Cell Design

For the most effective solar energy collection system it was decided to use high-efficiency low-weight solar cells. These triple junction cells have already seen extensive use in space applications and are constantly undergoing technological development. For the purpose of this report, a currently available cell will be used as the basis for small parameter scaling to fit the five year development timeline. Ideally, a custom cell is to be designed with tailored electrical and manufacturing characteristics, but that is beyond the scope of this design.

The baseline solar cell chosen is the 80 μm 3G30C from Azurspace¹. This cell from 2014 incorporates the current optimizations for the widely used GaInP/GaAs/Ge based cell, such as being lightweight and efficient. The design and its performance are representatives of the currently available space grade cells. The specifications can be seen in Table 4.1 along with the parameters for a 'V1.0' cell design, which is scaled to fit this paper. The rationale behind this scaling is explained afterwards.

Some of the parameters do not change or cannot be optimised for our purposes. The voltage is determined by the sum of electrical potentials created by the III-V compound semiconductor material layers within the subcells. It is affected by recombination and cell resistance, which is a function

¹"30% Triple Junction GaAs Solar Cell". Azurspace. Last accessed on 10-01-2022. https://www.azurspace.com/images/products/0004148-00-01_DB_GBK_80%C2%B5m.pdf

of material quality and layers. The thermal gradients could also be improved with semiconductor composition and bandgap optimisation, but this both is beyond the scope of this project. The 3G30C cell already has good voltage thermal gradients thus these are copied as no fundamental material changes will be made.

Table 4.1: Solar cell design parameters for 3G30C and 'V1.0'

Parameter	80 μm 3G30C	V1.0	Unit
Mass	50	45	mg cm^{-2}
Thickness	80	75	μm
Size	40 x 80	100 x 100	mm
V_{mp}	2411	2411	mV
V_{oc}	2700	2700	mV
I_{mp}	504.4	1938	mA
I_{sc}	520.2	2132	mA
η (BOL)	29.8	35	%
dV_{mp}/dT	-6.7	-6.7	mV K^{-1}
dV_{oc}/dT	-6.2	-6.2	mV K^{-1}
dI_{mp}/dT	0.24	0.924	mA K^{-1}
dI_{sc}/dT	0.36	1.387	mA K^{-1}

GaInP/GaAs/Ge is the standard for triple junction cells due to the fact that their lattice constants coincide nearly perfectly, as can be seen in Figure 4.1. For better thermal characteristics larger bandgap combinations are preferred, but no matching triplets exist. Lattice matching is extremely important for growing the individual layers of a solar cell. Stress concentrations in the mismatched lattices may lead to deformation and performance decreases. It is possible to combine off-lattice semiconductors, with much progress in recent years. For example, it is been researched that the thermal coefficients and achievable efficiencies of using InGaAs instead of Ge are better [5, 6]. However, the methods are not yet mature enough to be viable, mainly due to the increased complexity of manufacturing. Aspects such as this are a large reason to choose established designs. Custom designs are not guaranteed to benefit from current developments to decrease manufacturing costs. For these reasons, the industry standard configuration is taken.

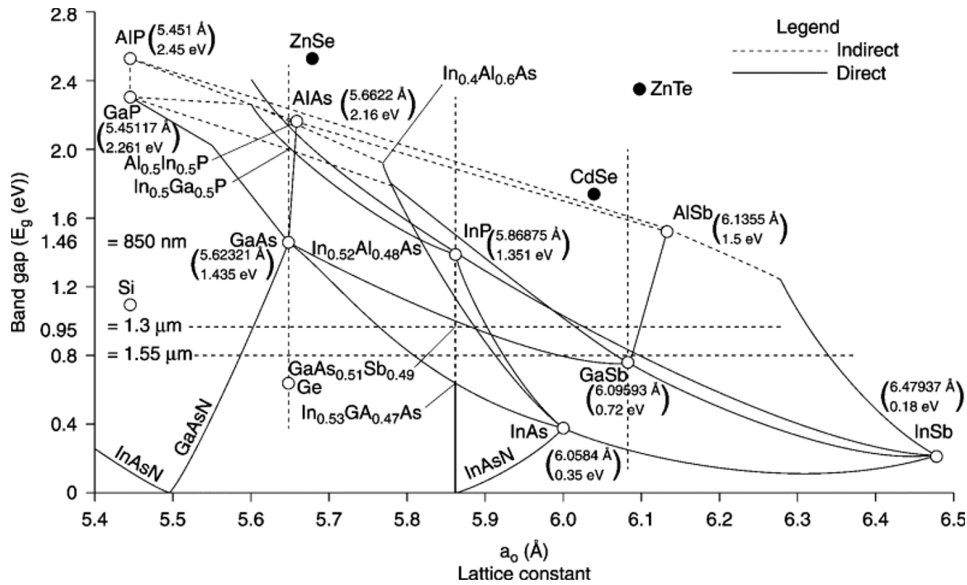


Figure 4.1: Semiconductor lattice constant versus bandgap [7]

The mass of the 3G30C cell is lower than contemporary solutions, this is due to a thinning of the Germanium growth substrate in manufacturing done by Azurspace. It is determined that further thinning of the substrate is possible, thus reducing the mass even more, as well as the thickness. Current metalorganic vapour-phase epitaxy growth wafers are limited to 6 inches diagonally². Further refinement of such large wafers means that square cells of 10 × 10 cm can be extracted from this wafer effectively. In scaling the cell area, the current increases with the area. Thus the I_{mp} and I_{sc} , as well as their temperature gradients, are scaled accordingly.

Triple junction cells are widely available at just over 30% efficiency, with the latest designs nearly 40% [8]. This difference is mainly due to advanced manufacturing techniques to decrease lattice defects and differing subcell materials. It is taken that 35% is achievable in the given time frame. To achieve 35% out of the 3G30C, the electrical parameters of the cell must be improved. Without a complete cell overhaul, the voltages cannot be improved. To achieve better performance, the current must increase. There are multiple ways to achieve this. The surface passivation may be improved, reducing recombination losses at the surface of the cell. The doping concentration may be increased as well, increasing the number of carriers available to contribute to the current output. These increased optical properties and collection probabilities can be achieved with only slight adjustments from the 3G30C. The values for I_{mp} and I_{sc} are calculated as needed to achieve 35% efficiency in this size cell. The according current temperature gradients are scaled with, overriding pure size scaling. This final cell design is rated to deliver 4.74 W under standard conditions. An approximation of the performance curves for this V1.0 cell design are shown in Figure 4.2, this is based on electrical parameters.

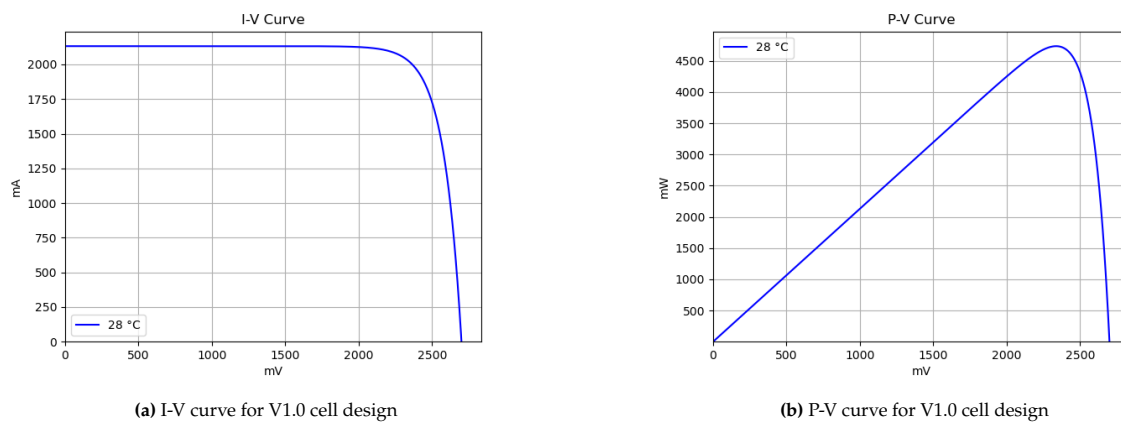


Figure 4.2: Performance curves for the V1.0 cell design for standard conditions

4.1.2. Photovoltaic Array Design

To incorporate the cells into the design they must be grouped electrically and physically to create usable panels. Cells can be connected in series to sum voltages, a so-called 'string'. They can also be connected in parallel to sum current, a so-called 'block'. Strings and blocks may be combined together to create an array. For our purposes, the large required area is divided into a multitude of panel areas. This is done to achieve the required electrical output, and simplify manufacturing and integration. The exact layout of cells is critical as multiple factors must be considered for an array of this size.

String mismatch

For a string of cells, the voltage of each is summed while the current is equal across each cell. In practise, the entire string operates at the lowest current as it cannot exceed that of the poorest cell in the string. This effect can drastically impact performance. The underperformance of a cell can be achieved by

²"Epitaxial MOCVD Growth and III-V Wafer Processing Services". SRI International. Last accessed on 13-01-2022. <https://www.sri.com/epitaxial-mocvd-growth-and-iii-v-wafer-processing-services/>

degradation or (partial) shading of it. Beyond that, all the additional current produced by other cells is dissipated in the poor cell, causing hot spot heating. This heating can be destructive to the cell and its neighbours. Even though the design will not experience shading during operation, this effect must be negated on the basis of cell degradation.

A bypass diode is always used in solar arrays. It is connected in parallel to a cell and is of opposite polarity. In normal operation, it is inactive until the cell becomes 'poor'. The current in the shaded part of the cell drops to zero, but the voltage remains at the open-circuit voltage. This results in a reverse bias voltage, where the voltage at the cathode is higher than that at the anode. A bypass diode then provides a low-resistance path for the reverse current. In practice, a bypass diode per cell is expensive in both area and cost. For space missions this may be done, but for most terrestrial applications of scale, a string may have a single bypass instead. Often Schottky diodes are used, but these possess a large voltage drop of around half a Volt, resulting in high power dissipation. An example of a better diode with a tenth the voltage drop is the SM74611³. For this design a similar diode is assumed with a maximum voltage of just over 30 V, this will simplify panel design.

Block mismatch

For a block of cells, the current is summed while the voltage is constant. The total voltage is not technically the lowest voltage in the block, but for our purposes may be treated as such. The voltage of a cell does effectively not degrade during its lifetime as it is inherent to the compound semiconductor materials used. Blocks cause effectively no issues for consistent cells.

Panel design

The maximum string length the assumed diode may handle is 12 cells, any more would exceed the maximum rated diode voltage of 30 V. Serially connected cells are connected from the anode (top contact) to the cathode (bottom contact). The top electrodes must be as small as possible so as not to block much of the incident light. Tiny parallel metallic strips called 'fingers' span the cell. Larger 'busbars' cross these, again parallel, and are used to connect cells together. Fingers collect the current and busbars transport it. Either the busbars continue between the cells or small wires could be used. The connection must be flexible due to the thermal expansion of the cells. The thermal expansion coefficient of used semiconductors is in the order of 10^{-6} K^{-1} . The 100 mm cells do not expand more than 0.1 mm under thermal cycling. For practical and manufacturing purposes a 0.5 mm spacing is taken for this panel design. This allows for thermal expansion as well as connectivity.

To minimise the electrical circuit for the diode, often a string is placed in a loop. Strings can then be placed in series and parallel. Combining strings and blocks leads to the same effects as cells in series. Take a block of two strings, which is in series with other such blocks. If a cell in a string becomes poor, that string is bypassed. The total voltage of the series of strings is now lower than its parallel counterpart. Thus the combination delivers less overall current than it does normally. All serial connections are now forced to operate at this lower current, compromising the performance of the array. This case is effectively similar to a series of individual cells. For any block in series with others, a single 'poor' panel means that the entire block must be bypassed as to not hamper the performance of the array. Thus it is preferred to minimise blocks that connect in series and use the so-called 'series-parallel' configuration.

For implementation purposes, it is preferred to keep standardised panels small and modular. Thus we define a panel as a single string of 12 cells with a bypass diode. This configuration is to be looped next to the diode to minimise electrical wiring. This can be done in two ways, as can be seen in Figure 4.3. The difference between these two layouts is the resulting shape of the panel. For panel A the panel will be squared, whereas panel B will provide a rectangular shape.

These panels are then connected in series to achieve a certain voltage with multiple of these chains then placed in parallel across the surface area. The IEC definition of DC voltages lists 1500 V as the

³"SM74611 Smart Bypass Diode". Texas Instruments. Last accessed on 10-01-2023. <https://www.ti.com/lit/ds/symlink/sm74611.pdf>

cut-off where one enters high-voltage operation⁴. It is preferred to keep the chains below this voltage for regulations. Each panel delivers 32.4 V maximum at open circuit, meaning a total of 46 may be chained. Each chain is to be put in parallel to achieve the required current for the energy harvesting requirement. The requirement SBD-PWR-01 states 'The balloon segment shall harvest at least TBD of solar power.', as the exact sizing of the solar array depends mostly on the balloon's carrying capabilities. The conditional solar array size also depends on thermal and irradiance characteristics, which are discussed in the next sections.

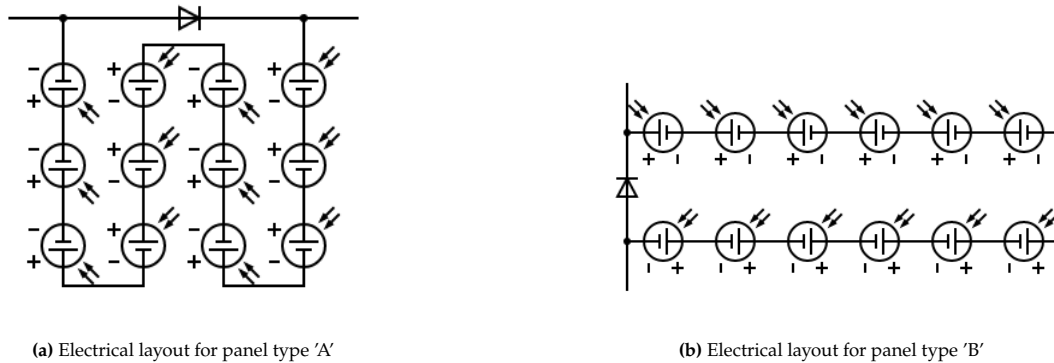


Figure 4.3: Electrical diagrams for the defined panel configurations.

4.1.3. Photovoltaic Cell Thermal Model

The performance of a solar cell is heavily temperature dependent. The thermal coefficients of the V1.0 cell were given in Table 4.1, these hold for a positive increase in temperature. The industry standard temperature is 28 °C and is used for modelling and certification⁵. This is the temperature at which nearly all solar cell specifications are given, including the 3G30C. As can be seen, the current increases while the voltage decreases. This is due to the inherent working effects of the semiconductor subcells. If the semiconductor holds more thermal energy due to a higher working temperature, the electrons in the valence band possess more energy. This reduced the effective bandgap of the material. This decrease means more, lower energy, photons are captured than previously. In a multi junction cell, the bandgaps are finely tuned, and disproportional bandgap changes in the semiconductors decrease the absorption efficiency. This is why the current increases, due to more photons, but the voltage drops steeply, resulting in overall power loss.

In order to calculate the effective efficiency of the solar cells, the temperature of the array at a given moment must be known. This is why a thermal model has been set up to investigate the heat balance of the solar array. To model a solar panel consisting of triple junction solar cells, certain assumptions have to be made. First of all, the thickness of the solar panels is negligible when compared to the total area. Thus the solar array is assumed to be a flat plate, such that the temperature of these plates is uniform with no internal convection. Regarding composition, it is modelled as a flat Germanium plate. This can be done because all other cell layers are an order of magnitude thinner and therefore do not influence the thermal model to the same extent. To get an indication of operating temperature this is the first layout.

The thermal model uses the environmental parameters of height, wind speed and incident solar flux as input, as well as germanium material characteristics and V1.0 cell electrical specifications. Regarding the incoming heat, it only considers the Sun's radiation as albedo and planetary radiation is blocked by the balloon. The exact solar spectrum, and consequently the power generated, depends on the altitude

⁴"IEC 61140:2016". International Electrotechnical Commission. Last accessed on 10-01-2022. <https://webstore.iec.ch/publication/23997>

⁵"Qualification and Quality Requirements for Space Solar Cells". American Institute of Aeronautics and Astronautics. Last accessed on 11-01-2022. https://aiaa.kavi.com/public/pub_rev/AIAA_S-111A-201X_PR.pdf

as well as location and time of the year. These are design factors later decided on. For this first thermal evaluation, a solar irradiance profile at 30°N 120°E on 21/06/2012 at 20 km altitude. This was chosen as it corresponds to the paper used for the solar incidence model and verification of it. Specifics on the solar incidence model are discussed later in section 4.2.

Heat generation in the cell is driven by the solar irradiance that does not get converted to electricity. For the V1.0 cell at 28 °C with efficiency 35%, 65% becomes waste heat. There are multiple processes that generate waste heat within the cell, but an efficiency based approximation is sufficient. The types of heat transfer that are included in this model are radiation and convection. Convection is split into free convection and forced convection. Convection is driven by the convection coefficient, area and temperature difference between the panel and the air. For the modelling of free and forced convection, the book 'Fundamentals of heat and mass transfer' was consulted [9]. Thermal radiation depends on the temperature difference between the panel and the air, as well as the emissivity of the cells. For germanium, the emissivity is 0.9 [10].

This first simple model can be seen as a solar array with bottom insulation, as is pictured in Figure 4.4a. Heat loads can alter the pressure distribution and structural integrity of the balloon, it is crucial to have sufficient insulation between the solar array and the airship [11]. The resulting temperature distribution can be seen in Figure 4.4b. This high temperature of up to 94.5 °C is unwanted as it lowers the efficiency of the solar array significantly. The operating efficiency of the array at peak power is now approximately 16.4% lower than the baseline. It was decided to investigate methods to lower this temperature in order to maintain the efficiency, and keep the required area minimal. One of the possibilities would be to increase the area over which heat can be dissipated through radiation and convection. Extending the area upwards, by using heat fins or similar methods, would result in induced shadows, lowering the solar array efficiency. Hence, the logical method would be to extend the area downwards.

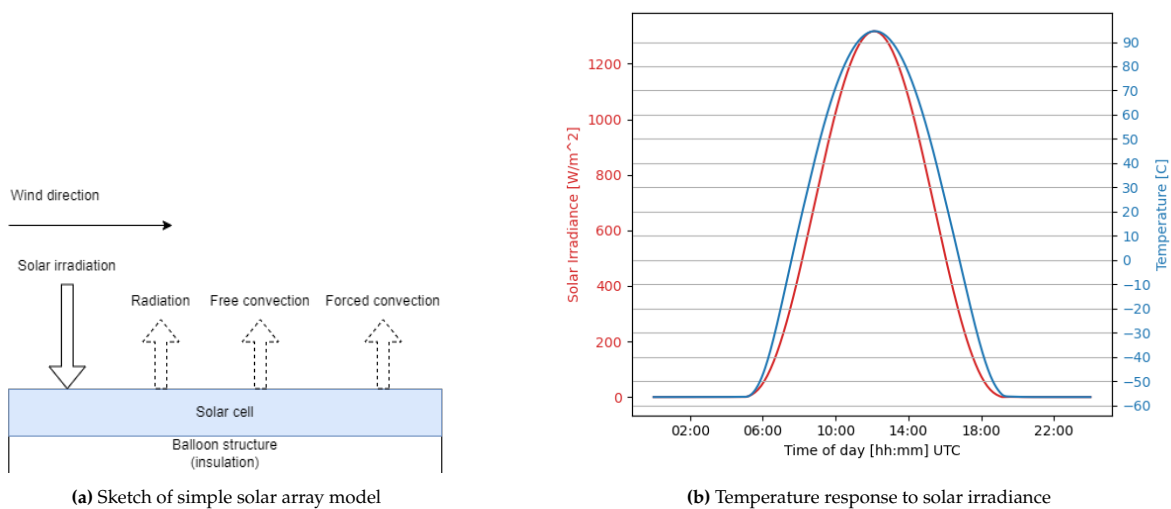


Figure 4.4: Simple thermal model setup and response for 20 km altitude and 5 m/s wind speed.

Extra surface area can be achieved by lifting the solar array from the balloon, to allow airflow at the bottom of the solar panels, effectively doubling the cooling area. The solar panels would then need some support structure to keep them in shape. This structure will be elaborated upon in section 4.6, but it is evident that a full size backplane is needed, which will be made of carbon fibre reinforced polymers (CFRP), as they provide a high strength to weight ratio and good emissivity. This full size backplane will also be very thin, which allows for neglecting the internal convection and the assumption that the temperature of the solar cells and the backplane are equal at all times. Updating the model to allow radiation and convection also from the CFRP backplane results in a solar cell temperature of 44.6 °C. Hence, the relative efficiency loss is reduced to 3.9% at peak power. The model and temperature

response when this change is implemented are shown in Figure 4.5.

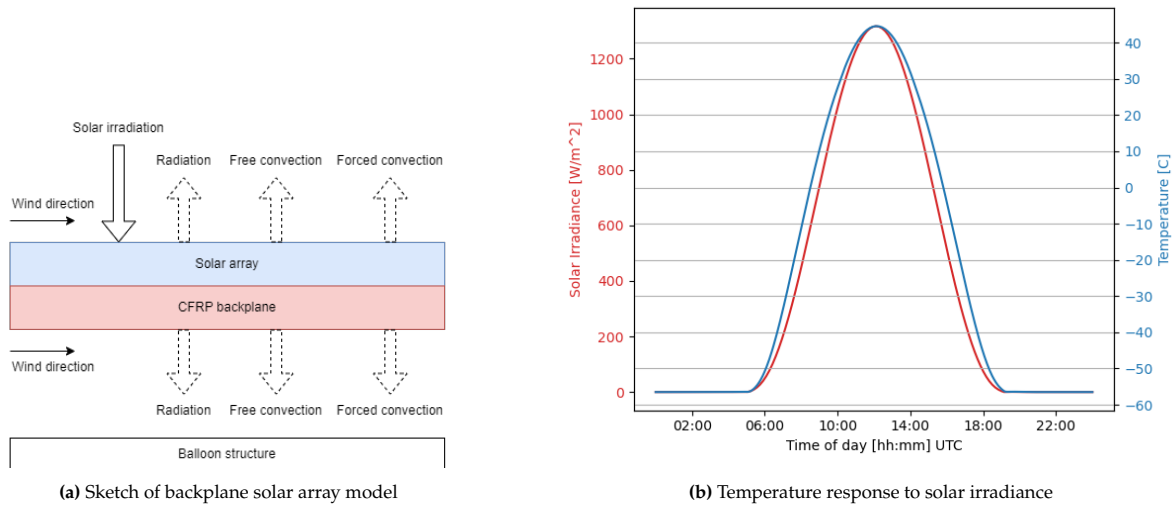


Figure 4.5: Backplane thermal model setup and response for 20 km altitude and 5 m/s wind speed.

From the model, it is noticed that the influence of the wind speed is low. Changing the wind speed from 0 to 30 m s⁻¹ for the simple model results in a decrease in temperature of 16%. This is comparable to the model set up by Jun Li et al., where a decrease of 12 percent was found over this same wind speed range and at the same 20 km height [12]. The relative contributions of heat transfer methods are given in Table 4.2. The solar array size and area is an input for the model, however the contribution of heat transfer methods is constant over a varying array at the same order of magnitude. Note that the wind speed, air volume between the backplane and balloon, as well as altitude do influence the relative numbers.

Table 4.2: Heat transfer contribution for backplane design (wind speed of 5 m/s, altitude of 20 km and plane spacing of 1 m)

Heat Transfer Method	Contribution
Cell radiation	47.08%
Cell free convection	3.90%
Cell forced convection	3.31%
CFRP radiation	39.73%
CFRP free convection	3.20%
CFRP forced convection	2.78%

By lifting the solar panels above the balloon, the temperature of the solar array can be decreased by 53%, which decreases the loss in efficiency due to thermal effects. With this backplane design, the loss in efficiency at peak sun hours will be only a couple percent depending on wind speed, which is deemed sufficient for this design. At a 5 m/s wind speed the loss in efficiency is decreased from 16.4% to 3.9% by lifting the solar panels. The performance curves for the V1.0 design at the maximum operating temperature are shown in Figure 4.6.

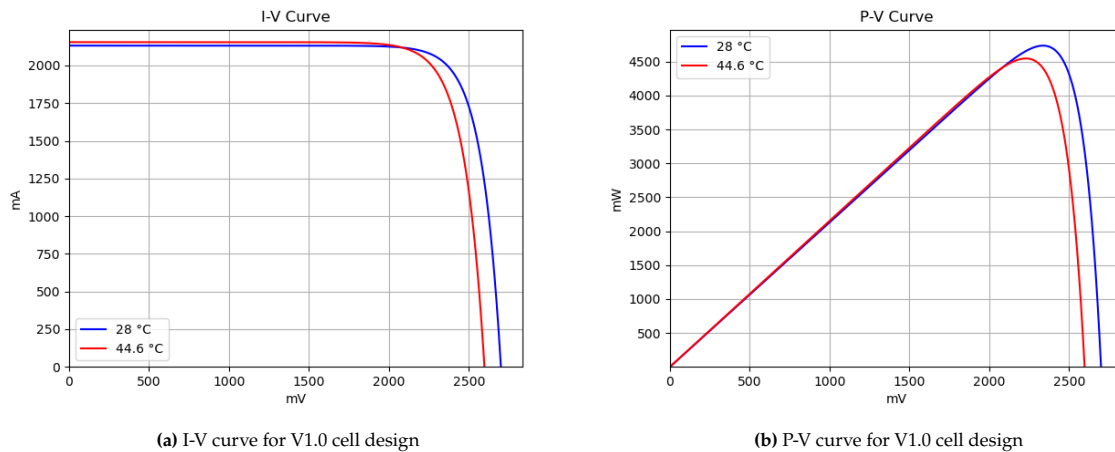


Figure 4.6: Performance curves for the V1.0 cell design for operational conditions (44.6 °C) compared to standard (28 °C).

4.1.4. Preliminary Array Sizing

Now that the specific performance characteristics of the V1.0 solar cell are known for the mission, the full array can be sized. The array must be large enough to deliver enough power to cover the balloon subsystem usage and transmit to ground. This design step is an iterative one. As a first estimate, according to the previous power budget the solar array must deliver 1 074 000 W. The sizing is done for the highest solar irradiance point of the day and the maximum power point of the solar cells.

On the used solar flux model, the maximum solar irradiance is 1317.3 W m^{-2} . This corresponds to a solar cell output of 4.55 W for an efficiency of 33.6% at 44.6 °C. A panel delivers 450.2 W m^{-2} total, meaning 19,698 panels are required. The size of a singular panel is $121,203 \text{ mm}^2$. Thus the array size must be 2388 m^2 .

One other consideration to be included in array design is the use of blocking diodes. Blocking diodes function to prevent the reverse flow of current from another chain of solar cells (or batteries) during periods of low or no sunlight. This backflow can occur when a chain of a higher voltage is connected in parallel with one or more chains with a lower voltage. The blocking diode allows current to flow in only one direction and prevents the reverse flow of current, protecting the other components of the solar array from damage. Each chain must possess a blocking diode for this purpose.

Environmental Considerations

The current solar array sizing is done for BOL conditions. However, requirement SBD-SCH-02 dictates an operational lifetime of 25 years must be designed for. The solar cells will degrade over the course of their lifetime, reducing power output. Redundancy and margins must be included in the array sizing to comply with all the requirements. Degradation factors that are evaluated are thermal cycling, particle radiation and UV radiation.

Due to the multi layered nature of triple junction solar cells, thermal cycling can lead to delamination and connection failure. It is not specified what the thermal cycling effects are for the 3G30C, nor the specific qualification requirement is has undergone. A comparable cell in the ZTJ from SolAero states no electrical performance degradation after 2000 heavy (-180 °C to +90 °C) cycles. Given that the V1.0 design must deal with lower intensity cycles, but for nearly 10,000 cycles, it can be determined that the effect will be minimal. A decrease of less than 5% in electrical performance is aimed for after 25 years for pure thermal cycling degradation.

Solar cells in space applications face the challenge of intense electron, proton and neutron flux from their radiation environment. They are radiation hardened designed with considerations such as protective layers and minimising subcell base layers. The 3G30C technical sheet lists no performance degradation

before 10^{14} 1 MeV equivalent electron flux. This performance characteristic is often listed for space application cells, stemming from the 'JPL Equivalent Fluence Method' for modelling radiation effects. The specifics are beyond the scope of this paper, but it provides an indication of the level of radiation hardening of a cell. To be plain, the radiation environment in the stratosphere is of low intensity. Most electrons and protons do not penetrate far enough to form a problem. However, at 20 km altitude, the atmospheric neutron flux is maximum. It does vary with latitude and longitude, but it does not exceed $1.4 \text{ cm}^{-2} \text{ s}^{-1}$ neutrons of 1-10 MeV [13]. The flux over 25 years would be $1.1 \cdot 10^9 \text{ cm}^{-2}$. This is not directly comparable to the JPL model rating, but it indicates that the flux is multiple orders of magnitude off. For the solar array sizing it can be determined effectively no degradation takes place from radiation effects.

Lastly, ultraviolet radiation may damage cell components, compromising electrical performance. High energy UV is known to cause damage to the surface passivation, which leads to an increase in recombination losses. It also causes carrier generation in the bulk of the solar cell. Both lead to a decrease in the open-circuit voltage. The exact mechanisms are not fully understood for multi junction cells, thus mainly protective layers are added to the design. In particular, the anti-reflective coating is tuned for this. Bare cells reflect a significant portion of incoming light. Consisting of two layers, TiO_x and Al_2O_3 in 3G30C, it is tuned to reflect UV and deep IR while passing intermediate wavelength. This is achieved by reflecting waves out of phase with a wave reflected from the semiconductor surfaces. This causes destructive interference, effectively resulting in no reflected energy. Specific UV characteristics cannot be found and depends on cell integration. According to literature, silicon crystalline cells degrade by $0.5\% \text{ y}^{-1}$ (median) [14]. Due to the flexibility of multi junction cell design, it is assumed this can be improved for the V1.0 design. A degradation factor of $0.3\% \text{ y}^{-1}$ is taken forward, or 7.5% after 25 years.

Redundancy Considerations

Besides degradation from operational conditions, the degradation of the array from physical defects. In its 25 year designed operational lifetime, all electrical components may be subject to failure. For example, the bypass diode in a panel may fail due to manufacturing defects. As explained before, this would cause the entire chain of panels to drop performance drastically. The consideration would be to include a redundant bypass diode, also in parallel, to each panel. The same holds for the blocking diodes, as a single failure compromises the entire array. Adding another for redundancy is as simple as connecting another in series. The array itself cannot be redundant, as every available area must be used for the operation to maximise generated power. If any cell fails, that would just result in a slight decrease in array performance.

4.1.5. Array Sizing

Introducing the total of 12.5% degradation of electrical performance from the cells at EOL, the array can be sized to meet all the requirements. Returning to the thermal model for the backplane design, now with 12.5% less power output, the effective power generation per cell is 3.982 W. The array sizing follows the same method as before. A panel delivers 395.2 W m^{-2} total, meaning 22,493 panels are required. The size of a singular panel is $121,203 \text{ mm}^2$. Thus the array size is 2726 m^2 to meet the EOL requirement. Calculating the produced power output of the solar array gives 8300 kWh over the course of 24h for this specific solar spectrum at BOL and 7200 at EOL.

Integration Considerations

The exact backplane sizing is mostly a structural consideration, rather than a solar array one. The CFRP must be slim enough to allow for the assumption that the internal heat flow is negligible. In the CalTech research the concept of an CFRP backplane is based on, it was found that a thin $<100 \text{ }\mu\text{m}$ layer is adequately thermally conductive [2]. A $90 \text{ }\mu\text{m}$ backplane combined with the solar panels results in approximately a 0.6 kg m^{-2} for the array.

The last item to consider is the wiring of the array. As described in subsection 4.1.2, a chain of panels is limited to 1500 Volt. This means that the order of 489 chains is needed. As all cables must converge to a central location, these hundreds of wires may span along the entire array area. In terms of integration, the connections are able to run below the backplane so as not to obstruct the solar array. This cabling

must be taken into account for the mass budget. On average a cable runs half the radius of the area, and possibly further along the balloon's internal structure. The area required for a 1500 V rated aluminium cable carrying 2 A along 15 meters is 0.21 mm^2 . Adding 0.5 mm of PVC insulation results in an approximate mass of 40 kg. Finally, the bypass diodes that must be wired into the system must be added as well. 978 blocking diodes are needed along with around 45 000 bypass diodes. This is needed to counter any manufacturing defects, uneven degradation or even delamination. The exact mass of the example diode is not provided, so an approximation is made. At 1 gram per diode, and 45,964 diodes needed, the mass is rounded to be 45 kg. Thus a total of 85 kg is budgeted for solar array integration.

4.2. Solar Flux Modelling

To realise its possible output power, the expected solar irradiance that reaches the solar array on the SBD is a critical parameter to evaluate. There are numerous steps to achieve the flux at a given time (or for a given time range), including the orientation and location of the solar array, the local time and Earth's position relative to the Sun, and Earth's atmospheric composition at the selected altitude. The irradiance values can then be used to size the solar array accordingly to meet the net power generation requirements, in addition to describing the thermal regulation system for the SBD. On the following note, this would entail the need for a parametric approach where combinations of various input ranges can be generated and analysed for reference.

This section aims to present the model used to determine the solar flux based on these different parameters. This starts by defining the model inputs and outputs, which are listed in subsection 4.2.1. Afterwards, the relationship between location and solar position is presented in subsection 4.2.2. Then, in subsection 4.2.3, the different radiation components are analyzed to account for variations in altitude. Finally, the influence of the height on the solar irradiance is presented in subsection 4.2.4.

4.2.1. Model Inputs and Outputs

First, it is important to characterise what can primarily affect the value used for the incoming solar flux. One of the key drivers for a stratospheric altitude than on-ground was the reduction of losses due to atmospheric scattering and absorption. The HadCM3 numerical model and dataset [15] has been used to show a difference of net solar irradiance at Earth's surface dropping to between 40-60% than as received at the top of the atmosphere, as well as general changes due to latitudinal and longitudinal changes⁶. Secondly, the total irradiance can be split into direct and diffuse irradiance values which each have their own relations with the aforementioned parameters as well as the geometric orientation of the given solar array relative to the sun and the local horizon. Lastly, solar time and Julian day affect the Sun's zenith in a given geographic location, and they consequently play a part in the length of the day and solar angle [16].

Listed below is a summary of base inputs that have been identified to be variants in the design and operation of the SBD. These can then be used to generate intermediate values for relative sun and earth angles for the various flux calculations.

- Year, month, and day
- Minute and hour
- Second (fractional)
- Longitude and latitude
- Elevation
- Local temperature and pressure
- Panel azimuth and slope

4.2.2. Solar Position and Angles

The first step is to have an accurate model of the solar position and relative angle to the array over time. Meeus' Solar Position Algorithm (SPA) [17] is a highly robust method to calculate

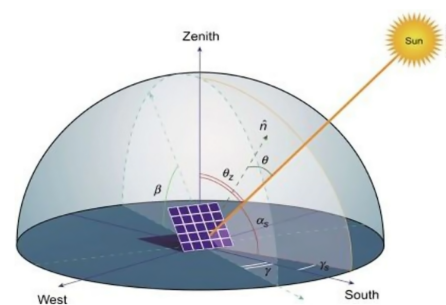


Figure 4.7: Illustration of the coordinate system and notable angles used in describing incoming radiation. Note that the astronomer's definition of azimuth γ , South moving Westward, is used here.

⁶"Solar Radiation". Jinyi Solar. https://www.jinyi-solar.com/Solar_Basics/solar-radiation.html

these values from the identified inputs, and it has additionally been verified and adapted for general use as a library routine by the National Renewable Energy Laboratory, under a contract of the United States Department of Energy [18]. It is able to calculate the solar zenith and local azimuth angles for instances within years -2000 to 6000, with uncertainties of $\pm 0.0003^\circ$ based on the date, time, and location on Earth - for arbitrary geometries. It utilises precise time arithmetic paired with VSOP87 [19], a semi-analytic model to describe the secular variation of planets from Mercury to Neptune - allowing for calculation of Earth's relative positions and orientation with respect to the Sun for long-term applications. The SPA algorithm also accounts for atmospheric refraction based on the altitude (angular distance of an object above the local horizon. Figure 4.7 demonstrates the different angles that are used to describe solar influx on the horizon plane and panel geometry.

A visualisation of one dataset that may be retrieved from the SPA algorithm is presented in Figure 4.8, which may be interpreted as a day/night cycle view of Earth. A plot of incidence angle θ would also be identical for a panel slope angle β of zero, i.e. the panel's normal vector \vec{n} is coincident with the zenith vector.

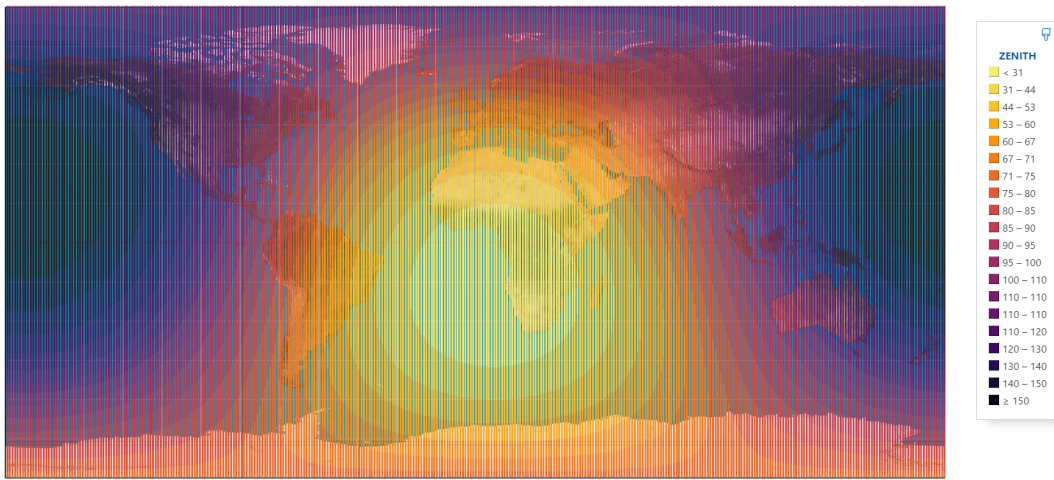


Figure 4.8: Variation of Sun zenith angle θ_z for February 2, 2023 at 11:45 AM UTC on an equirectangular projection of Earth. Colours represent isosurfaces.

4.2.3. Solar Radiation Components

With the parameters evaluated with the SPA implementation, the incoming solar radiation can be described for a wide range of scenarios. However, a key point is the high altitude aspect and its effect on solar radiation, which many available and common solar panel sizing models fail to account for in an extensive and straightforward manner [16]. The proposed model is a hybrid of Li et al. [20] and Kreith & Kreider [21] to reduce the overall complexity from obtaining various atmospheric transmittance and scattering coefficients.

The total incident solar radiation I_{tot} captured by a panel includes the direct solar I_{dir} , diffuse solar I_{dif} , and reflected I_{ref} radiation from Earth - as depicted in (4.1).

$$I_{tot} = I_{dir} + I_{dif} + I_{ref} \quad (4.1)$$

Angular Variation

Each of the above components have angular variance based on the parameters in Figure 4.7, and they can additionally be parameterised by two categories of irradiance fluxes: direct solar irradiance flux I_{DN} and diffuse irradiance flux I_{dh} . The decomposition of the three radiation sources is found in (4.2). Note

that ω is used as the solar elevation angle, which is found by an angular transformation of $\pi/2 - \theta$.

$$\begin{aligned} I_{dir} &= I_{DN} \sin \omega \cos \theta \\ I_{dif} &= I_{dh} (0.5 + 0.5 \cos \beta) \\ I_{ref} &= (I_{DN} \sin \omega + I_{dh}) (0.5 - 0.5 \cos \beta) \end{aligned} \quad (4.2)$$

Irradiance Fluxes

The irradiance fluxes for a horizontal plane on a clear day, which is assumed for the weather model in the stratosphere, have dependencies on the average solar irradiance at exospheric conditions I_0 (taken as constant 1361 W/m^2 [22]), true anomaly TA , Earth-Sun orbit eccentricity E (taken as constant 0.01671), atmospheric transmittance factor p_t (taken as constant of 0.65), and lastly an air mass ratio m to model altitude effects. The model equations are shown in (4.3).

$$\begin{aligned} I_{DN} &= I_0 \left(\frac{1 + E \cos TA}{1 - e^2} \right)^2 p_t^m \\ I_{dh} &= \begin{cases} \frac{1}{2} I_{DN} \sin \omega \frac{1 - p_t^m}{1 - 1.4 \ln p_t}, & \text{for } \sin \omega \geq 0 \\ 0, & \text{for } \sin \omega < 0 \end{cases} \end{aligned} \quad (4.3)$$

Air Mass Ratio

The air mass ratio (4.4) is prescribed as a function of the ratio of sea-level pressure P_0 to pressure at the considered altitude P_a . It also accounts for refraction, in terms of elevation angle ω .

$$m = \frac{P_a}{P_0} \left[\sqrt{1229 + (614 \sin \omega)^2} - 614 \sin \omega \right] \quad (4.4)$$

True Anomaly

The true anomaly TA defines the position of a body moving along a Keplerian orbit. It can be approximated from the mean anomaly MA via Fourier expansion and with local error of the fourth order [23] - which is applicable for low eccentricity orbits, such as the Earth-Sun orbit. The formulation is depicted in (4.5).

$$TA = MA + \left(2E - \frac{1}{4}E^3 \right) \sin(MA) + \frac{5}{4}E^2 \sin(2MA) + \frac{13}{12}E^3 \sin(3MA) + \mathcal{O}(E^4) \quad (4.5)$$

The mean anomaly can simply be obtained as the fraction of the year as in (4.6), where n represents the day number for a reference date, i.e. January 1st.

$$MA = \frac{2\pi n}{365} \quad (4.6)$$

4.2.4. Irradiance Output

From the equations above, we do see that the most optimal scenario for direct solar radiation is if the solar panels' normal vectors directly point towards the sun, thus a θ of 0 rad. Contrarily, the diffuse and reflective radiations are more dependent on the panel slope β , whereby the diffusive radiation increases for a lower β , while reflected decreases. A more obvious observation is that the resulting net solar flux for $\pi/2 < \theta < (3\pi)/2$ is zero. This is in correspondence with the day/night cycle analogue in Figure 4.8. Additionally, the model is height variant with the mass ratio, and hence pressure ratio. This change, using the International Standard Atmosphere model as a reference to attain the atmospheric pressure at

given altitudes, can be seen in Figure 4.9. From this graph, the vertical displacement of the balloon should be limited to avoid large reductions in power output.

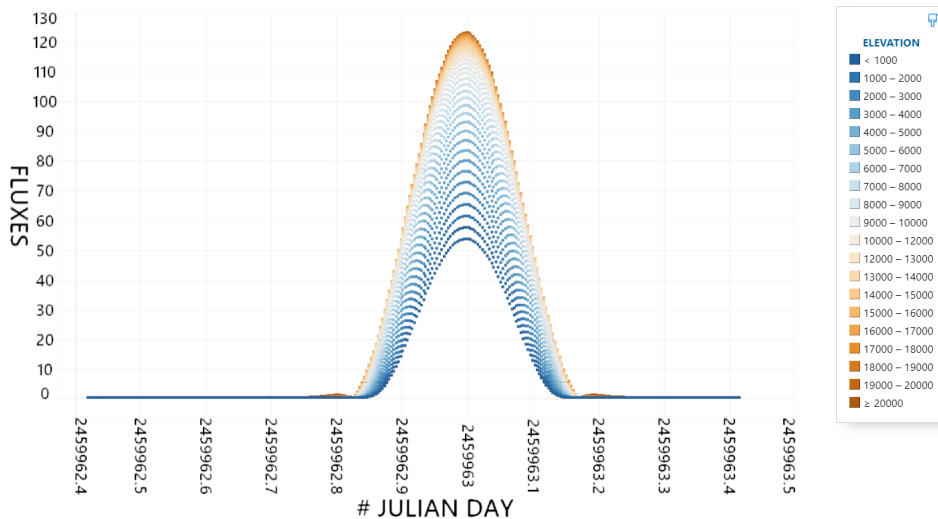


Figure 4.9: Variation of solar flux with heights for January 18, 2023, over Delft, The Netherlands (52.01° N, 4.36° E). Note that Julian Day is used to demonstrate the use of absolute time scales.

4.2.5. Model Verification and Validation

Given that the flux model is used as a basis for calculating the needs of the photovoltaics' specifications, it is essential the model is used correctly and the values it provides are representative of reality.

Verification

With regards to verification, the model utilises an analytical formulation and thus errors due to mesh spacing or time evaluation interval lengths are not present. This removes the need for a convergence test to verify output accuracy and precision.

Nevertheless, numerical errors may still occur due to the Julian Date being considered on an absolute basis - which may make for evaluating small changes in time (in the order of milliseconds) and give truncated outputs. To combat this, the intermediate & calculated values that the computational model uses are stored with high floating point precision (long double) [24]; while input and output variables are stored with lower precision (floats) to reduce memory requirements and output file size. The reasoning as to why the intermediate values require high precision mainly stems from the use of many trigonometric functions and notably those with asymptotic nature.

Furthermore, to ease program verification, only standardised and highly-developed libraries within the program were used, i.e. C/C++ standard libraries⁷, Python Standard Libraries⁸, Numpy [25], and Pandas [26].

Validation

The first model to validate is the sun model which is used to calculate the position and angle of the Sun at a given, universal time. This can be done by obtaining real life data and algorithms that have their parameters updated frequently SunCalc.org⁹ was taken as a reference for this. The case study in Figure 4.10 was taken as a reference input and its corresponding outputs.

⁷"C++ Standard Library reference (STL)". Microsoft. <https://learn.microsoft.com/fr-fr/cpp/standard-library/cpp-standard-library-reference>

⁸"The Python Standard Library". Python. <https://docs.python.org/3/library/>

⁹"SunCalc". SunCalc. <https://www.suncalc.org/>

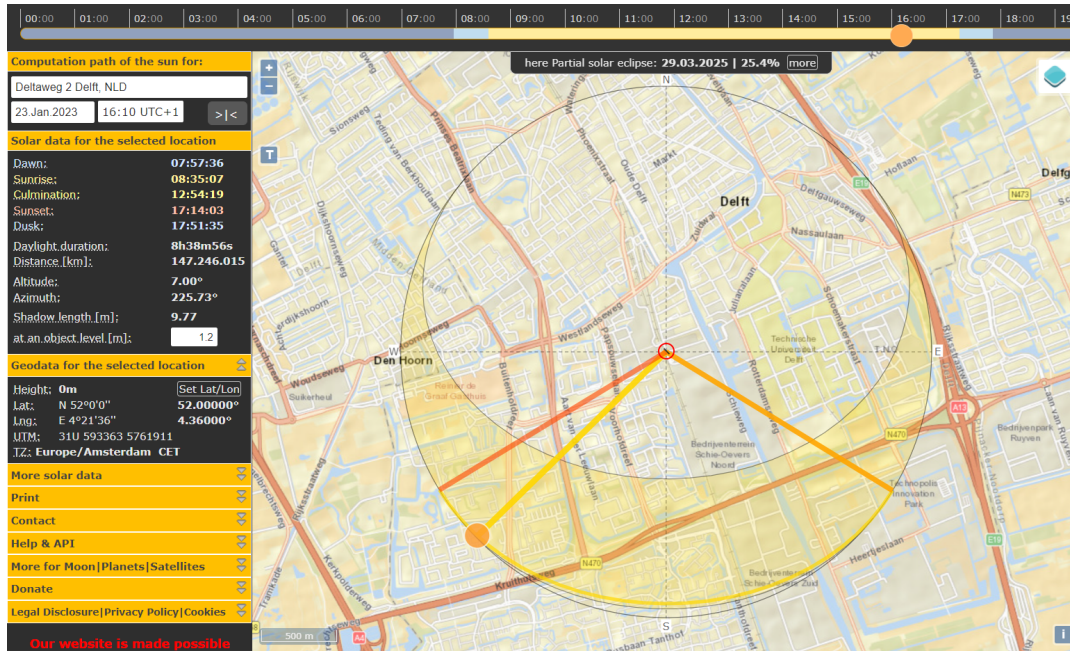


Figure 4.10: Case study used to validate solar position model

The following snippet represents the input arguments into the algorithm. Note that this is directly taken as a test C code, and is not the actual method of input for large datasets:

```

spa.year          = 2023; // 4-digit year,
spa.month         = 1; // 2-digit month,
spa.day           = 23; // 2-digit day,
spa.hour          = 16; // Observer local hour,
spa.minute       = 10; // Observer local minute,
spa.second        = 00; // Observer local second,
spa.timezone      = 1.0; // Observer time zone (negative
                        // west of Greenwich)
spa.delta_ut1     = 0; // Fractional second difference
                        // between UTC and UT which is used
spa.delta_t       = 69.184; // Difference between earth
                        // rotation time and terrestrial time
spa.longitude     = 4.36; // Observer longitude
spa.latitude      = 52.0; // Observer latitude
spa.elevation     = 0.0; // Observer elevation [meters]
spa.pressure      = 1013.25; // Annual average local
                        // pressure [mb]
spa.temperature   = 11; // Annual average local temperature
                        // [degrees Celsius]
spa.slope         = 0; // Surface slope (measured from the
                        // horizontal plane)
spa.azm_rotation  = 0; // Surface azimuth rotation (measured
                        // from south to projection of
                        // surface normal on horizontal plane,
                        //negative east)
spa.atmos_refract = 0.65; // Atmospheric refraction at sunrise
                        // and sunset
spa.function       = SPA_ALL; // Output Variables switch

```

After running the algorithm, the output dataset is displayed and can be seen below. Note that the intermediate values and a number of the final values are not being printed here.

Julian Day:	2459968.131944
L:	1.233453e+02 degrees
B:	2.050142e-04 degrees
R:	0.984310 AU
H:	48.917112 degrees
Delta Psi:	-2.510534e-03 degrees
Delta Epsilon:	1.932120e-03 degrees
Epsilon:	23.438225 degrees
Zenith:	83.001181 degrees
Azimuth:	45.731245 degrees
Incidence:	83.001181 degrees
Sunrise:	08:34:55 Local Time
Sunset:	17:14:12 Local Time

Comparing the results, and noting that the altitude is complementary to the zenith due to different coordinate frames and the differences in azimuth reference points, the output values are strikingly close. This procedure has also been tried for other timestamps and locations, and they also present extremely precise values. Thus, the SPA algorithm can be considered a valid model to use for solar flux input.

For the flux algorithm, the reference paper used in implementation [20] provide validated output reference data. Hence verifying that the values of the in-house irradiance model matches that of Li et al. can prove the validity and hence the applicability of the model. While the paper also elaborates on the temperature and 3-D geometry used, only the "slope" of an infinitesimal panel at a given time and location will be used to check the output results. Figure 4.11 presents Li et al.'s flux results for their high altitude airship for an altitude of 18 km, noon (UTC +8) on June 21, 2012, and 120°E & 30°N.

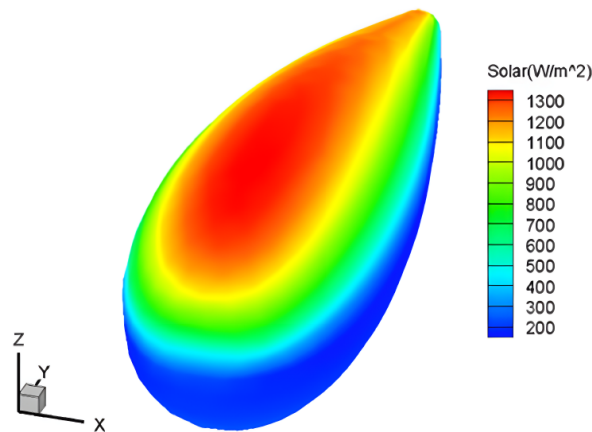


Figure 4.11: Li et al.'s flux distribution for the mentioned parameters [20]

For the above figure, the flux algorithm with the same parameters gives the following plot of net irradiance versus panel slope, i.e. the primary value that is variant across the given case study. This variation of the slope is given below in Figure 4.12, and has similar values. Recall that a slope of 0 degrees represents the panel facing the zenith, while 180 (or -180) implies the panel facing ground.

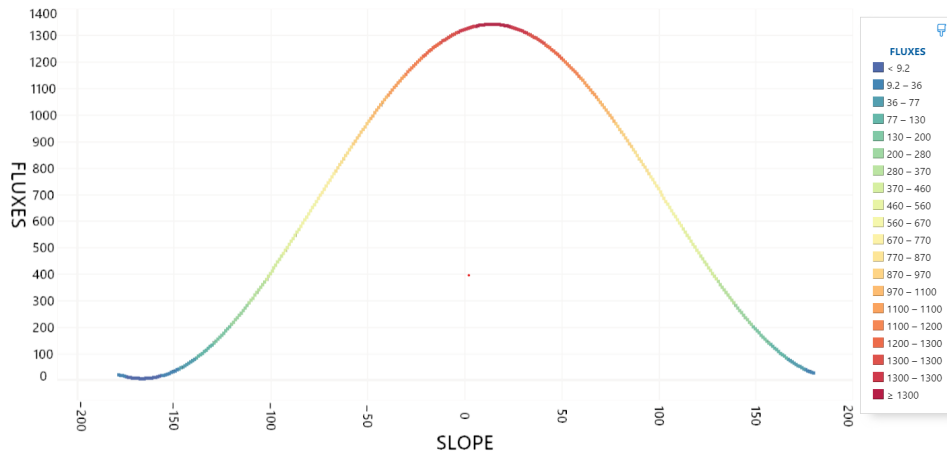


Figure 4.12: Plot of irradiance versus panel slope, with the slope in degrees on the x-axis and irradiance in W/m^2 on the y-axis

4.3. Tether Electrical Design

The main electrical task of the tether is to transmit the electrical power from the SBD to the ground. There are several factors that influence the design of this wire system, primarily the parameters that influence the losses within a power transmission cable. These are inductive, ohmic, and corona losses. These losses are listed and investigated in subsection 4.3.1. Afterwards, the internal design of the wire is shown in subsection 4.3.2.

4.3.1. Inefficiency types

Inductive losses

Inductive losses are caused by the inductance of the transmission wire. Although inductance is usually associated with components with coils, such as transformers and inductors, all electric systems will have some inductance. Inductance is the opposition to the change of current in an electric system and these losses are thus especially relevant in alternating current (AC) systems. Because the voltage alternates, often many times a second, the current will alternate as well. This causes a large rate of change in the current and thus induces inductive losses. A DC transmission cable would theoretically have zero inductive losses with a constant current and is thus used in sub-sea or long distance applications over AC transmission. Due to the mass-optimized nature of the wire, the inductive losses may be problematic, as they increase for thinner (and lighter) wires. As higher frequencies decrease the weight of transformers to alter the voltage, rectification of the AC signal is necessary as the inductive losses would completely negate any power sent through the wire at the frequencies these transformers operate [27].

Ohmic losses

Ohmic losses are the most basic of losses in electrical circuits. Every conductor has the inherent property of resistance which will cause losses proportional to the current flowing through the wire. As the power transmitted is both a function of the voltage and the current, high power applications often opt for a significantly higher voltage in order to reduce the current and thus the losses or necessary conductor material. Grid-scale power lines utilise voltages ranging from tens of kilovolts to over a megavolt for long distance, high power transmission lines¹⁰. Utilizing high voltages induces challenges in the insulation of the wires. Conventional insulation such as that of a simple lamp cord will not hold up against high voltage, the wire has to be specifically designed to resist the high electric field associated with these voltages.

Note that the ohmic losses scales up with an increase in resistance as well. With time, structural creep, chemical reactions, and microscale "chipping" of the material due to internal abrasion attribute to the

¹⁰<https://peaksstation.com/why-we-use-high-voltage-to-transmit-electrical-power/>

increase in resistance - and hence degradation of the tether's power-carrying capabilities.

For structural creep and deformation effects, the change in resistance is proportional to the change in cross-sectional area and length.

$$R = \frac{\rho * L}{A}$$

For a given amount of strain ϵ , the length L would increase by a factor $(1 + \epsilon)$. The tether diameter change Δd , which is proportional to the square root of the tether cross-sectional area A , can be found with the below equation, with ν being the tether's Poisson's ratio.

$$\Delta d = -d (1 - (1 + \epsilon)^{-\nu})$$

A similar effect of area reduction could be used to quantify the increase in ohmic losses due to chipping. However, for chemical reactions, the material's specific resistivity ρ would be affected.

Corona losses

The previously mentioned electric field is also what causes the corona losses in wires. Corona discharge is a phenomenon which happens in high voltage applications where the electric field (locally) exceeds the breakdown voltage of the air surrounding it. This causes the air to become conductive and a current to "leak". This corona discharge can be observed as a purple-ish hue or lightning resembling structure around charged conductors. These corona losses are especially significant in power transmission lines as the conductors are exposed to the air without any insulation. The losses can be reduced by reducing the intensity of the electrical field around the conductors. This is done by increasing the radius of the conductor and making sure that it is smooth, thus reducing the "sharpness" of the electric field. The distance between conductors can also be increased or insulation can be applied around the wires. Environmental factors also affect the actual breakdown voltage of the air, such as humidity or pressure. If the voltage remains under this limit there will be no corona discharge whatsoever.

Python model

The previously mentioned losses have been modelled in a python script. Combining the results gives an insight into the total losses compared to the design transmission power of 1 MW. Parameters such as the voltage and frequency were varied in order to investigate the effects. The voltage has an especially profound effect as this also affects the current, which is a big factor in the calculation of different losses.

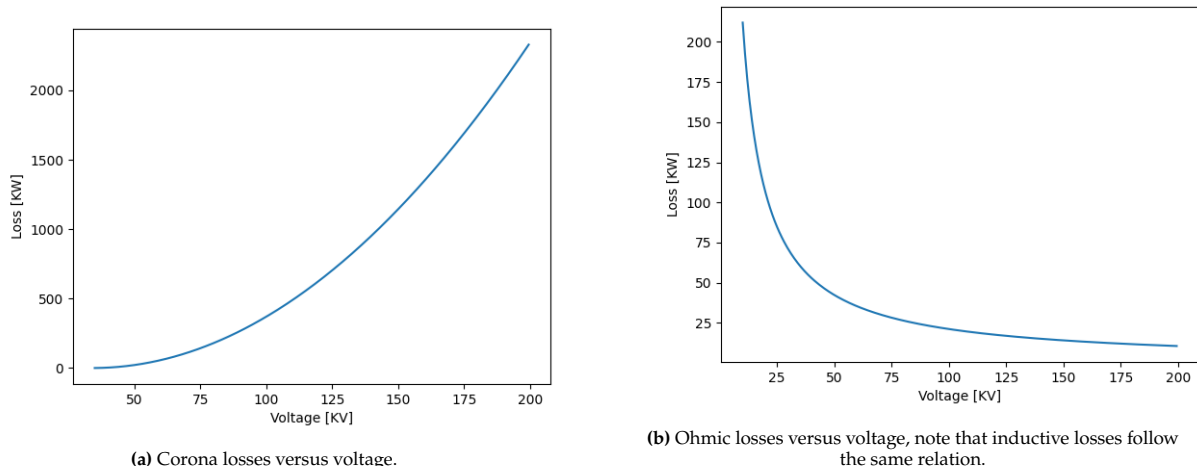


Figure 4.13: Graphs showing the effect of varying voltage on different loss types.

As can be seen in the figure above the effect of varying the voltage is quite significant. For the ohmic and inductive losses, a higher voltage is preferred as the losses are directly related to the (change of) current. For corona losses a conflict of interest is observed, as a higher voltage is desired for the other two loss types but the corona loss becomes incredibly large for voltages above the corona inception voltage, which is 34 kV for the estimated conditions. Summing the graphs for the three different losses an optimal voltage is obtained. The graph was realised for estimated conditions regarding wire diameter and frequency. These are subject to change but the general conclusions and shape of the graph are expected to stay the same.

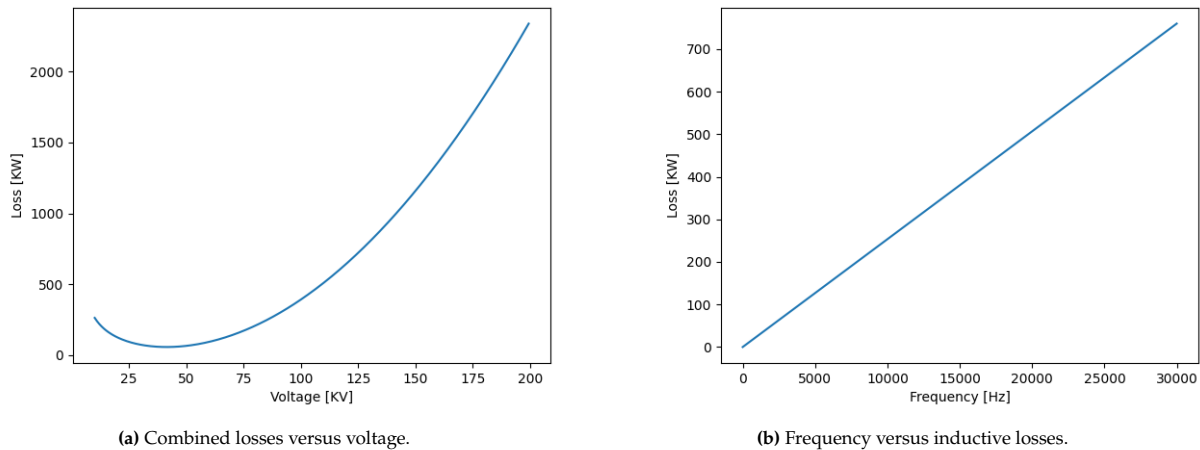


Figure 4.14: Graphs showing the total losses and effects of the varying frequency.

The effect of frequency on the inductive losses follows a linear relationship. For grid frequencies (50-60 Hz) losses are low, on the order of single kilowatts. Higher frequency transformers are lighter though, and these operate in the tens of kilohertz range, creating significant inefficiencies. It is therefore desirable to rectify the transformed signal to DC in order to completely negate this loss. It must also be noted that the corona loss formula contains the frequency as well, so this is an additional reason to use direct current.

It can be noted that the smallest loss is obtained just above the corona inception voltage, around 35 kV. Losses at this voltage amount to 60 kW, or 6% of the total power transmitted. A higher voltage will rapidly decrease the efficiency as the corona losses start growing swiftly after reaching the threshold. Although an efficiency of 94% is good compared to wireless power beaming, the relatively low voltage causes a need for a large conductor. With a current density of 4 A per square millimetre, the required area is 7 mm². Calculating the necessary tether weight and cross section using this weight a total tether mass of 2200 kg is obtained. If the voltage were to be increased this weight can be brought down tremendously as every kilogram of aluminium has to be supported by the fibre element of the tether.

4.3.2. Internal Wire Design

As corona discharge is the limiting factor for the maximum voltage in the tether design ways must be investigated to see if it can be mitigated. Since the discharge is caused by the high electric field associated with high voltages in conductors. A type of conductor which attempts to eliminate external electric/magnetic fields is the so-called coaxial cable. This cable consists of a conductive core with insulation around it, around which an outer conductive

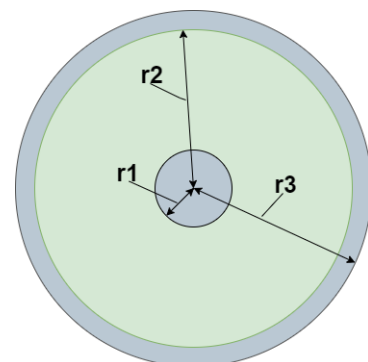


Figure 4.15: Cross section of the tether.

sheath is wrapped. This sheath is neutrally charged and thus the electric fields would only exist between the sheath and the core under ideal conditions. This would reduce the electric field on the outside of the cable below the corona inception voltage, even under non-ideal conditions. This would increase the allowed voltage in accordance with the insulative properties of the dielectric between the core and the sheath.

UHMWPE has favourable electrical properties for this particular application, as it can resist an electric field of 900 kV cm^{-1} [28]. Calculating the necessary radii of the insulation, core and sheath an estimate can be made of the allowed voltage across the conductors, taking into account a safety margin of 2. For initial estimates of the thickness of the cable, an allowed voltage of 130 kV is obtained. This reduces the necessary aluminium due to the lower current involved thus changing the geometry of the cable, leading to a different allowed voltage. This iterative loop must be performed with the finalized values.

The cross section of the tether is shown in 4.15. The core and sheath represent the aluminium conductors and are the same area in the final design as the DC current they carry are equal but opposite. The green area represents the UHMWPE core carrying the structural loads.

The total losses using a definitive voltage of 130 kV are calculated to be 1.4% due to ohmic losses. This voltage was chosen due to it being an intermediate voltage similar to the 110-150 kV range of some power transmission lines. In order to use this voltage with a safety factor of two an insulator thickness of 0.289 cm is needed. With this voltage the conductor surface area is 1.9 mm^2 per single wire, with the total mass for the positive and negative terminals being 187 kg.

4.3.3. Power transformation

The voltage produced by the solar cell strings is relatively low, especially compared to the voltages used in power transmission. Stepping up the voltage will decrease the losses as described in subsection 4.3.1. Stepping up voltages is usually done by transformers which require alternating current (AC), and solar panels produce direct current (DC). Using semi-conductors this current can rather trivially be turned into a pulsed signal which is suitable for use in transformers. Conventional transformers operate at grid-frequency: 50 Hz. This is appropriate for most applications, especially since weight is not a big factor for ground based power stations. The size of a transformer decreases with an increase in frequency, and therefore higher frequency systems will have less bulky, mass-intensive transformers[27].

High frequency transformers can have mass power densities of up to 20 W per gram and a volumetric power density of 50 W/cm^3 for the optimal frequency [27]. This is with small core geometry and ideal conditions though. Since an increase in core size will increase the heat generation more than the surface area to dissipate heat the numbers are halved to account for more inefficient mass and volume usage due to the need for cooling. With these figures the following table with transformer parameters is generated:

Table 4.4: Transformer characteristics

Power	1000000 W
Mass	100 kg
Volume	0.04 m^3

4.3.4. Switch Mode Power Supply

Turning the DC current into a high frequency signal, transforming the voltage and then rectifying the signal back to DC is a proven technology utilized in so called switch mode power supplies (SMPS). These power supplies have efficiencies higher than 90%, which is for systems with an additional step to rectify mains voltage to DC for use in household appliances [29]. In 4.16 the 4 main stages are represented in a block diagram. The first stage is the chopper which uses a type of semiconductor transistor which can handle high currents with a low resistance when conducting that has low losses during switching

between ON/OFF states. This "chopping" turns the signal into a signal resembling an AC wave. This is fed into the second stage, the transformer. Here the voltage gets multiplied in accordance with the turns ratio of the transformer coils. The transformer and chopper circuit are matched to each other as close as possible in order to reduce inductive losses due to high frequency components in the square wave. After the transformer, a rectifier will turn the alternating current signal into a direct current using diodes. This wave is still irregular though, and filtering is needed in order to make it a steady signal again. Using an assortment of components such as capacitors and inductors the signal is smoothed and harmonic frequencies are filtered out of the rectified signal.

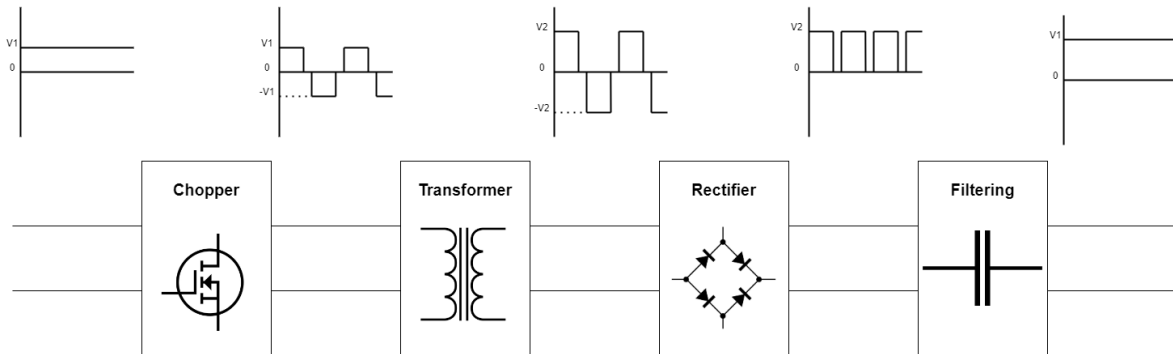


Figure 4.16: A high level overview of the stages of a SMPS.

4.4. Tether Structural Design

Next to the electrical function of the tether, it must also be strong enough to sustain the applied loads and keep the balloon in an acceptable horizontal and vertical range. To design for these demands, a dynamic model was set up which is used to simulate the equilibrium position of the tether under certain wind conditions. The worst case wind profile used as an input for this model is generated in subsection 4.4.1. Next up, the model is described in subsection 4.4.2. This leads to the generation of results and optimization in subsection 4.4.3. Lastly, the model is verified and validated in subsection 4.4.4.

4.4.1. Wind Profile

Due to the high altitude, it is not possible to consider wind to be constant along the tether. To use a realistic wind profile to act on the tether model, interpolation is used of data provided by Zhang et al[30]. This data has been used to get the shape of the wind profile and this shape is then scaled to fit the SBD-POS-09 requirement which states that the SBD shall be able to endure trajectory drifts due to stratospheric winds up to 30 m/s. This results in the wind profile as shown in Figure 4.17. Examining this wind profile with the direction of the wind fully to one side is seen as worst case scenario. If it can comply with this wind profile, it will also comply with the requirement regarding profiles with less wind speed or other distributions and orientations. In the same figure, the dynamic pressure q is also plotted. This is calculated using $q = \frac{1}{2}\rho V^2$. As can be observed, dynamic pressure closely follows the shape of the wind profile, however it drops faster at altitudes above 10 km due to a drop in density, which is calculated using the international standard atmosphere (ISA) model.

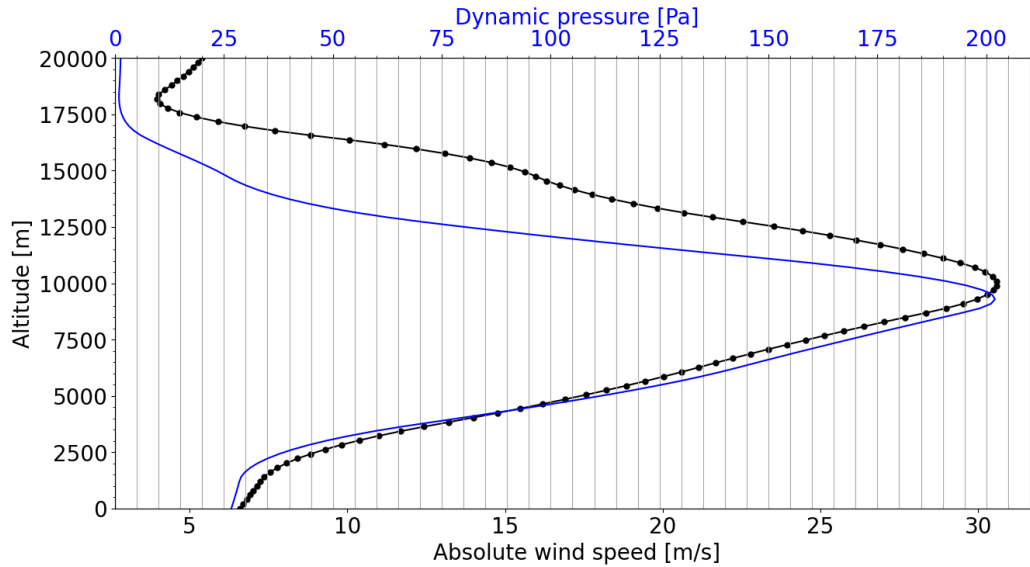


Figure 4.17: Profile of the wind speed versus altitude and accompanying dynamic pressure

4.4.2. Model Description

A simulation for the behaviour of the tether was set up in a similar fashion to the model described by Akita [31], where the tether is modelled as a number of nodes connected in a string by springs as shown in Figure 4.18. It has been decided after a number of simulations not to use tandem balloons, since these make the system as a whole more complex, both for maintenance and (de)commissioning, and result in much bigger horizontal displacement at the gain of only a slightly lighter tether. This means the tether is simpler and each node has two tension forces from two springs, a weight and a pressure drag split in a horizontal and vertical component. By applying a load at the top of the tether and a distributed load from the weight and drag of the tether and by fixing the bottom point, the movement of each node over time can be simulated using the spring equations in both dimensions, as listed in Equation 4.7 and Equation 4.8 [31].

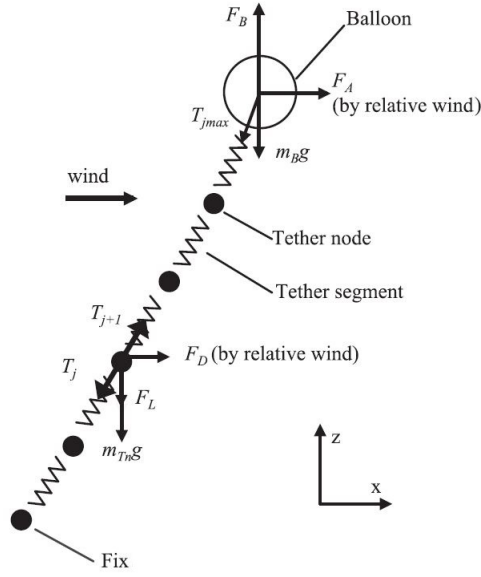


Figure 4.18: Sketch of how the tether was simulated [31]

$$m_j \frac{d^2 x^j}{dt^2} = T_x^{j+1} - T_x^j + F_D^j - C \frac{dx^j}{dt} \quad (4.7)$$

$$m_j \frac{d^2 z^j}{dt^2} = T_z^{j+1} - T_z^j + F_L^j - m_j g - C \frac{dz^j}{dt} \quad (4.8)$$

In these equations, j is the node index and m_j is the node mass, which equals the mass of the tether section between two nodes such that the springs are assumed massless. T is the tension in the springs above and below each individual node, in either x or z direction. The friction drag component of the drag on the tether is neglected, hence the wind velocity perpendicular to the local tether orientation is used to calculate the pressure drag of which F_D and F_L are its horizontal and vertical components. The drag coefficient used to calculate the pressure drag is 0.3 for turbulent cylinders [32] and the surface area is the frontal surface area (twice the radius times the length of a segment in between nodes). The damping coefficient C can be included because only the equilibrium position is of interest. It is chosen arbitrarily such that the simulation converges to a steady-state solution as fast as possible.

Contrary to Akita where the balloon mass was included in the model, the balloon was replaced with the lift and drag forces it generates. The lift is assumed to be kept at a constant level with the use of ballonets and the drag is calculated and updated with the local wind speed and density. The ballonets keep the volume of the balloon constant, meaning the drag coefficient and surface remain constant as well. For these parameters, a drag coefficient C_D of 0.112 based on the aerodynamic analysis as explained in subsection 4.5.3 and a surface area of $S_{balloon} = 1225 \text{ m}^2$ were used.

The simulation starts with the vertical tether without initial tension. It numerically integrates the movement of all nodes due to the applied forces while the lift force from the balloon puts all springs in tension and the tether moves to the equilibrium position. The lift force itself is set equal to the weight of the tether plus a chosen value for the excess lift. The excess lift is defined as the part of the lift force applied to the tether on top of the tether weight. With zero excess lift, the balloon is only just able to carry the tether.

A safety factor of 4 will be used for the tether strength [33]. As UHMWPE has an ultimate strength of 1 GPa, the maximum allowable stress will be 250 MPa. This is slightly higher than the conventional limit of 20% ultimate strength for creep of polymer tendons [34]. Since the part of the tether under the

largest load will be at a low temperature, where creep is less of an issue, and considering developments in creep resistant polymers in the coming 5 years, 25% is deemed valid.

The surface area of the UHMWPE is updated throughout the simulation to ensure that the maximum stress is 250 MPa. This changes the weight and therefore the required lift, which is also updated throughout the simulation. This means that the inputs for the simulation are the starting altitude, excess lift and initial guess for tether radius. The outputs are as follows:

- Tether weight
- Tether radius
- Equilibrium position of the balloon and tether
- Total lift applied on the tether

The simulation is animated and the final result of displacement and internal stress is plotted. An example of these plots is shown in Figure 4.19. This figure shows the final steady state solution to the wind profile for four different altitudes with different amounts of excess lifts.

4.4.3. Results Generation of Tether Simulation

A good combination of starting altitude, excess lift and tether radius was investigated to obtain a final displaced altitude of at least 15 km, as the altitude range of 15 to 45 km is specified by top level requirement SBD-POS-08. Additionally, the weight of the tether and size of the balloon (resulting from the required lift) should be minimized.

Because of large run times, it has been chosen to evaluate a number of altitudes with a 1 km interval, with excess lifts at an interval of 1000 N. The altitudes that are considered are 17, 18, 19 and 20 kilometres. 16 km and lower is not considered because the required loads to stay above 15 km result in an extremely heavy tether. Higher than 20 km is disregarded because the volume of the balloon would become too high at these altitudes.

Data for five excess lift values for 18 km altitude are shown in Table 4.5. The best value for this altitude would be 6000 N excess lift. Although 5000 N also seems viable from the table, the horizontal displacement is much more and the simulation did not end at a stationary position, indicating that the balloon moves very slowly into lower altitudes with increasing wind speeds. This would result in a non-acceptable design. This process has also been done for the other altitudes, for which the best values are shown in the same table. These best values are plotted in Figure 4.19.

Table 4.5: Simulation results for different excess lift values for 18 km and the excess lift for all considered altitudes giving the best results

Input parameters		Results				
Altitude [km]	Excess Lift [N]	Final altitude [km]	Horizontal displacement [km]	Tether radius [mm]	Tether weight [kN]	Final applied lift value [kN]
18	4000	9.27	14.93	7.69	32.43	36.43
18	5000	15.97	6.85	5.26	15.76	20.76
18	6000	16.78	5.02	5.59	17.66	23.66
18	7000	17.02	4.44	5.92	19.67	26.67
18	8000	17.17	4.04	6.24	21.69	29.69
17	8000	16.27	3.78	5.90	18.43	26.43
18	6000	16.78	5.02	5.59	17.66	23.76
19	4000	17.33	5.18	5.18	16.18	20.18
20	2000	16.91	7.69	4.60	13.72	15.72

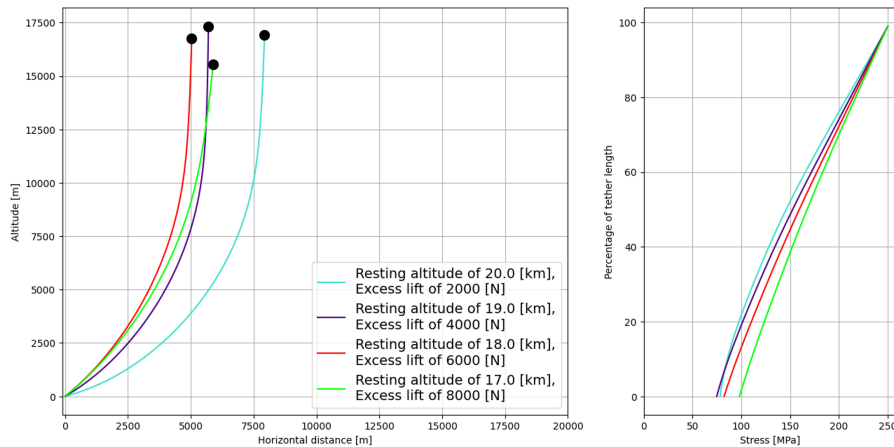


Figure 4.19: Best solutions for altitudes. The left figure shows the final steady state converged solution. The right figure shows the stress in the tether.

In the choice of an optimum combination of variables, a few results have to be balanced against each other. First of all, it is required that the final altitude is above 15 km for this worst case wind profile. Secondly, the radius of the wire should always be at least 3.7 mm to have at least 2.89 mm insulation between the conducting parts, as explained in subsection 4.3.2. It can be seen that the radius of the wire for all altitudes is sufficient enough from an insulator point of view, hence this consideration is not limiting.

Furthermore, the final applied lift should be minimized, as it can be related directly to the volume of the hydrogen needed in the balloon. Larger volumes require a larger structure, which significantly increases the weight. Hence, the final lift is not driving for the design altitude. The second consideration regarding the volume is the design (or starting) altitude. Because of the decrease in density with increasing altitude, the hydrogen expands, hence also requiring a larger volume. Hence, a balance between the final applied lift and the design altitude has to be made.

Regarding this, the influence of altitude on the solar panel output has also been investigated. From subsection 4.2.4, it was found that the decrease in solar flux over a decrease in height was in the order of 0.4% per km at 20 km. Hence, this consideration was also not decisive. The horizontal displacement of the balloon in the equilibrium position is the largest difference between the results for different starting altitudes. As this is the worst case horizontal displacement, the airspace that needs to be cleared for one SBD is dependent on this value. Hence, this value should be kept in a reasonable range.

Considering all points made previously, it was decided that an 18 km design altitude gave the best overall performance, mainly regarding the lower volume required when compared to 20 km and the lower vertical displacement. This altitude is subsequently fixed and used for further sizing and design iterations.

Further design should look into more detailed optimization of design altitude and excess lift to find a potentially lighter, smaller and cheaper design.

4.4.4. Model Verification and Validation

To ensure accuracy of the results of the simulation, the model has to be verified to ensure it outputs what is expected of it and subsequently validated to reflect the physical problem.

Verification

The model to simulate the dynamic response to wind needs to be verified and validated. Verification of the code has been done in multiple ways. A lot of unit tests have been performed by printing values and visualizing responses. Also manual checks have been done to check if equations and values were used correctly. To check if the model responded in a natural way, not only the final state has been generated, but also the response over time was simulated. Also a convergence test has been performed with different amount of nodes and time steps. It was observed that only increasing the amount of nodes resulted in an unstable system. But decreasing it to a too low amount resulted in a non-convergent solution. This behaviour resembles the "Courant–Friedrichs–Lewy stability condition"¹¹ for numerical advection. In essence, the numerical domain of dependence of any point in space and time must include the analytical domain, where the initial conditions has an effect on the exact value of the solution at that point, to ensure the scheme can form the solution.

To thus compare different solutions, the number of nodes and time step should be scaled accordingly to each other. Doubling the nodes means halving the time step. To compare solutions, an amount of 50, 100, 150, 200 and 1000 nodes have been run. 1000 nodes were primarily run to get an "analytic solution" and to get an estimate on the error. All of these conclusions are visualized in Figure 4.20. As mentioned before, this is visualized for 50, 100, 150, 200 and 1000 nodes, but has been zoomed in on the top balloon, and the strain curve at 50 % of the tether.

It can be observed that increasing the number of nodes with a set amount moves the solution gradually closer to the solution with a very high number of nodes, indicating a reduction in error when simulating more nodes. This indicates some level of consistency, but not fully. This has likely to do with the sensitivity of the model. There are many variables connected that slightly change the stress, affecting radius, drag on the wire, and final position, and the iterative procedure may amplify any perturbations.

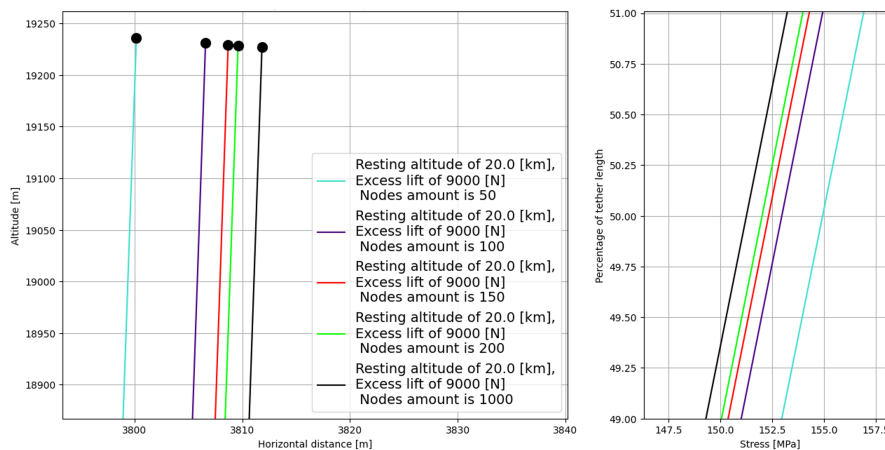


Figure 4.20: Zoomed in versions of the steady state solutions for 50, 100, 150, 200 and 1000 nodes. The left figure shows the final steady state converged solution. The right figure shows the stress in the tether.

Besides the final response also the radius over time is plotted in Figure 4.21, with the amount of iterations on the x-axis. It can be observed that for all the different amount of nodes all converged to a final solution for the radius. They all converge to a similar value. This is however done in a different time scale. This is due to the fact that doubling the number of nodes results in halving the time step. Resulting in more steps to be computed to end up at the steady state solution.

¹¹CFD Online. Courant–Friedrichs–Lewy condition. <https://www.cfd-online.com/Wiki/Courant-Friedrichs-Lewy>

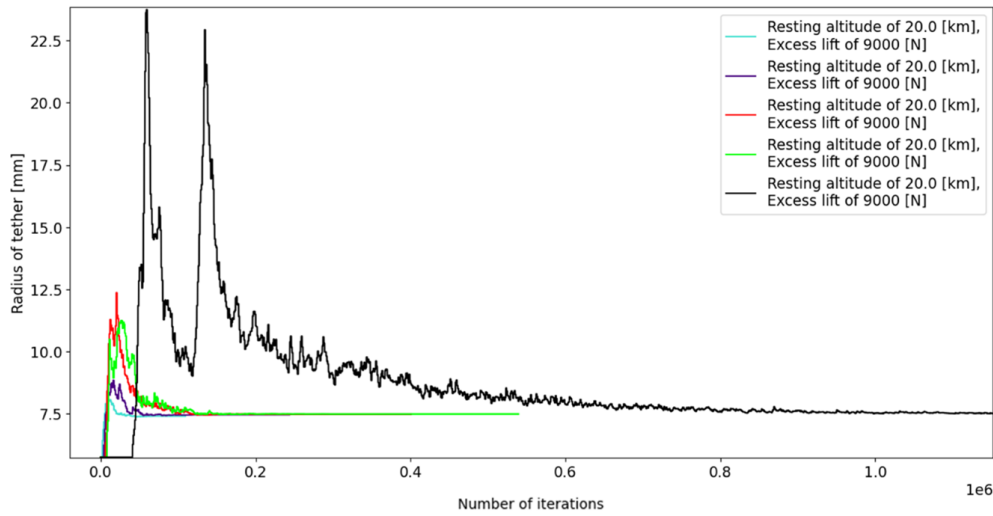


Figure 4.21: Radius update over iterations amount for 50, 100, 150, 200 and 1000 nodes

Validation

Besides verification, also validation has to be done. There is however no data similar enough to make a good comparison for validation. It is thus required to generate data for validation. This can be done with a small scale real life test. This should be done as early as possible in the next design stages. One example would be to lift a tethered balloon to 2 kilometres altitude without any power generation, to use that data as input for validation. This can be done as cheaply as possible, but still getting realistic data. Sensors used would measure stress in the tether, altitude and position, temperature and wind-speed at balloon altitude and wind speed and air density measurements along the tether.

4.5. Aerostatics & Aerodynamics

This section aims to cover the aerostatic and aerodynamic characteristics of the SBD. It starts by investigating the lifting capabilities in subsection 4.5.1. Afterwards, the functioning of the ballonets, which assist in the commissioning and decommissioning, is explained in subsection 4.5.2. Finally, the drag coefficient of the SBD is approximated in subsection 4.5.3.

4.5.1. Lifting power

The lifting power has been calculated using Equation 4.9 [35]. It takes into account the differential pressure and temperature, using the ideal gas equation.

$$L(H) = g \cdot V(H) \cdot \left(\rho_{air}(H) - \frac{p_{gas}(H) + \Delta p_{gas}}{R_{gas} \cdot (T_{air} \pm \Delta T_{gas})} \right) \quad (4.9)$$

Where g is the gravitational constant, $V(H)$ is the volume of the balloon at altitude, ρ_{gas} is the density of air at altitude, $p_{gas}(H) + \Delta p_{gas}$ is the pressure at a certain altitude plus the differential pressure of the balloon, R_{gas} is the specific gas constant, $T_{air} \pm \Delta T_{gas}$ is the outside temperature and the differential temperature of the gas inside the balloon. The differential pressure is set to twice the dynamic pressure with a windspeed of 30 m/s with the density of the design altitude, because the shape of the balloon should not deform due to the wind experienced. If this pressure is too low, deformation will occur of the balloon risking the mission to fail.

From Equation 4.9 the volume of the balloon can be calculated using the mass of the balloon and the

excess lift needed to stay afloat and have the designed for horizontal displacement and altitude, which has been described in section 4.4. Figure 4.22 shows the volume increase over its altitude. The ambient air pressure decreases the higher the balloon will go, so the pressure on the balloon will decrease and would make the hydrogen expand to keep a constant differential pressure. The differential temperature is set to be 40 degrees Kelvin and the mass used for this plot is the mass from the final budget of 5125 kg.

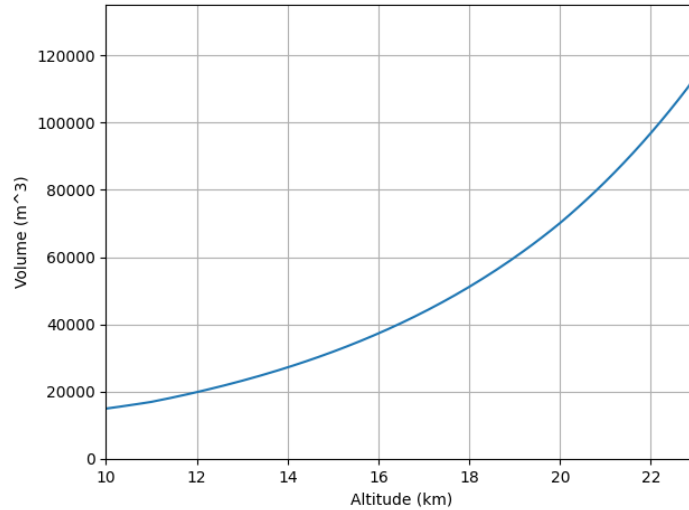


Figure 4.22: Differing volume of the balloon for changes in altitude

The balloon will differ in temperature due to the cycling of the solar irradiance on the balloon[36]. This results in a volume due to the isobaric expansion of the balloon and therefore an increase in lift. The pressure inside will stay the same, and for this to happen the volume would need to increase because the molecules have more energy.

The solar panels will endure the highest temperatures since it is right on top of the balloon, which is discussed in subsection 4.1.3. Some of that heat flow will reach the balloon and the area not covered by the solar panels will still heat up the outer skin and therefore the hydrogen itself. Figure 4.23 shows the effect of the differential temperature on the lift. A 100 Kelvin positive differential temperature might be very high, but it might reach between 40 and 60 Kelvin, which is around 1 kN of extra lift [36]. To realise the isobaric expansion the ballonets are implemented, which is described in the next subsection.

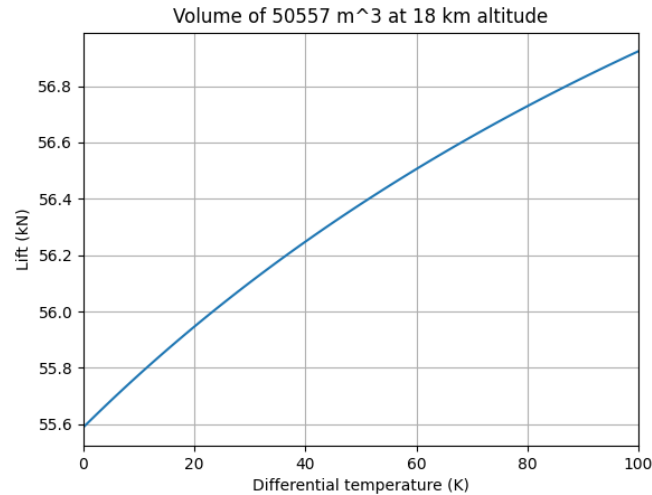


Figure 4.23: Lifting capabilities of the balloon varying over positive differential temperature from its ambient temperature

The system also has been validated through the input of the numbers from multiple papers [35][36]. The numbers from those two papers closely resembled the program made to calculate the lifting force and its volume. Their final values were within 5 % of the program made, this is due to the variance of wind and thermal effects of the models. Where the papers included a differential pressure over time and their temperatures did not conform to the ISA temperatures. But the final values are deemed to be in the same ballpark and therefore validated. However further tests are needed to fully validate the system, and to fully optimise the lifting capabilities of the balloon at higher altitudes and varying atmospheres.

4.5.2. Ballonets

Without the use of a ballonet, the balloon will deform immensely the higher it goes. The ballonets are able to regulate the inside pressure and therefore the shape of the balloon. Keeping a close-to-constant form is essential for the structure, otherwise, the loads might rise above the designed level. That is the reason must include a ballonet, which can be seen in Figure 4.24.

Ballonets will thus mainly be used to account for the density changes of the hydrogen used over increasing altitude. The volume of the hydrogen will approximately increase 10-fold at a height of 18 km compared to the volume on the ground. This will lead to a size of 90.1 % of the total volume of the balloon for the ballonets on the ground. This will be filled up with ambient air and have the same differential pressure as the hydrogen, which has been discussed in the previous subsection. There will be a thin sheet of latex since it will not have to carry any loads because the pressures are the same and just needs to divide the two gasses.

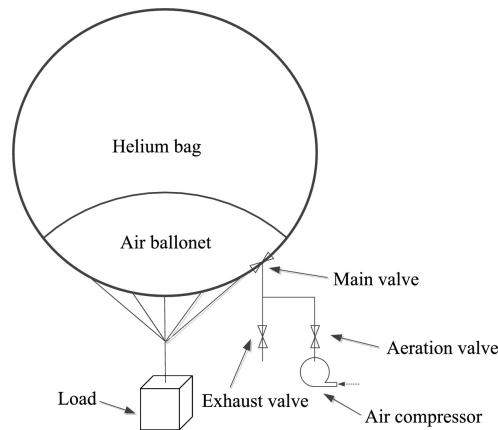


Figure 4.24: Sketch of the altitude adjustment mechanism of the balloon [37].

The ballonets could also be used for altitude control. More ambient air could be pumped in and increase the weight of the balloon, which leads to a new equilibrium. This would be better than dumping some of the hydrogen, since the hydrogen is a scarcity in the stratosphere. Figure 4.25 displays the required volume percentage of the ballonets compared to the total volume for different design altitudes, when the balloon is located on ground. At design altitude, the ballonets will be empty in ideal conditions, but to introduce a bit of margin and to compensate for thermal effects, as explained in subsection 4.5.1, the ballonets will still be filled with a bit of air when operational.

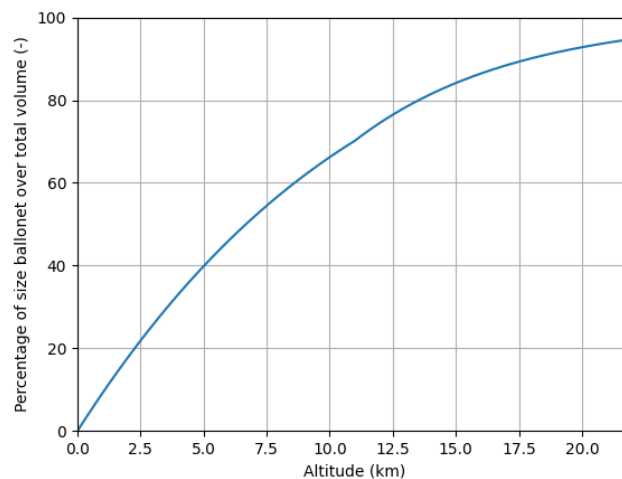


Figure 4.25: Sizing of the ballonet for a specific design altitude

4.5.3. Aerodynamic Drag

The aerodynamic drag of the balloon is important in describing the drift experienced due to wind. But with its unique shape - described as an oblate spheroid - evaluating the drag coefficient of the vehicle is difficult to compute analytically for the length scales and flow velocities at hand. In addition, most research for ellipsoidal particles deal with low Reynolds number ($Re < 10^4$), thus making their provided drag coefficients incomparable. The Reynolds number ($Re = \rho VL/\mu$) can be used to non-dimensionally assess the flow regime for this, and its variation can be seen in Figure 4.26. The graph indicates that for the selected SBD parameters and operating altitudes, $Re \sim O(10^6) - O(10^7)$, which is uncommon to find

aerodynamic characteristics for such a shape and low speeds.

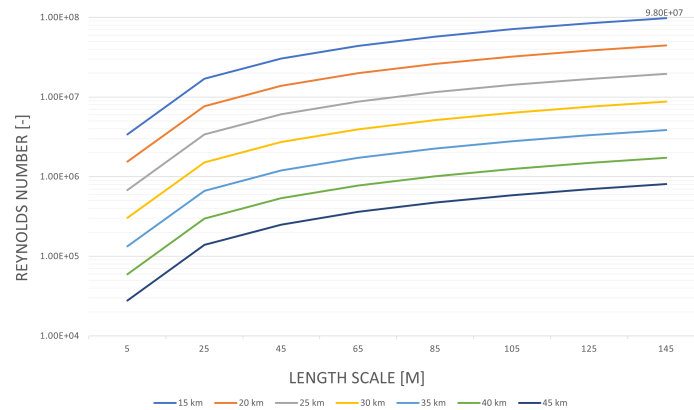


Figure 4.26: Variation of Reynolds number with length scale, at different altitudes and at 50 m s^{-1}

Thus, it was decided to numerically compute the drag coefficient C_D of the oblate spheroid, of 1/4 slenderness, using 3rd party Computational Fluid Dynamics (CFD) software. However, some key assumptions & simplifications were made in the analysis and are listed below.

- A small change in scaling, due to sizing iterations, has a negligible effect on the drag coefficient, due to remaining in the same Reynolds number order.
- Geometric elements protruding from the balloon are not considered
- The flow is incompressible throughout the domain, as the expected velocities are less than Mach 0.3
- The state variables, and thus drag values, are taken for steady aerodynamic conditions.
- The boundary layer thickness can be described by flat plate skin friction using Blasius turbulent and laminar solutions [38].
- An infinite mass "wind-tunnel" simulation resembles the steady-state finite mass model
- Small changes in the angle of attack result in the same C_D
- The use of a symmetry boundary condition is sufficient to reduce computational complexity and chances of running over software license constraints

Simulation Domain and Geometry

A solid model was created in CAD to give Figure 4.27, which is an ellipsoid of 4:1 slenderness ratio rotated about its axis of polar symmetry. An enclosure was then created around the body in Figure 4.28, with a depth of 60 000 mm (not shown in the figure), to act as the fluid domain. However, as per the final assumption, the computational domain was sliced in half in favour of a symmetry boundary condition.

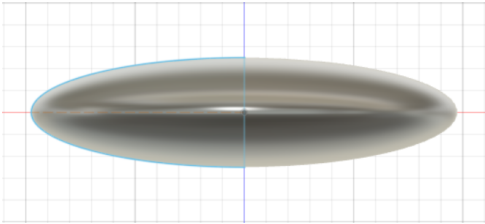


Figure 4.27: CAD model used for CFD analysis

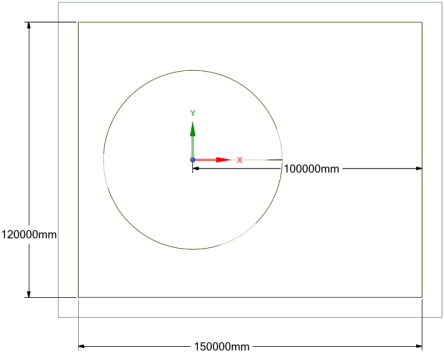


Figure 4.28: Enclosure geometry used for creating fluid domain

The boundary conditions used can be seen in Figure 4.29. The yellow colour represents the symmetry condition, blue for the velocity inlet, red for a pressure outlet, and white for walls (non-slip).

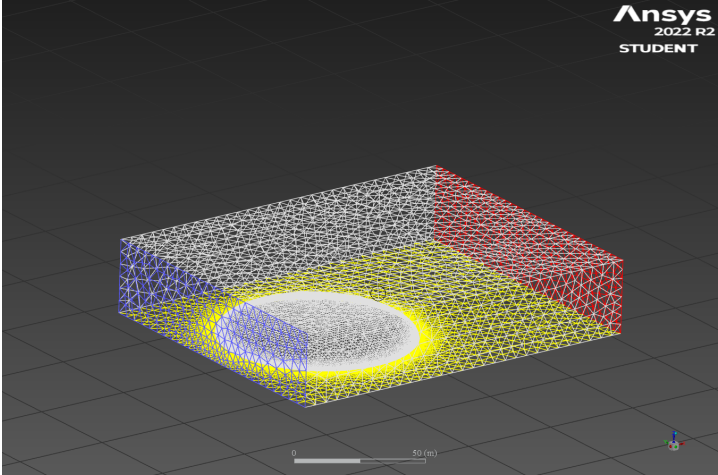


Figure 4.29: Transparent view of domain with colours indicating different boundary conditions

Meshing

The next important step is meshing the fluid domain, notably in the vicinity of the spheroid. An unstructured tetrahedral mesh with a based element edge length of 5 m was created, with 4 m mapped for the inlet and outlet faces. The spheroid’s face has a custom edge length of 1.85 m to better capture its geometric curvature and possible points of separation. These characteristics may be visualised in Figure 4.30

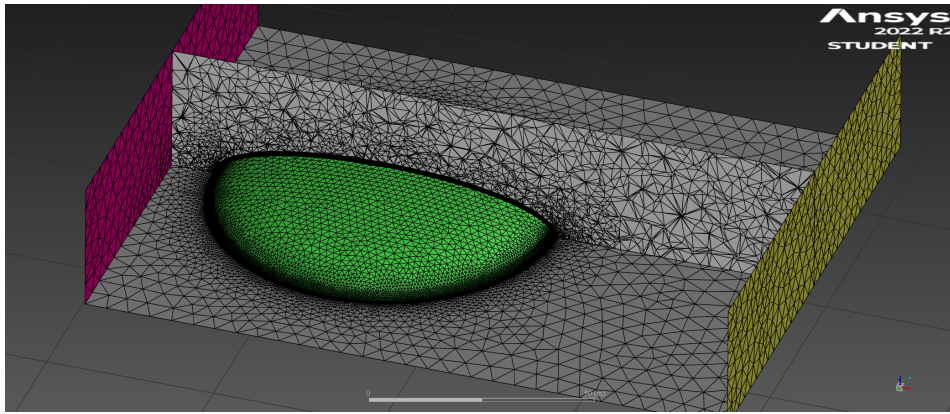


Figure 4.30: Isometric visualisation of the mesh used. A visual cutting plane has been added for section detail

Note that this base mesh is not effective at capturing the boundary layer, leading to the need for inflation layers around the object of interest. Using Schlichting solutions [39] to calculate the initial cell height from Reynolds Number, frictional coefficients, stresses, and velocities - and for a target y^+ of 30 and altitude of 18 km - a first layer height of 1.85 cm was attained. Using Blasius, a boundary layer thickness δ_{99} of 1.03 m was estimated with a growth ratio of 1.07. Given limited mesh cells due to licensing, only 23 layers were taken for inflation, leading to a final layer thickness of 8.74 cm. The inflation layers may be seen in Figure 4.31.

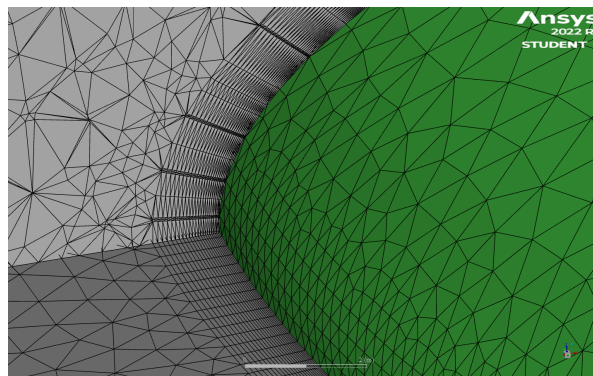


Figure 4.31: Magnified view of the same mesh, with focus on the boundary layer inflation mesh

Simulation Parameters

The simulation was performed in Ansys FLUENT 2022R2¹², as it provides a very systematic and streamlined approach for this application compared to the other considered option of OpenFOAM [40]. FLUENT can additionally be used for easy post-processing of data and directly attaining drag coefficient metrics as the simulation runs to check for convergence of the value. The setup used for FLUENT is listed below.

- Coupled and implicit PISO-SIMPLE solver (pressure-based)
- Realisable $k - \epsilon$ RANS turbulence, for high-Re applications and near-wall resolution
- Non-slip walls with zero roughness
- Velocity inlet of constant 30 m/s
- Zero total pressure outlet

¹²"Ansys Fluent: Fluid Simulation Software". Ansys. <https://www.ansys.com/products/fluids/ansys-fluent>

- Convergence check of 10^{-4} for all monitored residuals
- Reference area set to 1 m^2

Results

After about 140 iterations, the solution reaches its steady-state solution. The static pressure plots of select views are presented in Figure 4.32, and these may be used to indicate points of separation and reverse flow, as in the trailing edge. However, there are no other points of flow separation over the rest of the spheroid geometry that attributes to increased drag.

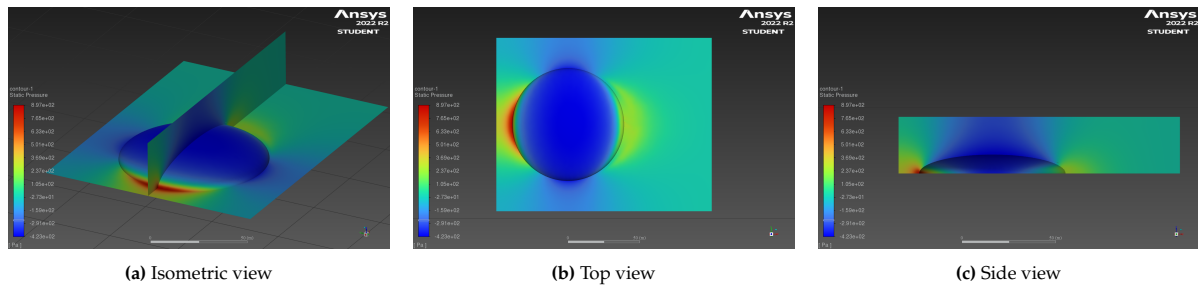


Figure 4.32: Static pressure plots over the simulation domain

The drag of the spheroid element can be found by integrating the pressure profile over the body's area and taking the x-axis projection of the resulting force vector. Taking this surface integral leads to a pressure drag of 27 500 N and viscous drag of 10 200 N, totalling to 37 700 N; and for a reference area of 1 m^2 , a *non-normalised* drag coefficient of 68.45827 for half the spheroid (due to the symmetry assumption). To the *non-normalised* drag coefficient of the entire sphere, this value can be multiplied by two. Lastly, to get the non-dimensional drag coefficient of the body, the value should be divided by the object area perpendicular to the incoming flow which is generally used as the reference area in aerodynamics applications. This can be found from the CAD model to be 1152 m^2 , and the C_D can be finally found to be 0.112.

Addendum on Slip Boundaries

Note that due to the size of the flow domain, the velocity plot of the converged solution still illustrated reverse flows and numerical dissipation errors at the walls with the no-slip conditions. In addition, the walls do not have a boundary layer in reality, hence making the slip condition applicable. Thus, in the next iteration of the aerodynamic numerical simulation, the non-slip walls were changed to slip walls, i.e. enforcing zero wall shear stresses in X, Y, and Z directions. Intuitively, this change would lead to a lower drag acting on the spheroid. A comparison of the velocity profiles of no-slip and slip boundaries are given in Figure 4.33.

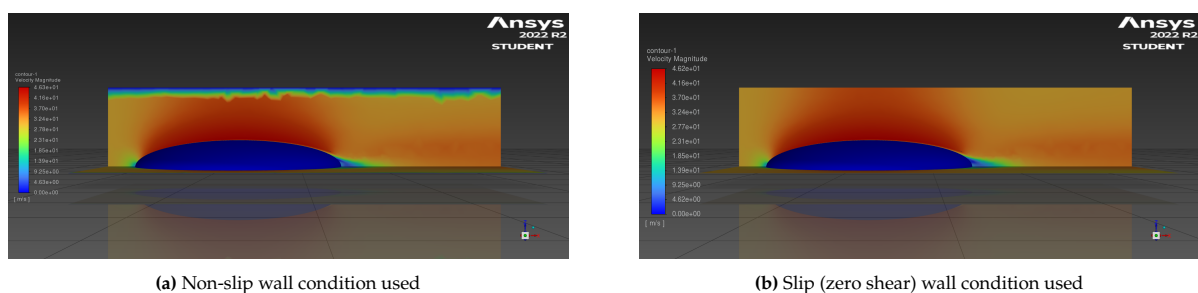


Figure 4.33: Velocity contour plot comparison

Despite the seemingly distinct change in velocity profile around the walls. The evaluated C_D was only

marginally lower than the no-slip condition, at 0.108 or 4% lower.

Verification

The numerical algorithms and turbulence models used in Ansys FLUENT have already been used to a great extent in industry and research applications, hence making verification of program functionality redundant. Nevertheless convergence testing may still be done to check the resolution of the mesh. Note due to limited time and mesh resolution limits only boundary layer resolution was increased, i.e. the number of layers within the inflation regime. This is essential in providing information on viscous drag and its contribution to the C_D . The simulation was rerun for 30 inflation layers, instead of 23, with the drag coefficient only marginally changing by +0.05% more. With this metric, the drag coefficient can at least be said to be consistent in its calculation.

Validation

While oblate spheroid drag coefficient models from simulations and empirical analyses do not exist at this scale of Reynolds numbers, comparisons may still be made with papers to at least have an idea of the range of drag coefficients and how it develops for increasing orders of magnitudes of Re . With the models presented in Maramizonouz and Nadimi [41], ellipsoids with flatness & elongation factors and flow regimes can be used. For $Re \sim O(10^5)$, Bagheri and Bonnadonna's model [42] proposes an ellipsoidal model that is most resemblant of the case being studied here. Their semi-empirical model does display a good correlation with the CFD model, with their results seen in Figure 4.34.

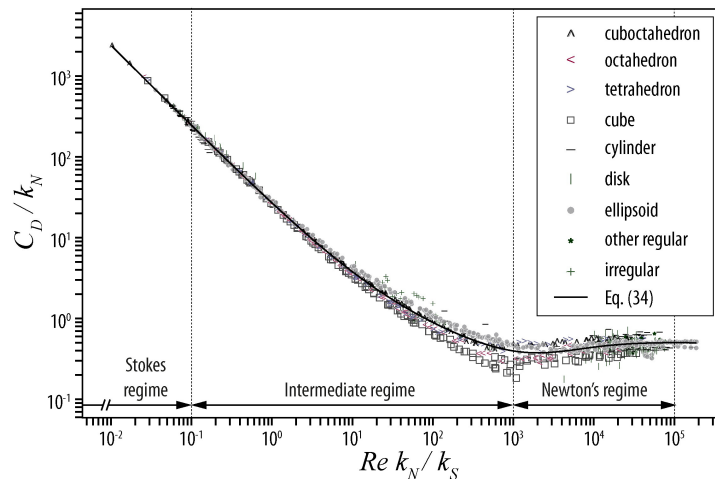


Figure 4.34: Dependency of normalised drag coefficient of freely falling particles on normalised Reynolds number [42]. The shape dataset is provided in the reference.

4.6. Balloon Structural & Material Design

To model the balloon structure, it has been decided to subdivide the full SBD structure into multiple distinct parts, being firstly the tether and the balloon. The balloon is subdivided into the central rod and the top structure. The central rod is the central load carrying element of the structure. This rod is loaded in tension and connects the wire tension and the payload to the top structure. Lastly, the top structure is the part connecting the upwards force generated by the balloon to the solar panels and the central rod. This top structure consists of ribs orientated in a circular layout. The tether and central rod are covered in subsection 4.6.2, where a simple calculation for this central rod is carried out. Furthermore, the structural analysis of the top structure is explained in subsection 4.6.3. Finally, considerations regarding the balloon shape and skin material are listed in subsection 4.6.4, where initial sizing is also done.

4.6.1. Structural Design Overview

The Skydancer is designed to harvest solar energy and deliver it to Earth. To make it possible, it needs to have a structure that provides enough space for lifting gasses that could maintain the structure at the altitude of 18 km. The Skydancer also needs to have a structure that is able to support its own weight and to house all the required payload, as well as to allow solar panel placement in such way, that maximises efficiency.

The Skydancer is hence aimed to have a maximised top area to accommodate solar panels, which is possible due to the flattened shape of the balloon. It allows for easier flat (horizontal) placement of the solar array, which is needed in order to maximise the efficiency for a wide range of solar inclination angles and to prevent from formation of a shadow due to placement of nearby panels. Solar panels should be lifted up from the balloon skin to ensure cooling of the solar panels, and to prevent hydrogen from collecting too much heat from the solar panels, which could lead to hydrogen explosion.

The structure connecting balloon surface with the solar panel array and providing point of connection to the solar panels is further referred as the "Top structure". It consists of top beam, compression rod, and curved rod, that are connected with central rod and placed on the balloon skin. Curved rods are expected to prevent a phenomena of the shrinkage of the panels into the balloon, by providing rigidity in the upper balloon part, while top beams provide rigid support to the solar panels. Both beams are interconnected with the compression rod, which aid to relieve critical moment bending loadings at both beams.

The central rod is a part of the balloon providing a load passage for all rigid parts of the Skydancer. It is hollow inside, which allows for internal placement of the tether (wire) and cables stretching from the solar panels. It carries payload weight at the bottom, at the middle is connected with the end of the tether and curved beams, and at the top is rigidly connected with top beams. It is enclosed by the balloon skin. All lifting forces in the balloon are transmitted to both the central rod and curved beams via the balloon skin.

Finally, payload is located below the balloon to increase stability of the balloon. The wire, which enters the payload compartment via a small hole, goes through the central rod and connects to the top of the balloon, keeps balloon in place and provides restoring forces. High attachment point allows for more stability compared to a possibly of connecting wire directly to the payload. General layout of the Skydancer is provided in Figure 4.35.

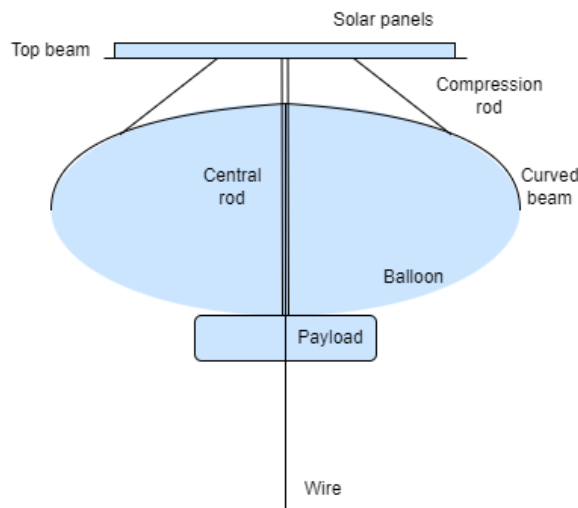


Figure 4.35: Sketch of the Skydancer

4.6.2. Tether & Central Rod

For this structural design, the free body diagrams of the wire and this central rod are shown in Figure 4.36. The forces shown in the free body diagram of the wire are the tension force in the wire, which is the summation of the excess lift and the weight of the wire itself, which is a distributed load of the full wire length. This wire tension follows from the stability analysis done in section 4.7.

The central rod is the main structural element of the balloon, connecting all rigid parts. Its main function is to provide a structural connection between the top structure, the wire and also to acts as a connection point for the balloon compartments. In Figure 4.36b, the forces at the bottom are the tension force of the wire and the weight of the payload. This payload consists of the transformer, onboard computer and other payloads which might be brought on. The total mass budget for this payload box will be 150 kg, which includes the external structure shielding it from the environment and the connection of this box to the rod. Furthermore the weight of this rod is taken into account as a distributed load and the load at the top is also included, which acts at the connection point to the top structure.

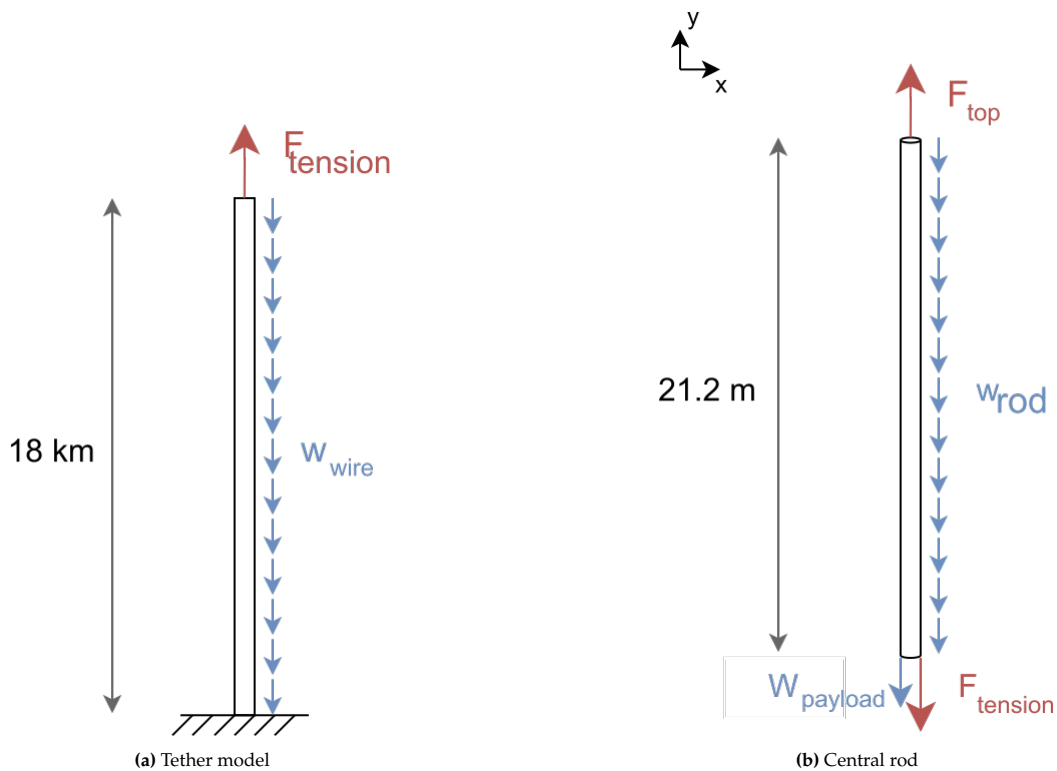


Figure 4.36: Free body diagrams

A quick sizing for this rod was done, using a tubular shape which would allow wires on the inside. It has been decided to use carbon fibre composite which has great properties of carrying tensile loads along the fibres. Since tension is the most prominent in central rod loading, and the rod is designed for axial load carrying, the material choice seems to provide great benefit in mass reduction while providing the required axial strength. For a carbon fibre rod of this length, the required area to stay under the ultimate tensile strength, taking into account a safety factor of 25%, was found to be 62.2 cm^2 , which resulted in a weight of 197 kg.

After this initial sizing, methods were investigated to lower the weight of this central rod. The main loads of this rod were due to the tension of the tether, but this tether is also designed to carry these tensional loads. Hence, it was decided to connect the tether not to the bottom of this central rod, but instead to make this central rod hollow for the length of the balloon such that the wire can be on the

inside. The central rod then only has to carry the payload weight, its own weight and can still act as a connection for the balloon segments. With this implementation, the central rod is essentially split into two parts, being a hollow part of 18.4 m where the wire tension does not have to be carried, and a solid part of 3 m, where the wire tension is introduced and linked to the forces resulting from the top structure. By this change, the weight of the central rod is reduced to 78 kg.

Finally, since the central rod is hollow and the wire is enclosed in it, the wire might experience stress concentrations at the bottom of the central rod, when the Skydancer gets tilted due to lateral loads. To prevent wire from snapping, the central rod features conical geometry, where the hole at the bottom part of the central rod is larger than the hole at the upper part. Allowing displacements in the rod and avoiding sharp edges close to the wire is necessary for this design configuration.

4.6.3. Top Structure

The top structure connects the upwards force of the balloon to the weight of the solar panels and the central rod, to carry the other subsystems and payload as well. This top structure consists of 12 ribs orientated in a circle. These ribs consists of a straight beam at the top, where it is supporting the solar arrays, and a curved beam at located at the balloon skin, where the upwards force is generated. The top view of the balloon and a simplified structural model of one of these ribs are shown in Figure 4.37. Here the solar array area is shown in yellow, and the dimensions are indicated in the side view.

For both the straight top and the curved bottom beams, the sizing is based on the distributed loads acting upon them and the maximum shear force and moment acting on these beams. These beams will be analyzed separately, with a connecting compression rod between them to allow for bending relief.

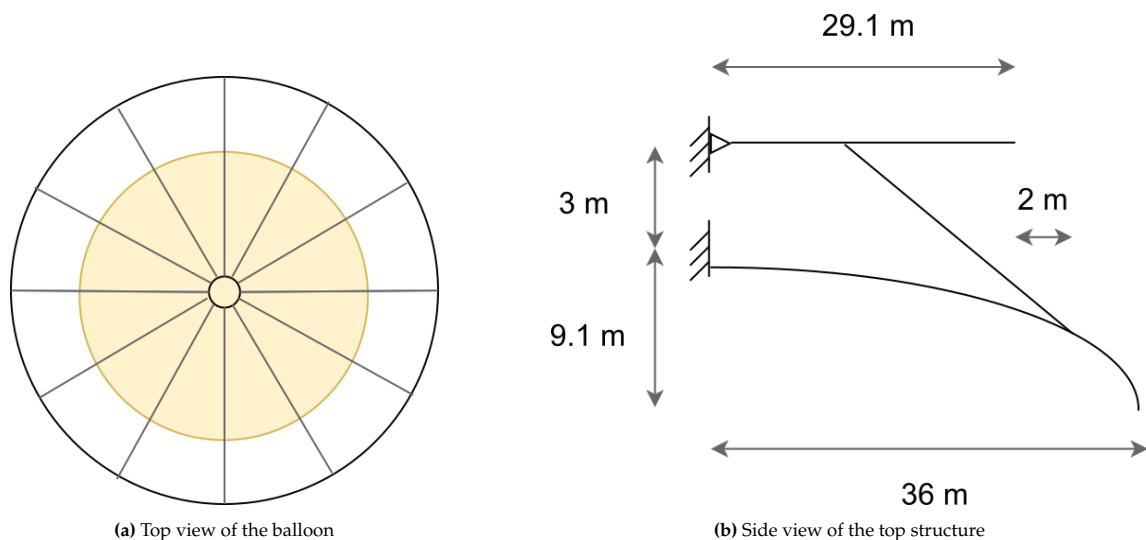


Figure 4.37: Top view and side view of top structure

Top Beam

For the internal loading within the top beam, the following procedure was followed. The density of the solar panels and supporting carbon fibre flat plate is determined in subsection 4.1.5, and equals 0.6 kg m^{-2} . Each rib is carrying the load of a pie point of the circle, of which the size depends on the number of beams and the length of this plate of solar panels. The area of the loads that have to be carried is shaped as a pie point, which follows a linear distribution for the most part and follows the shape of a circle for the last small part. It was assumed that this could be approximated by a simple linear increasing load, where the equivalent load acts at two third of the total length and the force is simply the integration of the total distributed load, which is the area of a triangle. For a solar plate diameter of 29.1 m and 12 beams, the actual load distribution was also calculated and compared to the

simplified linear load. It was found that the influence of the circle on this distributed load was relevant for the last 3.4 %, hence, the assumption of a linear load distribution is deemed valid.

A free body diagram of this top rod, solely regarding the y-direction, is shown in Figure 4.38. As shown in Figure 4.37b, the connection of the top beam to the central rod is modelled as a hinge, as it was deemed undesirable to have moments acting on this point as the solar panels are located there. Because of this, the support force is solely a force in the y-direction. The force F_{solar} is found to be 1330 N. From this FBD, the force within the connecting rod in the x-direction is easily found to be $2 * F_{solar}$ and F_A is equal to F_{solar} . The maximum shear force will act at the location of the connecting rod and the maximum moment will also occur at this location.

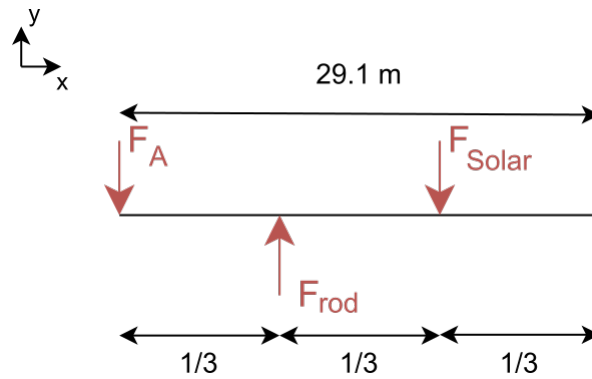


Figure 4.38: Free body diagram of top beam

Curved beam

The curved beams are designed to carry balloon lift loads and a part of structural loads from the top balloon structure (structural and solar panels). The curved beams follow the outline of the balloon's top surface and connect to the central rod at the root, which is modelled as a wall support. This curved rod is providing a shape for the upper part of the balloon and can hence be described by the formula for an ellipse as shown in Equation 4.10

$$\frac{x^2}{a^2} + \frac{y^2}{b^2} = 1 \quad (4.10)$$

where $a = 36$ m and $b = 9.12$ m. The rod shall have a minimised weight while allowing minimal deflections due to forces acting upon shall be able to withstand internal bending moments that are introducing internal stresses.

For the loads acting on the curved beams, the area under these rods also follows the shape of a pie point. However, the load on a unit area is not as evenly distributed as the load of the solar panels, as the load is dependent on the column of hydrogen below the unit area. As the height of this column decreases when the location moves further away from the central rod, as this hydrogen volume is shaped as an obloid, this linear load had to be adjusted to account for this decrease in load when moving closer to the edge. This has been done by integrating the area under the eclipse and defining the side view of the obloid. Multiplying this distribution of the side view due to the obloid shape by the distribution of the top view, which follows this pie shape, leads to the final distributed load on the curved rod. It was found that the resulting force acts at approximately 55% of the distance of the distributed load.

For the curved I-beam, the free body diagram in just the x-direction is shown in Figure 4.39 which incorporates the resulting force instead of the distributed load from the hydrogen. The values for the forces and moments in this graph are $F_{hydrogen} = 4590$ N and $F_{rod} = 2660$ N. With these values and distances known, the reaction force and moment at B are found to be 2930 N and 7.8 kNm respectively. From this diagram, it is immediately clear that the maximum moment will occur at $x = 0$. The maximum shear force will be located at the point where the connecting rod is acting.

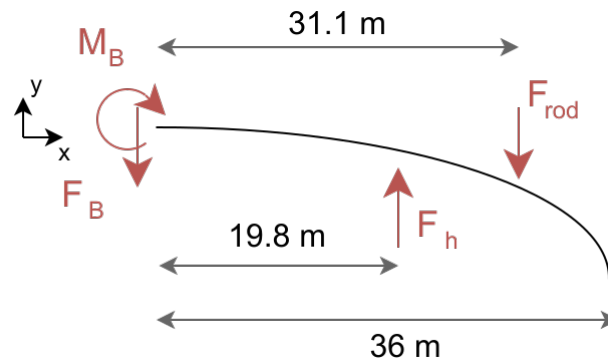


Figure 4.39: Free body diagram of bottom beam

Sizing of the beams

Now that the location of the the maximum shear and moment force are known for both beams, the actual values for these limiting loads are calculated using a python script, where the full distributed load is used instead of the resulting forces. With these loads known, the beams can be sized. The material used for these beams is Aluminium 6601, with a tensile yield strength of 276 MPa. For the sizing, it is crucial to know which of these stresses is the most limiting. This is done using Tresca's yield criterion, which states that the maximum tensile stress is half of the yield strength, as listed in Equation 4.11 [43].

$$\tau_{max} = \frac{\sigma_{yield}}{2} \quad (4.11)$$

To allow such a sizing, the dimensions of the beams need to be known too. As the beams mainly have to resist bending in one direction, the chosen shape for such a beam is an I-beam. The dimensions of this beam are parameterized and related to one base dimension, which is the thickness of the web. The nomenclature for the dimensions of an I-beam are shown in Figure 4.40¹³. For a large moment of inertia compared to the area, it was chosen to go for a flange thickness of twice this web thickness. Furthermore, the width and height of the flange and web respectively are related to their thickness by a ratio of 1:25. For performance, this ratio should be as high as possible, but it is limited by manufacturing aspects. For a thin-walled assumption, this ratio needs to be at least 1:10. From literature it was found that a ratio of 1:25 is valid for such I-beams [44], and that higher ratios can be achieved for high precision engineering.

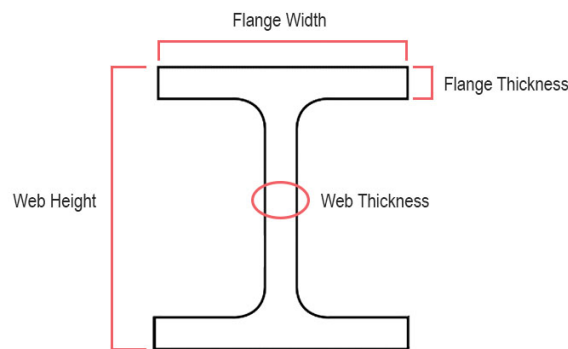


Figure 4.40: General lay-out and nomenclature for an I-beam

¹³"Wide Beams", North York Iron Corporation, Accessed on 17-1-2023, <https://northyorkiron.com/wide-beams/>

For both beams it results in the bending stress being the limiting case over the tensile stress. For the top beam this maximum bending occurs at the point where the connecting rod acts, as this is where the shear force will switch from being positive to negative. For the bottom beam, the maximum bending occurs at the root, where it is connected to the central rod. Sizing the I-beam such that it reaches the maximum allowed yield stress at these locations, while incorporating a safety factor of 20%, results in a web thickness of 1.6 mm and 1.8 mm for the top and bottom beam respectively. The area of these cross sections can then also be calculated straightforwardly. The web thickness, area and weight of both beams is tabulated in Table 4.6. It should be noted that the cross-sections of these beams can be further optimised to increase strength and thus decrease weight, which is a task for further structural analysis. Also for the curved beam, tapering is an option to further decrease the weight here.

Table 4.6: Parameters of the beams

	Top beam	Bottom beam
Web thickness [mm]	1.63	1.77
Area [cm ²]	5.36	6.26
Weight [kg]	42.1	49.2

Connecting Rod

The last thing that should be included in this overview is the connecting rod, which is loaded in pure compression. Sizing a solid aluminium rod with these forces results in a weight of 60 kg per rod, which is deemed too heavy for this purpose. After considering the literature to find another material for this purpose, it was found that it is not necessarily the material, but instead the shape is the aspect where this rod can be improved. Recent research has shown that gyroidal shapes are extremely strong in compression. Researchers at MIT managed to create a 3D printed graphene shape that has a density of 5 percent of steel, while being 10 times as strong [45]. Further research concluded that this was not linked to the graphene directly, but that also other materials' compressive strength over weight can be massively improved by implementing a gyroid as shape [46, 47]. Using this technology for the connecting rod should be able to reduce the weight by 90%. Again, this is only possible because of the fact that this connecting rod is loaded solely through compression.

Deformations

For a successful top structure design it should be ensured that beam deflections are small enough and do not affect the functionality of the balloon in any negative way. The critical point of deflection is the end point of the curved beam since it is a loose end of a long beam that is being introduced to uniform loads along its structure. To estimate the approximate deflection at the tip of the rod, the beam can be assumed to be horizontal along x-axis, and the load due to balloon pressure is uniform. The actual total deflection would be larger due to the pressure forces acting on the sides of the balloon (x component of the balloon induced loading is neglected). The following formulas can be used for the estimation of deflection due to linear load distribution as well as due to the point load acting at the connection with the compression rod. The deflection of a beam tip due to the uniform load can be calculated using the formula below:

$$v_{uniformload} = \frac{w \cdot L^4}{8 \cdot E \cdot I_i} \quad (4.12)$$

The deflection of a beam tip due to the point loading at the compression rod is calculated as:

$$v_{pointload} = \frac{F \cdot a^2 \cdot (3 \cdot L - a)}{6 \cdot E \cdot I} \quad (4.13)$$

where $F = 2660$ N is the downward point force due to the compression rod, $a = 32.1$ m is the location of the F on the x-axis, $w = 127.5$ N/m is the value of the uniform force acting upon the rib rod due

to the balloon pressure acting on the rib rod, assuming that balloon skin does not carry any loads. Adding up the individual contributions of those deflections, it has been calculated that the maximal deflection would result in a total vertical deflection of 38 m, which is unacceptable. However, in reality, the deflection is limited by the compression rod. When the compression rod would be fully fixed, the displacement of the tip would only be 6 mm. However, in reality, the connection is not fixed and is prone to deformations. Assuming a realistic case where 3% of loads due to balloon pressure are transferred to the curved beam, while the remaining 97% is in the balloon skin, only 2.5 m would deflect, which would cause no issues for the SBD.

This example shows that it is crucial to address the deflection issue by, for example, allowing the skin to carry most loads. The future design of the top structure of the SBD would require either ensuring that at 97% of the pressure, the load is carried by the skin in maximal loading conditions (while allowing curved beams to carry the rest 3%), or negating the bending issue by other means, e.g. attachment of supporting wires at the ends of the curved rods. The current design accommodates the idea of using strengthening tendons in a pumpkin-like shaped balloon (see 4.6.4) on its skin that ensures the required strength of the skin balloon to carry stresses on its own, as well as compression beams, limiting the movement of the curved beam. However, the current design is also sized for the worst-case-scenario in the top-structure (where all loads are carried via curved beams). The load path should be optimised in future design iterations, allowing to settle on an optimal value for loads introduced to the top structure via balloon skin. To summarise, the deflection of the curved beam is not expected to rise issues in the design where most loads are carried by the balloon skin and where compression rods are present. Also, due to the reduced carrying capacity of the curved beams and the introduction of multiple compression rods in the future, the weight of the top structure is expected to decrease.

Discussion

In conclusion, the introduction of a compression rod can drastically reduce the weights of both beams. A downside of this rod is that it will introduce tension and compression in the bottom and top rod respectively. As this supporting rod is a two-force member, the relation between the horizontal and vertical forces has the same ratio as the horizontal and vertical distances. Preliminary calculations relating this tension and compression to the area of both beams and the allowable tensile and compressive strengths show that solely these axial forces will not introduce any problems. In further structural analysis, a Mohr's circle can be used to assess the maximum stresses, where the stresses on an element in all directions are combined. If this combination of stresses would pose problems, a solution would be to increase the height between the top of the balloon and the plate with the solar collectors, as this would increase the angle of the connecting rods and would decrease the compressive and tensile forces in the beams.

Another possibility to improve the structure and optimise it further would be considering the usage of multiple compression rods or a truss structure for a more uniform distribution of loads along the top and bottom beams, which would allow for a more lightweight structure and construction of more efficient load paths.

It should be noted that this is only a very initial and over-simplified structural model and that more attention should be given to the structure in further design stages. In further structural analysis, it is recommended to initiate a full scale FEM model to calculate the internal loads for all elements. However, with these initial estimates enable the further sizing of the balloon, as an estimate for the top structure mass is now provided.

4.6.4. Balloon

The balloon is taking on the form of a pumpkin balloon, as shown in Figure 4.41. The outer skin is divided into tendons. The benefits of the pumpkin shape with respect to an oblate spheroid, are the following [48]:

- Pumpkin shapes can have more payload whilst maintaining the same lift due to their larger volume-to-surface area ratio.

- Usage of strengthening structures - tendons - ensures that balloon withstand higher pressures and extreme temperatures, increasing durability.

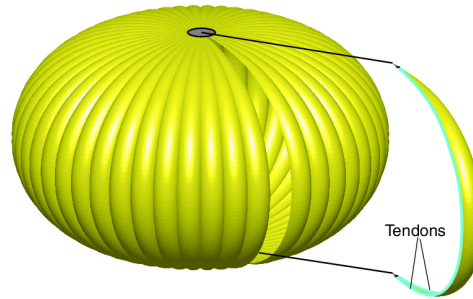


Figure 4.41: Pumpkin balloon shape [48]

For the sizing of the balloon skin, the inputs are the balloon's volume, the area of the solar panels, differential pressure, the excess lift and the admissible stress.

The material used in the wire, UHMWPE, is also used for the balloon skin. The material is strong for its weight and has good UV-resistance. Furthermore, a layer of PVDC (Polyvinylidene chloride) is added to the skin for permeability characteristics.

The formula used to calculate the skin thickness of the UHMWPE is shown Equation 4.14 [49].

$$t_b = \frac{\Delta p R}{2\sigma_b} * 1.2 \quad (4.14)$$

Where t_b is the fibre thickness, Δp the differential pressure, R is the radius of the balloon and σ_b is the admissible stress. A safety factor of 1.2 is introduced because the formula is applicable to use for a perfect sphere, whereas this design looks at a pumpkin shape (comparable to an oblate spheroid). The solar panels are placed as a disk on top of the balloon. The radius is a fraction of the solar panel area radius. The admissible stress is one-fourth of the yield stress of UHMPWE, 0.25 GPa, as used for the wire sizing before. The differential pressure is obtained from the results from the lift calculations, shown in subsection 4.5.1. The resulting thickness is 9.4 μm . The density of UHMPWE is 970 kg/m^3 [50].

The permeability of the balloon skin is also an important consideration for the sizing of the thickness of the outer balloon skin. Equation 4.15 shows the flow rate of the hydrogen over time [51].

$$J_s = \rho \cdot \frac{\Delta atm \cdot A}{t_{PVDC}} \quad (4.15)$$

where J_s is in $cm^3 \cdot day^{-1}$, Δatm is the differential pressure in standard atmosphere, ρ in $\frac{cm^3 mm}{m^2 day \Delta atm}$, A is the circumference of the balloon and t is the thickness of the PVDC used.

ρ is 0.07 for nitrogen at 23 degrees Celsius and the average ratio of permeabilities of nitrogen with respect to hydrogen is 0.160, since hydrogen is a smaller particle than nitrogen and would have a higher permeability factor [52][53]. The permeability factor only decreases with lower temperatures. Together with the thickness of 1 μm of PVDC, an area of 8625 m^2 and a differential pressure of 100 Pa, this will result in a 3.72 L per day of loss of hydrogen. The hydrogen leakage is deemed to be negligible for a long-duration mission since this results in a loss of 1.4 cubic meters of hydrogen a year. Therefore the hydrogen supply does not need to be replenished.

For the calculations for the balloon's area and mass of the balloon skin, the shape is assumed to be comparable to an oblate spheroid. The volume, based on a given total mass, is derived in the method discussed in subsection 4.5.1. Using formulas for an oblate spheroid an area for the surface area can be calculated.

The amount of gasbags needed such that the excess lift or less is lost when one of the bags pops is 10, considering an excess lift of 6000 N and a total lift of 55086 N . Since the decision was made to have 12 ribs supporting the solar panels, connected to rods in the balloon top skin, it is decided to have 12 gasbags. Next, it is determined that the number of tendons should be between 16 to 145, this is standard for smaller pumpkin balloons [48]. Hence, twelve tendons are too few to ensure the benefits of a pumpkin shaped balloon, and as such, the number of tendons is increased to double the number of gasbags to ensure a symmetrical design: 24 tendons.

The 12 walls added for the gasbags have the same thickness as the balloon's skin in order to assure that once one of the bags pops, the compartments next to the compartment pop maintain the permeability and strength characteristics. Moreover, the UHMPWE is able to carry structural loads occurring due to the balloon wanting to take on the form of a sphere.

An input of a volume of 49518 m^3 and differential pressure of 108.58 N/m^2 , with 12 gasbags, results in a mass of 160 kg for the inner and outer skin.

Another feature of the balloon are the ballonets which are incorporated in the balloon structure. They help to provide variable lift to the Skydancer, which is extremely useful for commissioning and decommissioning stages. Ballonets also allow to save hydrogen since it is not necessary to get rid of the lifting gasses in order to lower the balloon. Commissioning and decommissioning stages and use of ballonets are explained in more detail in section 5.1

4.6.5. Material Choice

The chosen materials for each component of the SBD are summarised in Table 4.7. It is important that chosen materials are not only strong, but also durable, since they will be constantly exposed to atmospheric conditions. Furthermore, the cost, lightweightness, manufacturability and sustainability (cradle-to-cradle classification) are also some of the important factors determining the choice of material.

Table 4.7: Material selection

Component	Material	Reasoning
Top and curved beam	Aluminium alloy 2014	Aluminium alloy is an attractive decision as it allows for good resistance against shear, tension, bending, while is also a relatively cheap option. Aluminium is more lightweight than steel. At the end of life all aluminium parts can be easily recycled. Aluminium alloy 2014 has good corrosion resistance, and local corrosion on a small scale should not interfere with structural strength. Aluminium is completely resistant to UV rays. Aluminium is easy to shape into desired geometries while not influencing properties of the material unpredictably.
Compression rod	Aluminium	Provides a lightweight and strong structure when combined with gyroidal geometry. Requires coating to prevent corrosion, but itself has good
Central rod	Carbon-fibre-reinforced polymer	Carbon fibres have great performance in tension, which is the most critical loading condition. Large part of fibres could be arranged along the length of the rod, while the remaining fibres could carry aerodynamic loads acting perpendicular to the central rod. Homogeneous material qualities are not necessary in this loading case and such fibre distribution would help to reduce weight.
Balloon skin	UHMPWE with PVDC	UHMPWE (Ultra High Molecular Weight Polyethylene) provides a lightweight and strong solution for the balloon skin. The fibres are non-rigid, but with excellent performance while in tension, which is the most important aspect for a balloon design. Connecting the top and bottom of the balloon with fibres (via tendons and "legs") allows those fibres to act in tension, where they excel, while keeping the balloon outline in a "squished" shape. Furthermore, the coating of PVDC would minimise gas leakage through the skin. It is also important that materials would be UV-resistant, and placed on the outside of the balloon, the UHMPWE would provide good UV-resistance.
Tether	UHMPWE with aluminium	UHMPWE is UV-resistant and has good tensile strength qualities. It is important that the tether is as lightweight as possible, and UHMPWE allows for that. Finally, it is possible to purchase commercially available wires made of UHMPWE, or to weave them into other geometries, which makes the manufacturing process simple. The aluminium core is used for its electrically conductive properties and high breaking length as a conducting material.

4.7. Stability & Control

The stability & control characteristics are dependent on passive methods, as active station keeping has been ruled out. The SBD uses multiple passive control elements that will provide stability to the balloon, the main two being the tether, as touched upon in section 4.4, and the ballonets, which were covered in subsection 4.5.2. Furthermore, the balloon was designed to have good aerodynamic performance, with a drag coefficient of 0.112.

With the weights of all subsystems known, the centre of mass can be found. As the subsystems with the highest weights lay on top of the balloon, the centre of gravity will be located in the upper part. For a freely floating or flying system, having this centre of gravity lie above the centre of pressure would result in an unstable system, as any disturbance could cause the system to tip over. However, this SBD

is connected to a tether, which limits any angular movements except yaw, hence this will not pose any issues. This also goes for changes in the location of the centre of gravity or centre of pressure during launch or decommissioning.

Inflating or deflating the ballonets allows the system to change the weight and the weight distribution. Because of that, the balloon will be able to counteract disturbances in pitch and roll angles. The weight change also allows for the balloon to control its altitude when ascending and descending for maintenance and (de)commissioning.

Table 4.8: Axial stability control methods

Table 4.9: Rotational stability control methods

Translation	Tool	Rotation	Tool
x-axis	Tether, streamlined z-y face	Roll (x-axis)	Tether, ballonets
y-axis	Tether, streamlined x-z face	Pitch (y-axis)	Tether, ballonets
z-axis	Tether, ballonets	Yaw (z-axis)	None

All mentioned methods of stability control are summarised in Table 4.8 and 4.9. In this table the internal body coordinate system is used, where the x-axis is orientated towards the "nose", the y-axis to the left "wing" and the z-axis is orientated downwards along the wire. As the balloon is rotationally symmetric, the difference between these x and y axes is trivial. The only allowed rotation would be yaw, but the yaw inside of the tether should be limited, as this will introduce torsional forces. To allow the balloon to rotate while minimizing the torsion on the tether, a swivel is used at the point of connection between the tether and the balloon.

4.8. Payload Design

Aside from solar panels and the lifting structure, there are other systems on board the balloon which are critical for mission success. In this section, the payload is defined and sized. First off the sensors and meters package is designed in subsection 4.8.1. Then the wireless communication system and its data handling constituents are sized in subsection 4.8.2. Lastly, the supporting components such as the battery are defined in subsection 4.8.3. At the end of the section, an overview will be given of the total electrical architecture.

4.8.1. Sensors & Meters Package Design

Some specific sensor types are needed for proper operation of the balloon. One such sensor is the temperature sensor of the battery packs. The batteries must be kept within operating temperature to avoid degradation or failure. A small and redundant temperature sensor is simple to include. Two other critical sensors are voltage and current sensors to keep the solar array in check. Due to the electrical design of the array, it will monitor itself. However, failure and degradation measurements must be taken to keep the system fully operational. A set of redundant current sensors as well as voltage sensors is included in each chain.

Finally, other sensors and meters required to keep the system in operational conditions are internal and external sensors. The internal hydrogen status must be monitored with temperature, density and pressure sensors. The balloon skin can also be monitored with a strain sensor. To contrast the hydrogen internal sensors, external atmospheric sensors of the same kind are needed. Moreover, altitude, attitude and wind speed are also required to get a complete data set. All sensors to be included in the payload are listed in Table 4.10 according to the design group.

Table 4.10: All sensors and meters to be present in the payload.

Atmospheric sensors	Extended sensors	Balloon sensors	Electrical sensors
Temperature	Pyranometer	Temperature	Voltage
Density	Hygrometer	Density	Current
Pressure	Geiger counter	Pressure	Temperature
Wind speed	Magnetometer	Strain	
Altitude	Imaging camera		
Attitude	Ozone		

The payload also carries additional science instruments, listed as 'extended sensors'. Besides mission non-critical information, these provide valuable long term in-situ measurements that are used to bolster the business case. In particular, there is an opportunity to measure exact local solar incidence, humidity and ozone concentration with pyranometers, hygrometers and Geiger counters respectively. Other science data can be obtained with magnetometers and imaging cameras.

Most of the sensors are to be placed in the lower payload bay, such as the atmospheric sensors. Others such as the pyranometer are required to be placed on the upper layer with the solar array. Most are flexible in positioning and configuration. Nearly all sensors are of insignificant size compared to the volume available in the lower payload bay. Similarly, the mass of the sensors package is negligible compared to the rest of the system.

4.8.2. Data Handling System Design

The data handling diagram of the balloon is rather simple as the system revolves around monitoring itself and its environment, as opposed to actively interacting with its surroundings. The block diagram is given in Figure 4.42, where it can be seen that all information flows through a central data handling controller. There are two actions the controller can perform, either transmit collected data or command the power control module. Data from critical sensors are continuously fed into the controller which autonomously performs elementary tasks given the sensory inputs. For example, the temperature regulation of the battery pack, done by an electric heater. Most data simply gets transmitted to the ground segment where the non-science data gets monitored for the correct functioning of the system. The source of outside input comes from the receiving antenna, which may overwrite the controller to deviate from its standard operation.

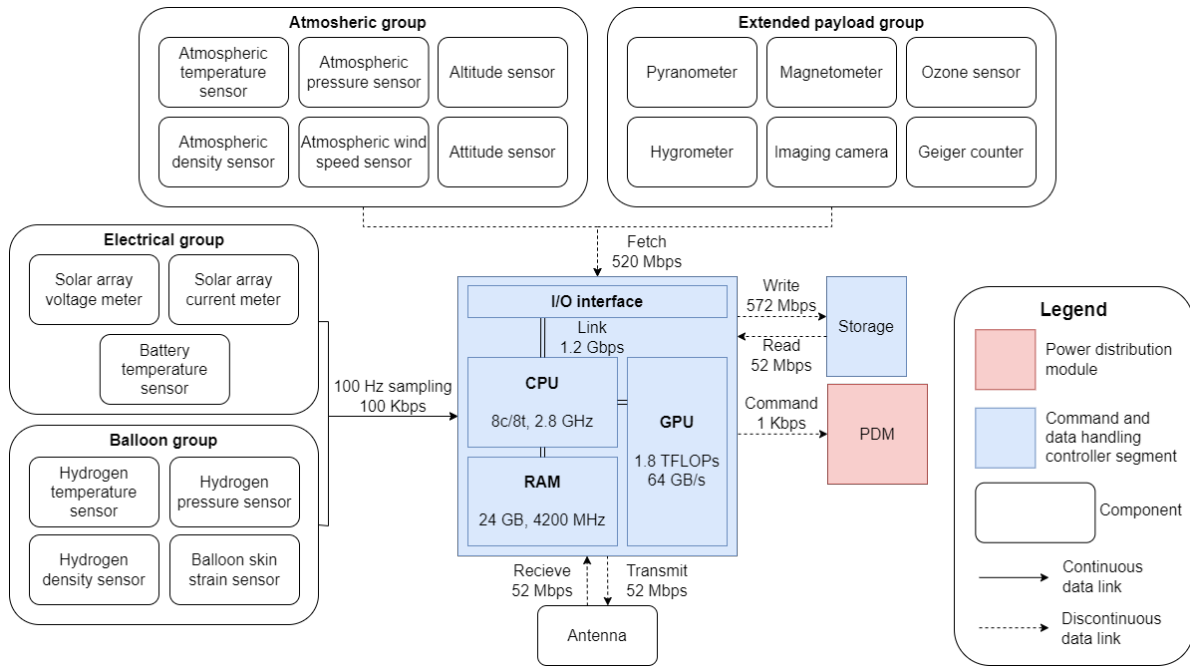


Figure 4.42: Data handling block diagram for a singular balloon

Using the technical specification from the midterm review, an analysis can be made of the bit-rate capacity that the communication array has. All of the sensors onboard produce significant data, but the largest data concern is the camera. The extreme case of a 4k camera was considered. This sensor was chosen as a potential ridesharing scientific payload that is more data intensive. The required data rate for a compressed 4k video is 25 Megabit per second. This is thus the minimum data transfer capacity that is necessary. Table 4.11 shows the characteristics of the data transmission segment.

Table 4.11: Downlink budget at 18 km with a transmission power of 15 W.

Item	Gain (dBW)
Transmit power	23.5
Cable loss balloon	-0.21
Antenna gain	28.9
Free-space loss	-79.1
Receiver gain	45.4
Cable loss ground station	-2.1
Low noise amplifier	20
Signal to noise ratio	36.4

Table 4.12: Technical parameters of the data transmission system.

Parameter	Value
Height	18 km
Transmission power	15 W
Transmitter diameter	0.3 m
Receiver diameter	2 m
Bandwidth	20 MHz
Frequency	12 GHz
Balloon transmitter cable	1 m
Ground station cable	20 m

With this calculated signal-to-noise ratio, the bitrate per hertz of bandwidth can be calculated, which yields the total bitrate. This is given by the Shannon-Hartley theorem:

$$C = B * \log_2(S/N) \tag{4.16}$$

Where C is the capacity in bs^{-1} , B is the bandwidth in hertz and S/N is the signal-to-noise ratio. Filling in the numbers yields a bitrate of 51.86 Mbps^{-1} . This is over twice the necessary capacity for a 4k video, which has been defined as the minimum required. Since the power required for the data transmission is insignificant compared to the total power used, 15 W will remain the transmission power. The excess

capacity allows for upgradeability, sensor data transmission and margin if for example, the weather worsens transmission conditions.

C&DH Controller Specifications

The command and data handling controller must be able to handle the total incoming data of all sensors, process it and pass on the required bits. It also has to run operating software to regulate subsystems, such as a maximum power point tracking (MPPT) algorithm. To perform these tasks the controller must consist of a CPU (Central Processing Unit), GPU (Graphics Processing Unit), memory controller and have I/O interfaces. Such a complete set in a small package is referred to as system-on-a-chip, or SoC.

The sizing for individual data rates is derived from the maximum operational capabilities. For example, the SoC may need to record the maximum sensor data rate and at the same time receive the maximum amount from the communications array. The SoC internal links and the storage must be capable of these data rates. Any high-end SoC, like the ones found in modern smartphones¹⁴, is capable of this level of data handling. The consideration of data storage size depends on whether video footage is required to be stored. It is not deemed essential to store video, meaning that even long term sensor data may be stored on common NAND drives. For redundancy considerations, the entire SoC is to be run in parallel with an identical twin. A failure in SoC leads to communications loss, which may lead to catastrophic system collapse.

4.8.3. Battery Pack Design

Considering that there will be no onboard hydrogen replenishment system and fuel cell (see subsection 4.6.4), the electricity needs of the system is greatly reduced. During the day, power is supplied by the solar panels, thus storage is only necessary during the night. As the ambient temperature is far below zero Celsius at operating altitude, the battery must be kept at a more appropriate temperature. Batteries have a lower capacity and voltage at decreasing temperatures, inhibiting the system from working as intended. The battery is therefore to be insulated using lightweight insulators with a low emissivity, such as metal foils. An electric heater is added to the battery to keep its temperature constant during the many temperature cycles.

In order to control the altitude of the system air pumps are used to inflate the ballonets, decreasing the lift of the system below buoyancy. The pumps are sized to lower to the ground within 24 hours so the system can be protected from heavy weather, which can be predicted over 36 hours in advance, as will be explained in section 5.1. The difference in ballonet volume between 18000 and 0 meters is approximately 45000 m³. In order to pump this much air within 24 hours at an overpressure of 100 pascals a continuous power of 150 W is required, assuming 60% motor and pump efficiencies¹⁵. This required power is similar to the power used by non-essential onboard systems such as sensors. In the event of a hypothetical storm warning the power can be diverted during the night, making use of the battery power reserved for these sensors. During the day solar energy production can be used, having no effect on the battery needs.

As mentioned in 4.8.1 there are possibly more than 100 differing sensors including redundancy. Some sensors have power usage in the milliwatt range, others approaching the single digit watt range. Considering the wide range of sensors an average power of 1 W per sensor type was chosen. A single SoC as sized accordingly does not require more than 10 Watts and the electric heater 50 watts, based on convective and radiative heat losses for a reference cuboid at high altitude. The antenna will add an additional 15W of continuous usage. This yields a continuous power usage of 185 W which has to be accounted for by the battery at night, 14 hours in the worst case scenario. This means that the battery must have a capacity of at least 2.6 kWh, which has a volume of approximately 6.2 litres and 10.2 kg at lithium ion energy densities.

¹⁴"SNAPDRAGON® 8 GEN 2 MOBILE PLATFORM". Qualcomm. <https://www.qualcomm.com/content/dam/qcomm-martech/dm-assets/documents/Snapdragon-8-Gen-2-Product-Brief.pdf>

¹⁵<https://www.e-education.psu.edu/eme811/node/710>

4.8.4. Payload Sizing

The combination of all electrical systems is shown in Figure 4.43. At the heart of the circuit is the power distribution module (PDM), which acts as an intersection for all subsystems. The electrical design of the solar array means it acts as a power source for the system. Most of this power is transported to the ground segment for energy delivery. Some of the power is divided into payload elements such as the sensors and electrical heater. The estimated voltages stem from standard units used in the electrical design of the individual constituents. For the purpose of the balloon, the transformer is not considered part of the PDM.

The transformer is by far the largest contributor to the payload mass at 100 kg. The rest of the payload is insignificant or hard to size in terms of mass. Considering this, and that the lower payload bay is to be made of a lightweight structure, a total payload system mass of 200 kg is estimated. The volume is neglected as of now, at the lower payload bay is not volume limited in any way.

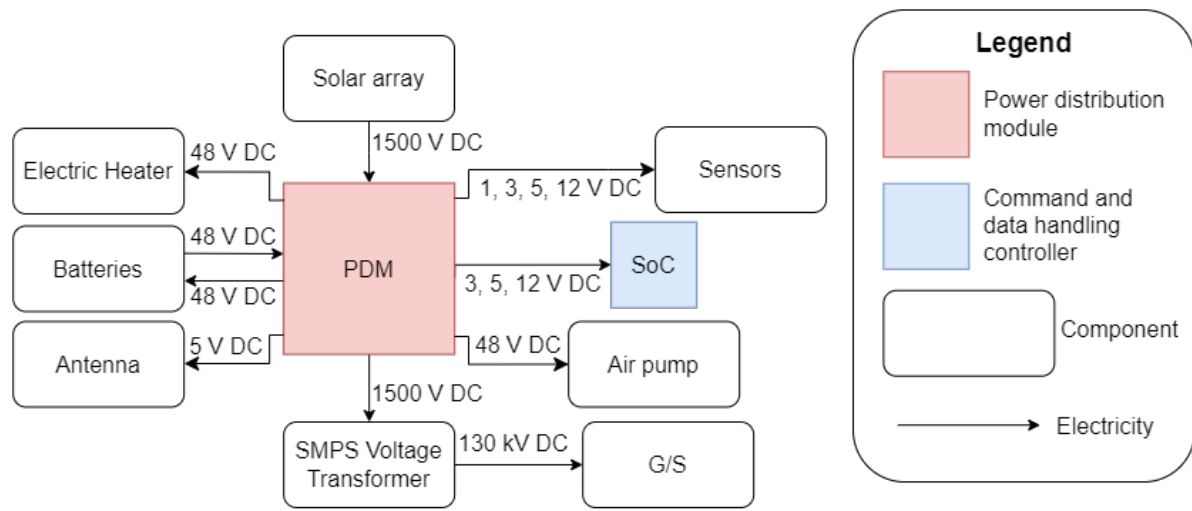


Figure 4.43: Electrical block diagram for the complete system

5 | Design Realisation

The realisation of the design is worked out in this chapter of the report. Future steps are discussed as well as the engineering budgets. section 5.1 will discuss the logistics and operations, including the choice of having a sea based ground segment, commissioning and decommissioning and maintenance. section 5.2 will discuss the production plan of Skydancer. In section 5.3 the engineering budgets are presented. The Design & Development Logic flow diagram is presented in section 5.4. Lastly, the project Gantt chart after DSE is visualized in section 5.5 to show the post-DSE activities.

5.1. Logistics & Operations

In this section, choices are elaborated upon for ground segment characteristics in subsection 5.1.1. For the logistics and operations, the three phases of commission, perform operations and decommission are defined in subsection 5.1.2 to subsection 5.1.4. Additionally, a plan for maintenance and operations is given in subsection 5.1.5.

5.1.1. Ground segment

The ground segment is defined as the setup provided on the ground that is attached to the tether. Considering the novelty aspects of this design, there is a wide range of possibilities to be considered for the design.

There is the option to deploy the design either on land or at sea. At land, a distinction is made between remote and densely populated areas. It is not sensible to deploy near densely populated areas. The risks associated with this design that may cause the design to crash are sincere. These are listed in chapter 7. Moreover, often in densely populated areas, more air traffic is expected, therefore this design is more probable to interrupt busy airspace. When it comes to remote areas, it is possible to deploy the balloon if the facilities are in place for all the different phases, and the area is accessible, so for example crew is able to travel there and the product can be delivered on site. The same goes for sea-based deployment. When looking at possibilities to deploy the product on land, at extensive northern and southern latitudes the wind speeds are often high enough for wind energy, at 4 to 5 m/s a wind turbine starts to operate and a minimum of 7 m/s is desirable for profitable operation¹. Moreover, hydropower is more common at these latitudes [54]. When looking at locations around the equator, the ground profile exists mostly of dense (often protected) rain forests and wide-spread plains. On the wide-spread plains, a ground based solar farm is preferable when it comes to cost. In the case of the rainforest, deploying the balloon in a remote area of the forest greatly disrupt the environment. Hence, it seems favourable to operate at sea near the equator. More elaboration on this decision is provided in chapter 8.

A ground segment at sea would consist out of the following components: a sea platform, sea cables and a potential grid transformer. Figure 5.1, shows the different components. The water level is depicted in blue, the electrical wiring in red and the tethers in yellow. Moreover from left to right, one sees the following components: electricity grid, potential grid transformer, sea cabling and then lastly, the sea platform with the tether attached to the top.

¹Wind energy's frequently asked questions (FAQ). (The European Wind Energy Association. Last accessed on 20-01-2022. <https://www.ewea.org/wind-energy-basics/faq/>

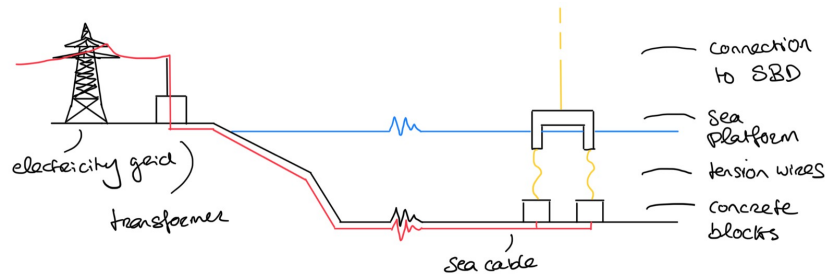


Figure 5.1: Visualisation ground segment

The sea platform is a tension-leg platform, a concept adopted from offshore wind energy. This method is often used for water depths ranging from 300 to 1600 *m*, beneficial for the sea around the equator [55]. Furthermore, this type of platform is beneficial to other floating platforms in the following aspects [56]:

- The platform has good heave motion, entailing up and down motion of the platform with changing circumstances.
- Can be assembled and commissioned onshore.
- Small hull size.
- Small mooring footprint.

5.1.2. Commission

The commissioning of such a big system needs special attention. The sea platform is temporarily expanded to facilitate the commissioning. This is done by adding floating platforms around the permanent tension-leg platform.

The different components of the SBD will be delivered to the site by boat. The long carbon fibre rod in the middle of the design is one of the challenging parts to transport. Additionally, for example, the solar panels are transported in stacks to the operating site.

The realization of the ground segment is done by an external party. An additional component to the platform is a coil placed on top, around this coil the balloon's full tether can be wrapped. This coil assists in the progress of launching and taking down the balloon in a controlled manner.

The permanent tension leg platform can be seen as follows. There are big blocks of concrete on the bottom of the ocean used as anchors. Then there are wires connected from the blocks to the platform floating on the sea. These wires will always be in tension, hence the name tension-leg platform. These concrete blocks will be adjusted such that marine life will have as less disturbance as possible. Maybe it is even possible to support it by starting a new coral reef by adding coral and holes into the blocks. All temporarily floating platforms are attached by wire to the surrounding platforms but only on the sides, not in a diagonal fashion. This process is illustrated in Figure 5.2, where a top view is given of the platform, and the wire is depicted in yellow wrapped around the coil. In the left picture the standalone permanent tension-leg platform is depicted, in the middle one the modular pieces of the platform are added and in the right picture it is shown how the balloon is laid on top of the platform with a red marking.

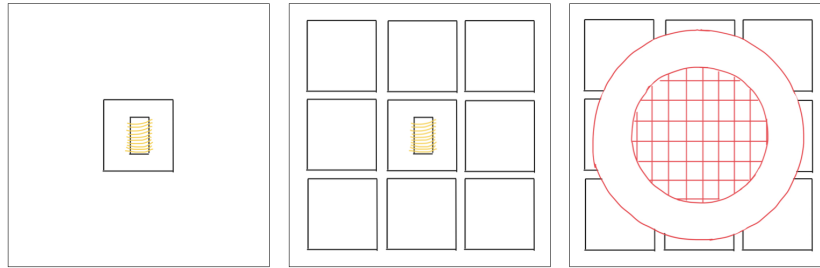


Figure 5.2: Modular sea platform

On the sea platform, the assembly work takes place. The full design is assembled, whilst the tether is wrapped around the coil and only attached at the last moment to the bottom of the balloon. There is a supporting structure needed to hold the structure because the stiff rod of carbon fibre encasing the top part of the wire is unable to carry loads of the payload and structure on the top part of the balloon. Pre-launch checks are then performed. Next, the hydrogen is pumped into the balloon and the ballonets are inflated to their full size, to keep the balloon in shape. During the launch, the coil turns to unwrap the wire gradually and the air is let out of the gasbags to let the hydrogen expand. After the balloon is successfully deployed, the modular sea platform pieces are removed and mission systems are initialised.

5.1.3. Perform operations

In the operational phase four functions are fulfilled, as mentioned in section 3.1, these are: supply energy, perform baseline operations, communicate and scheduled operation. Scheduled operation is elaborated upon subsection 5.1.5.

Due to the cyclicity of nature, there will also be cyclicity in the operations. There will be two parts of every cycle. The first part will be when sunlight is available to supply energy to the grid, or solar mode. Second part is when there is no sunlight available, hibernation mode. Both modes will have the need to handle data. Data needs to be gathered from certain systems. Also, data needs to be able to received and transmitted from and to the ground segment. This is all powered with the electricity generated from the solar panels, since this is green energy. During the night, the energy will be used from small batteries on board or send up by the tether.

During solar mode, there is the need of course to supply energy. It needs to harvest the solar energy, then process the energy and lastly distribute the energy. This is also visualized in the Functional Flow Diagram in Figure 3.2. With the data acquired during the day and night cycles, maintenance can be scheduled. This will always be during the day for safety reasons. The systems will be shut down and maintenance will be performed. After maintenance there will be commissioning again and the systems will be turned on generating power once again. There is some optimal window for commissioning with optimal power generation. This could be found in the future with a more detailed commissioning plan.

Lastly it should be noted that during operations there are regulations to comply with. Since the tether will be in the airspace almost continuously this is a potential hazard. Therefore an airspace restriction is necessary for safety reasons. One could only guess what will happen when an aircraft hits the tether during flight. What exactly the safety range around the movement range of Skydancer can be analyzed in future design stages

5.1.4. Decommission

For the decommissioning, the ballonets are filled with air and simultaneously the coil is bringing in the wire. The modular sea platform is deployed once again to facilitate disassembling the balloon partially on the platform. The remaining components are transported back to land. The life-cycle ends with the reuse of some components, and recycling of other materials and for some, the only option is to dispose of them as waste.

There is a minimum speed for the decommissioning of the balloon, due to the weather conditions. The very strong winds of hurricanes or tropical storms can affect the balloon substantially. The NOAA (National Oceanic Atmospheric Administration) mentions a 36 hour advanced warning². From this, a requirement was set up stating that the system should be able to land within 24 hours, this requirement is labeled SBD-POS-12. It does require more research as to what the effects are on the balloon and what the most efficient way of decommissioning is. Preferably all of the hydrogen is saved, however there is an excess of lift and this might need to be reduced to the extent where it will move down by itself.

5.1.5. Maintenance and emergency operations

During the balloon's lifetime, the balloon has to be brought down to the ground to perform maintenance checks. Especially with first deployment, the balloon needs to be taken down frequently, commencing with each year. Next, after gaining familiarity with the degrading and deeming it to be acceptable, the balloon is to be taken down every five years, so four times during its lifetime. Moreover, for safety reasons the balloon needs to be taken down when an emergency scenario occurs such as extreme weather scenario's (cyclones for example).

The maintenance checks and emergency scenarios to be encountered are provided in Table 5.1. Housekeeping data is provided by the sensors described in subsection 4.8.2.

Table 5.1: Maintenance and emergency procedures

Type	Type	Approach	Frequency
Regular inspection	Corrosion	Inspection on ground	Every five years
	UV radiation		
	Wire performance		
	Internal fogging		
	Wire attachment points		
Regular inspection	Gas leakage	Atmospheric sensor group	Daily by housekeeping data
	Solar panel performance	Electrical sensor group	
	Electrical system performance	Electrical sensor group	
	Balloon performance	Balloon sensors group	
Emergency procedures	Troubling weather conditions (e.g. tornado)	Indication by weather forecast	After first indication within 24 hours
	Wire snap	Indication by power outage	
	Ballonet failure	Indication by balloon sensor group	
	Communication failure	Indication by some or all sensor groups	
	Fatal damage due to lightning	Indication by power outage and/or electrical sensor group	

5.2. Manufacturing, Assembly and Integration Plan

The production plan dictates the steps to be taken in order to produce the full system, it is shown in Figure 5.3. It shows concurrent assembly timelines for the balloon, sea platform and tether. These parts are required separately before the commission. The focus is on the constituent parts and key materials

²"NHC Issuance Criteria Changes for Tropical Cyclone Watches/Warnings", National Oceanic and Atmospheric Administration, accessed on 24-01-2023, https://www.nhc.noaa.gov/watchwarn_changes.shtml

required.

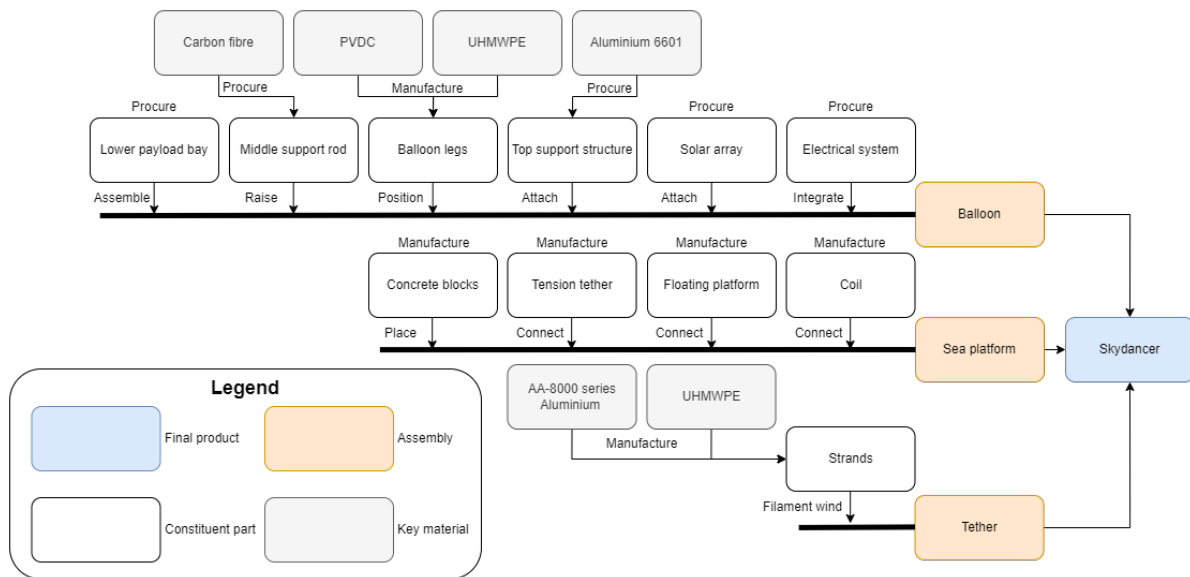


Figure 5.3: Production plan for Skydancer

Manufacturing

Most of the constituent parts are to be bought as shelf products. These would include electronics and the support structure for the top balloon. These are all off the shelf products or are estimated to be within 3 years. These require no new methods of manufacturing since these have an already proven concept. Other components such as the solar panels are to be procured in arrangement with a future plant. A cost breakdown and economic roadmap is presented later in section 8.2, however generic manufacturing aspect must be taken into account regardless. It should also be noted, that if applicable a lean manufacturing approach should be adopted to make the production as sustainable as possible.

The solar cell cost and performance estimations are based on an efficient, high production volume plant. For best performance, the lattice defects must be minimised. Improper cells are more susceptible to thermal cycling degradation, which endangers the mission in both effectiveness and long-term performance. The substrate recycling as described in the proposed manufacturing process is both key to the cost of the system as well as the sustainability goals. These aspects are to be taken into special consideration with the manufacturer.

The balloon itself will consist of PVDC and UHMWPE as explained in subsection 4.6.4. The inner part of the skin will be made of PVDC. This material will reduce the leakage of hydrogen significantly to a level that is acceptable. The outer part of the skin will consist of UHMWPE for load carrying characteristics. They will be joined together to form one skin by the use of an adhesive material. How exactly and what adhesive material will be decided in future design stages.

On a first glance, the size of Skydancer seems too big to manufacture the skin efficiently. This is however deemed not a problem. To this day one of the biggest balloons, "Big 60", is made by NASA³ in 2017. It had a total volume of 1.7 million m³, considerably larger than Skydancer's 50 thousands m³. Moreover, Skydancer will have twelve gas bags, instead of one big balloon, improving the ease of manufacturing. Also, the skin of this balloon is almost the same thickness, proving manufacturing of the balloon is of no issue.

The tether is however a completely new concept, as it is meant to be capable of carrying loads and

³"Touchdown! NASA's Football Stadium-sized Scientific Balloon Takes Flight". NASA. <https://www.nasa.gov/feature/goddard/2018/touchdown-nasa-s-football-stadium-sized-scientific-balloon-takes-flight>

transmitting power over long distances. UHMWPE materials are lightweight and have high specific mechanical properties, thus making them ideal. However, as they are non-conductive, another material would need to be used for providing an electrical path, i.e. aluminium, for its excellent conductive qualities and specific weight. These two materials can be used together by combining the fibres of UHMWPE with strands of aluminium and the manufacturing technique of filament winding. The resulting blended filament can then be wound into larger diameters and eventually the final tether dimension ⁴.

Lastly, the sea platform needs to be manufactured. It consists of three big parts as is described in section 5.1. The concrete blocks can easily be manufactured and same is possible for the connection tethers, for which the material can be decided upon later. The floating platforms have to be worked out in more detail in the future to more precisely define the production plan and material selection. The same is true for the coil.

Assembly

After manufacturing, all components need to be assembled into one product. Before this quality checks should however be performed, this is described in more detail in Figure 3.1 in the lower left of the figure in section 3.1.

Assembly can be done at different levels. The assembly of the sub-sub components can be done at factories and at a smaller scale. After this is done the assembly of the final product needs to be performed and quality checks need to be performed. Due to the sheer size of the final product, the assembly can not be done before it arrives at its final destination, as is explained in section 5.1 in more detail. This would require the workers who perform the assembly to work at the sea platform instead of at a factory.

When it comes to attaching the tether to the ground station setup and Skydancer, an analogue can be drawn to rope joining and termination methods. While knots tend to be prevailing due to their ease in making them, they drastically reduce the effective breaking strength of the tether at the endpoints due to stress concentration and out-of-plane loads being exerted on anisotropic fibers⁵, by up to 60%. Splicing is an alternative that involves reinserting the tail end of a rope into itself and can better retain the breaking properties of the material (about 20%). Given that a solid core tether is used however, special care needs to be taken to lock the splice at the ends, and by having a hollow core at the end [57]. The eye made by the splice may then be latched onto a swivel or eye-bolt-like structure.

5.3. Resource Allocation

This section shows the division of the technical resource, specifically the mass and power budgets. There are also some contingencies taken into consideration for the possible changes that could be included in the further design stages.

5.3.1. Mass budget

The mass budget is essential for the sizing of the balloon, mainly the volume sizing and the tether design. The iterations started with assumptions for size and drag for the balloon to calculate the mass and size of the tether. This led to the resizing of the top balloon itself, for which the structure, skin and payload and solar cells are dependent. A few iterations have been performed to close in on a converging mass. So essentially, everything is inner connected, except the payload which is mostly independent of the rest. The final mass budget can be seen in Table 5.2.

⁴"E-Textiles". Bally Ribbon Mills. <https://www.ballyribbon.com/products/e-textiles/>

⁵"Strength reduction of textile materials by knots". Edelrid. <https://edelrid.com/int-en/knowledge/knowledge-base/strength-reduction-of-textile-materials-by-knots>

Table 5.2: Engineering mass budget

Component/subsystems	Mass (kg)	Margin (%)
Solar cells + backplane integration	1600	5
Electrical payload	85	10
Top structure	1200	10
Middle rod	80	20
Skin	160	10
Payload	200	20
Tether	1800	10
Total	5125	-

The table displays that there are 3 major beneficiaries, being the solar cells, the top structure and the tether. This is leading to the top requirements, which are the harvesting and transportation of solar energy. The top structure is the main component for carrying loads of the full system, since the loads from the wire carry through the middle rod and dissipate the load over the entire structure.

Moreover, the margins show the certainty in each subsystem of how detailed it is and what is expected to still change. Since this report is on the concept design of a balloon, there might still be substantial changes. There is high confidence in the solar cells that Skydancer will be utilising because these have been studied a substantial amount and are already being used on current space missions. The structure is still due to change, and more analysis is required, for example in vibrational modes. Lastly, the payload is not finalised yet, there could be an addition of ridesharing scientific payload or the inclusion of a bigger transformer.

5.3.2. Power budget

The power system is designed to provide 1 MW of energy at the end of life. The main consideration is the selection of solar panels and their sizing. The solar arrays will deteriorate over their design life of 25 years, due to environmental factors like UV radiation. The power delivered from the start is therefore considerably higher. The efficiency at beginning of life has been calculated to be close to 32.86 % and at end of life 28.75 %, this is a change of approximately 12 %. The division of the losses and the transmission can be followed in seen in Figure 5.4.

Besides the photovoltaic losses, there are also other minor losses. The distribution losses are set at 0.5 % of the incoming solar irradiance, from which the system uses 185 W. Moreover, there are losses due to the tether, which are described in section 4.3, and result in a loss of 1.47 %. The last loss is the use of the uplink from the ground station. This results in a total efficiency at BOL of 32.2 % and at EOL of 28.2 %.

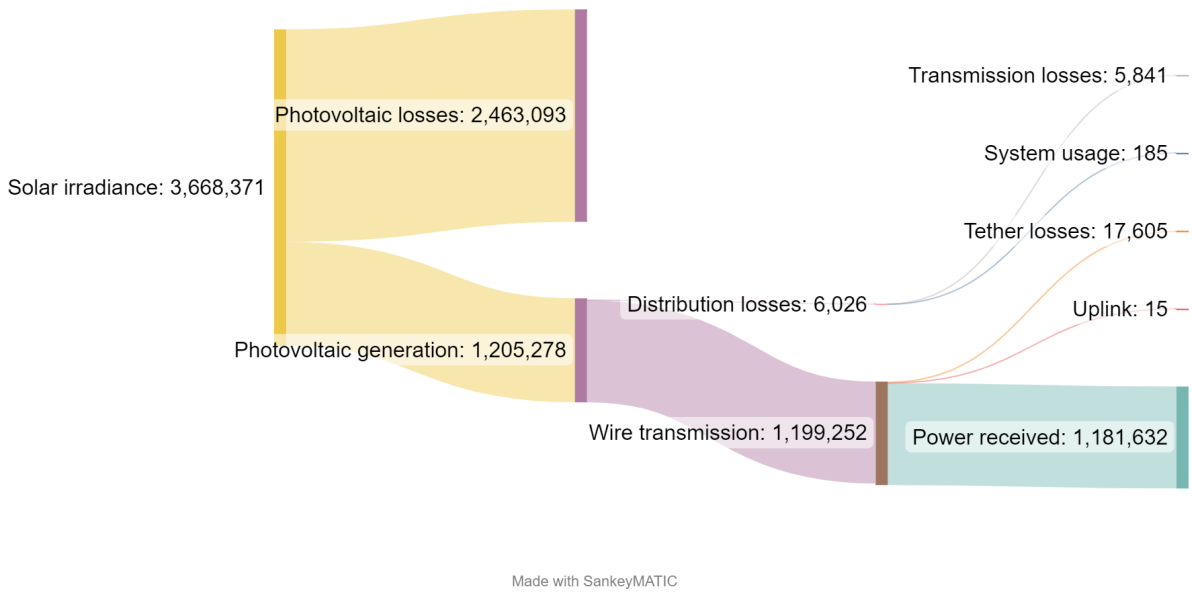


Figure 5.4: Power breakdown in Watts

Table 5.3: Updated power budget with margins

System components	Power (W)	Margin (%)
Photovoltaic losses	2,463,093	5
Transmission losses	5,841	15
System usage	185	20
Tether losses	17,605	10
Uplink	15	10

Just like the margins for the mass budget, Table 5.3, there is high confidence in the photovoltaics and their losses. The transmission losses might require adjustment, an estimate has been made based on similar systems. However, no calculations have been made to the extent of the losses through the wiring of the balloon itself will be. Finally, the margin for the system usage, so the command and data handling module, is rather high since there might still be substantial changes.

5.4. Project Design & Development Logic

An initial plan for the activities to be done after the DSE is made, and the logical flow between them is shown in Figure 5.5. Flow is shown between the different phases (validate the initial design, further design, verification and validation, certification, construction and delivery product) and between the activities in each phase. The design & development logic considers activities in the categories of design, verification and validation, certification and production, starting off with the validation of the initial design before the detailed design of individual parts and assemblies.

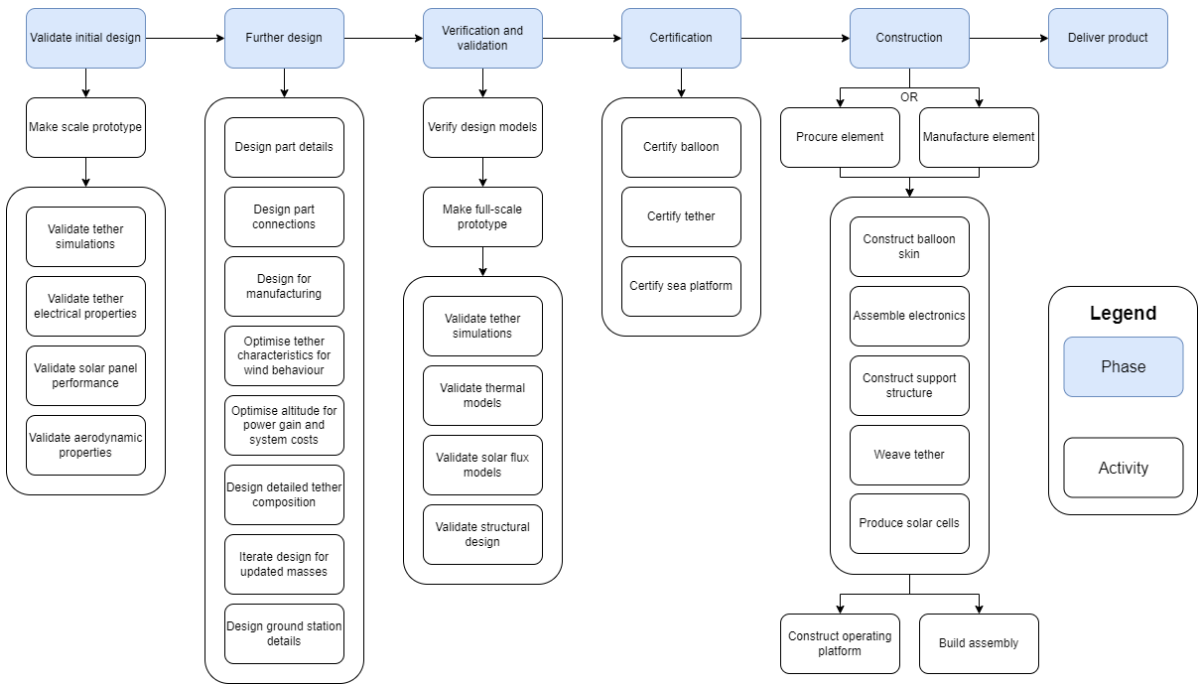


Figure 5.5: Project design and development flow diagram

5.5. Project Gantt Chart

The project Gantt chart also presents the post-DSE activities but also shows a (first version of a) time planning. It contains the duration and starts and end date of each task. Work Breakdown Structure identifier numbers are counted from 5 onwards, as the DSE Gantt chart ended at task 4. Additionally, it defines relations between tasks to show when a task can happen at the earliest. Critically, the schedule for the post-DSE activities is finished in February 2027, which allows the system to be operational in November 2027 (within 5 years after the start of the project, as specified by requirement SBD-SCH-01), even with minor delays in some tasks.

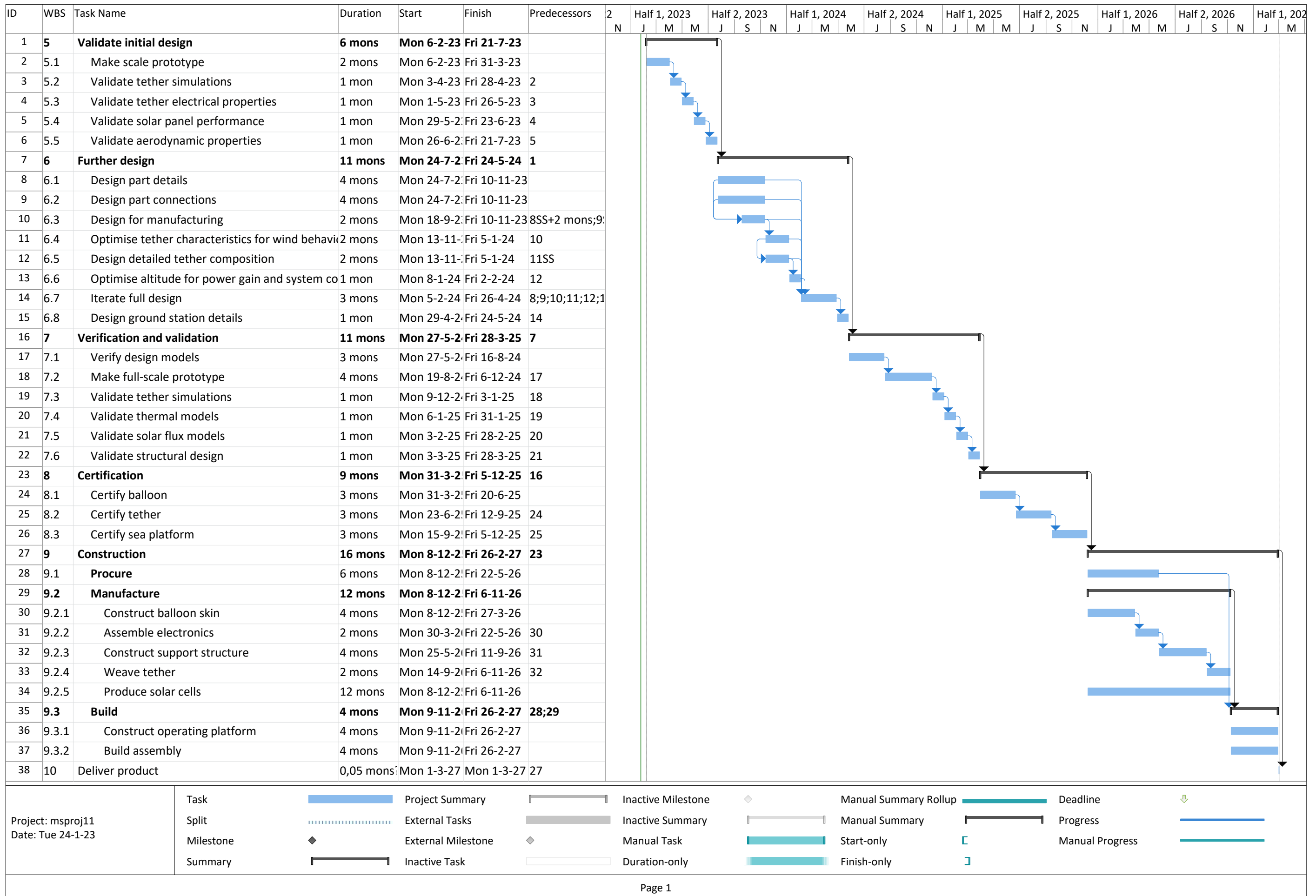


Figure 5.6: Gantt chart for the activities to be performed after the DSE

6 | Design Overview

This chapter displays the total design overview of the stratospheric balloon design. It goes more in-depth for the non-technical aspects of the design and analysis of the performance of the system, regarding the sustainability approach and the performance of the balloon. section 6.1 displays the hardware and software flows from components and systems. section 6.2 shows the final sizing and layout of the final design of the Skydancer. section 6.4 explains the verification and validation of the full system, where further tests, reviews or analysis are needed. section 6.3 analyses the carbon footprint of the balloon over its lifetime for the different subsystems. section 6.5 displays the operational performance from the side of solar harvesting and its transmission. section 6.6 elaborates on the reliability, availability, maintainability and safety of the product. And lastly, section 6.7 investigates the sensitivity of the design when parameters are changed.

6.1. Configuration & Lay-out: H/W and S/W diagrams

The hardware diagram shows all components of the system that require a resource. This is mostly power, but also includes data lines and the hydrogen. They are interconnected to show the flow of resources within the system. It is shown in Figure 6.1. The software diagram shows the interactions between the components of the system which the software must accomplish. It serves to illustrate the mutual relations of the systems constituents. it is shown in Figure 6.2.

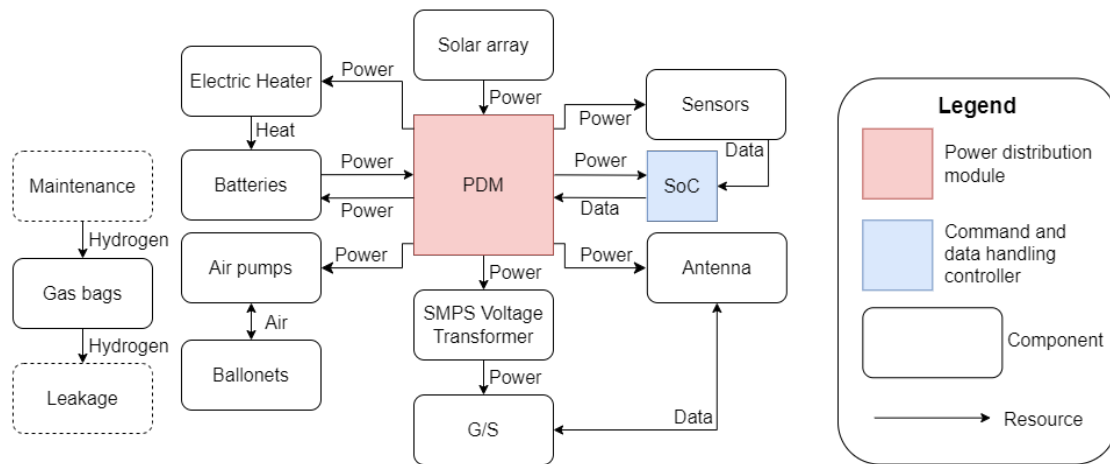


Figure 6.1: Hardware block diagram

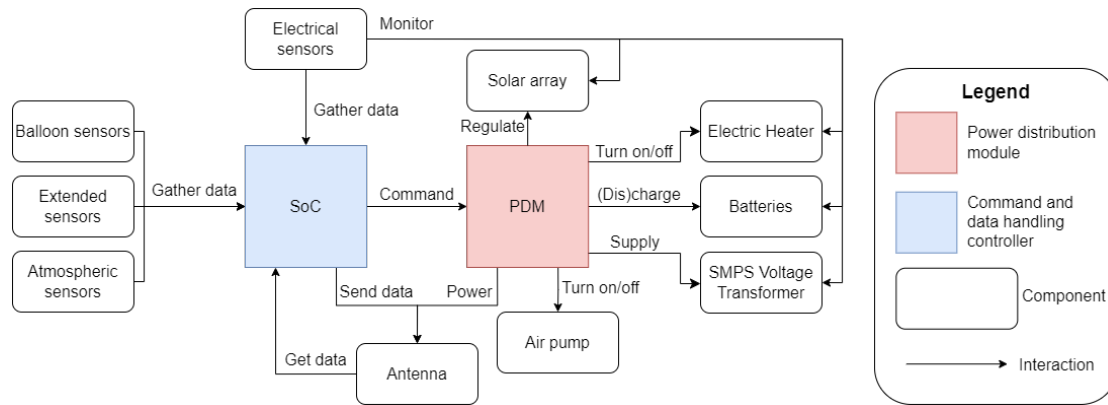


Figure 6.2: Software block diagram

6.2. Configuration & Lay-out: Structure of the SBD

Once structural parts have been sized, a CAD model has been created for the SBD. All created parts have been created up-to-scale, apart from the tether, which is enlarged for better visibility. Payload structure is larger than required to accommodate all the payload as well, and the actual sizing and design for a payload of such scale would be too detailed at this design stage. The model therefore portrays expectations of a possible payload configuration, given the required payload volume. Solar array thickness is very small (< 1 mm) and not taken into consideration for this model. The SBD dimensions for each component are summarised in Table 6.1.

Table 6.1: Final dimensions of the SBD

Part	Length	Width	Height
Balloon	72 m	72 m	18 m
Central rod	14 cm	14 cm	21.2 m
Curved beam	38.6 m	5.7 cm	12.2 cm
Compression rod 18 m	2cm	2cm	22.8 m
Top beam	29.1 m	4 cm	8cm
Solar Array	58.2 m	58.2 m	-

Values are derived from the CAD model. The model itself is presented in figures 6.3 to 6.7 that feature isometric, cross-section, top view, side view and exploded views.

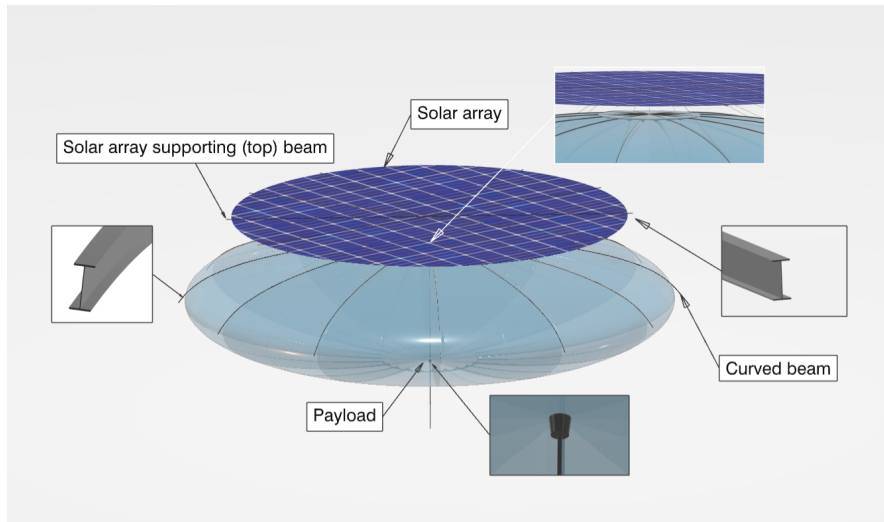


Figure 6.3: Isometric view. Cross sections of top and curved beams are shown. The payload is hidden behind the balloon skin.

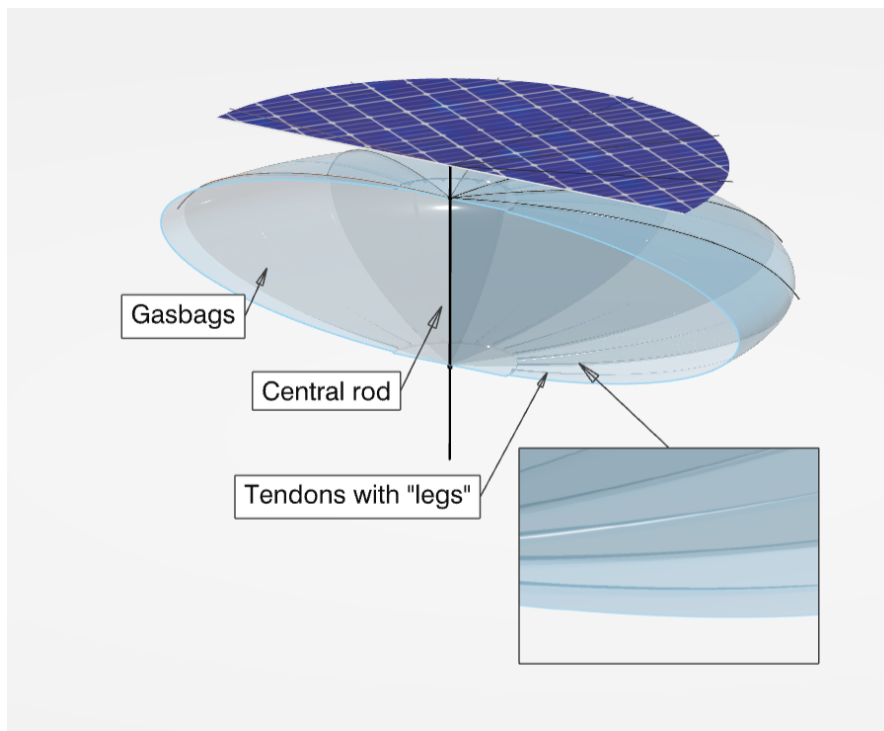


Figure 6.4: Cross-section view. The cutting plane is located at the middle section, and is twisted under an angle that allows to inspect internal structure of the gasbags.

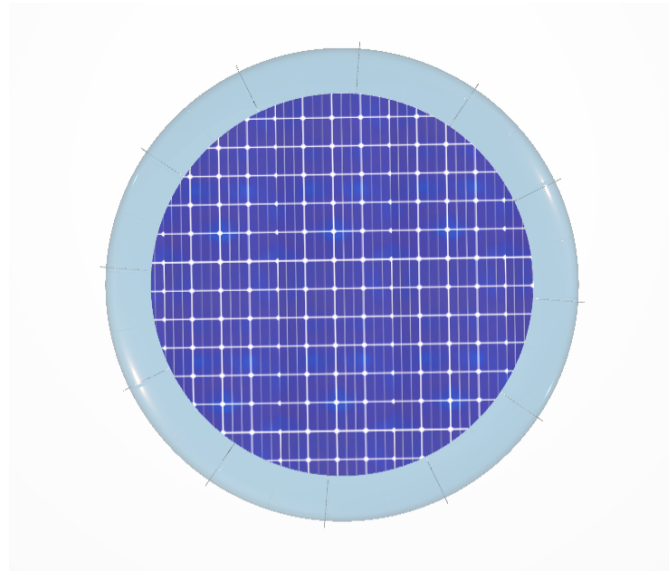


Figure 6.5: Top view. At the outer balloon edges, longer supporting rods would be needed to enable flat layout of the solar panels, so the radius of solar panel plate is smaller than the radius of the balloon.

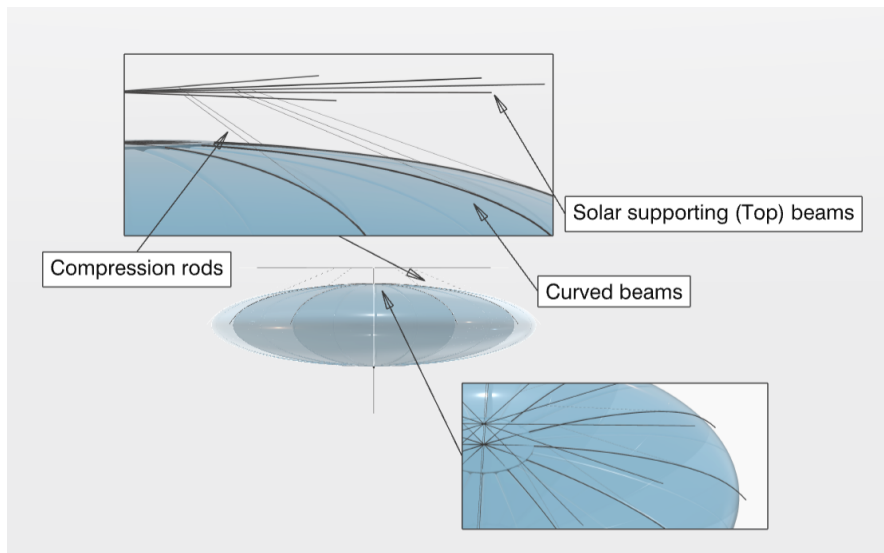


Figure 6.6: Side view. Note that the solar panels are not shown in this picture, which allows to have a better look at the configuration of the top structure

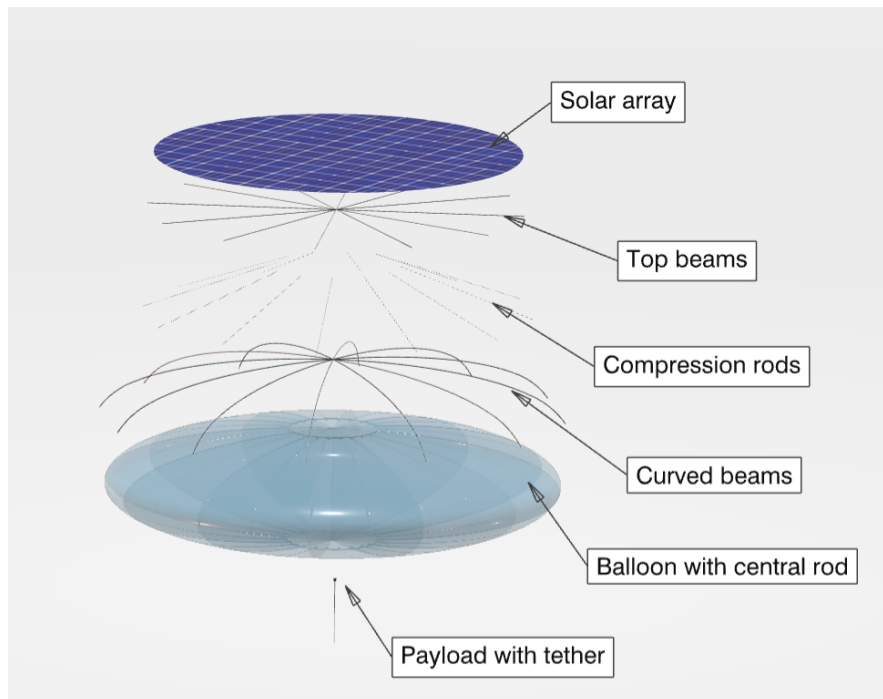


Figure 6.7: Exploded view. Top beams, compression rods and curved beams compose "Top structure". Central rod is inside of the balloon.

6.3. Carbon footprint

The life-cycle carbon footprint of the SBD is provided in this section.

First of all, the amount of CO₂ emitted by the production of the materials is calculated. The values used are depicted in Table 6.2.

Table 6.2: Carbon footprint SBD materials

Material	Fraction of CO ₂ emission per material [kgCO ₂ /kg] [3][58][59] ^{1 2}	Mass [kg]	Recycle factor [-] [60]	CO ₂ emission [kg]
Solar panels	6.5	1,200	0.8	6,240
PVC	3.5	43 (Electrical) + 5 (Air pumps)	0.5	84
Silicon	9.9	43 (Electrical)	0.5	213
Aluminium	13	20 (Payload) + 5 (Air pumps) + 178 (Structure)	0.15	396
CFRP	18	450 (Support solar panels)	0.5	4,050
Copper	4	50 (Transformer) + 20 (Air pumps)	0.15	42
Steel	1.85	50 (Transformer) + 20 (Air pumps)	0.15	19
UHMPWE	3.5	1,613 (Wire) + 135 (Skin)	0.5	3,059
PVDC	3.5	25 (Skin)	0.5	44

Hydrogen is to be produced in a carbon neutral manner. The total amount of CO₂ expelled by material production is 14,147 kg.

The other components contributing to CO₂ emissions and their magnitude are listed in Table 6.3. Moreover, the total carbon footprint is provided: 266,612 kg of CO₂.

Table 6.3: Carbon footprint SBD

Component	CO ₂ emissions [kg]
Materials production	14147
Manufacturing (10% of materials production)	1415
Transportation product to site (from Shanghai to Jakarta) ³	175
Maintenance (4 times transportation)	700
End-of-life (same as transportation)	175
Ground segment (off-shore structure) [61]	250000
Total	266612

For renewable energy, the carbon footprint is often provided in the unit 'gram CO₂ per kilowatt-hour'. The predicted power output for this product's 25 year lifetime is 52 GWh, resulting in a carbon footprint of 5.4 gCO₂/kWh.

6.4. Verification & Validation

With a more detailed design of the individual subsystems baselined, steps on verification and validation of the product need to be performed. First verification and afterwards validation will be addressed.

6.4.1. Product Verification

Product verification is done by verifying compliance with the SBD requirements, listed in chapter 9. The three methods used for verification are described below [62]. The proposed

verification method used for each requirement is presented in Table 6.4. The full design approach has a lot of similarities with other HAPS designs, such as Zhang et al [30] and Akita [31]. Using similar approaches as these gives an indication that the design approach is verified as well.

- Test: testing (sub)system on ground within reasonable time and money constraints.
- Analysis: establishment and analysis of the mathematical or computational model.
- Review of design: inspection of design documentation or product

Table 6.4: Verification Matrix. Requirement statements can be found in chapter 9

Requirement ID	Verification Method	Verification Method Description
SBD-PWR-01	Analysis	Simulations and calculations can be done to verify power generation met amidst operating conditions
SBD-PWR-02	Analysis	Simulations and calculations can be done to verify power transmission met amidst operating conditions
SBD-PWR-05	Analysis	Calculations can be done to estimate losses
SBD-PWR-06	Review of design	Prove by reviewing the purpose of components used in power conversion
SBD-POS-01	Test	Emulate environment conditions in scaled tests and relevant sensors' abilities to operate
SBD-POS-03	Test	Emulate environment conditions in scaled tests and relevant sensors' abilities to operate
SBD-POS-05	Test	Emulate environment conditions in scaled tests and relevant sensors' abilities to operate
SBD-POS-06	Test	Emulate environment conditions in scaled tests and relevant sensors' abilities to operate
SBD-POS-08	Analysis	Simulations can be used to integrate forces experienced throughout mission life
SBD-POS-09	Analysis	Simulations can be used to integrate forces experienced throughout mission life
SBD-POS-12	Test/Analysis	Scaled tests may be performed. Calculations and numerical models demonstrate controllability
SBD-POS-13	Test	Emulate environment conditions in scaled tests and relevant sensors' abilities to operate
SBD-POS-14	Test	Emulate environment conditions in scaled tests and relevant sensors' abilities to operate
SBD-COM-02	Test	Emulate environment conditions in scaled tests for antenna directionality losses
SBD-COM-03	Review of design	Follows from link budget parameters
SBD-COM-05	Test	Emulate environment conditions in scaled tests for antenna directionality losses
SBD-COM-06	Review of design	Follows from link budget parameters
SBD-COM-07	Review of design	Follows from link budget parameters
SBD-COM-08	Review of design	Follows from choice and design of antenna
SBD-STR-01	Analysis	Loading calculations and simulations can be used to show operational stresses are under material yield stresses

SBD-STR-02	Test/ Analysis	Small-scale, accelerated testing can be done to check resistance to light of materials. Calculations based on analytical and empirical models may be used.
SBD-STR-03	Review of design	Technical drawings and system architectures can be referred to
SBD-STR-04	Test/ Analysis	Scaled testing and multiphysics simulations can be done to check mission performance in various environmental conditions and anomalies
SBD-STR-05	Analysis	Thermal models can be used to attain temperature distribution
SBD-SUS-02	Review of design	All energy used should be generated by onboard solar array
SBD-SUS-03	Review of design	Decommissioning stage should be designed to not produce any waste products
SBD-SUS-05	Review of design	Review ecological metrics of used materials
SBD-SUS-06	Review of design	System interfaces' adaptability and compatibility requirements shall be reviewed
SBD-SUS-07	Analysis	Calculations of emissions can be done for various stages of the project
SBD-SUS-08	Review of design	Check recyclability characteristics of materials used
SBD-COS-01	Analysis	Market analysis to evaluate costs and revenues can be done
SBD-COS-02	Analysis	Market analysis to evaluate costs and revenues can be done
SBD-SCH-01	Review of design	Check product release and resource allocation
SBD-SCH-02	Review of design	Check product release and resource allocation
SBD-SCH-03	Review of design	Check product release and resource allocation
SBD-SCH-04	Review of design	Check product release and resource allocation
SBD-REG-01	Review of design	Check manufacturing guidelines and regulations documents
SBD-REG-02	Review of design	Check logistical guidelines and regulations documents
SBD-REG-03	Review of design	Check operational guidelines and regulations documents
SBD-REG-03.01	Test	Perform voltage measurements of DC power lines
SBD-SFT-01	Analysis	Perform RAMS analysis
SBD-SFT-01.01	Analysis	Perform RAMS analysis
SBD-SFT-03	Analysis/Review of design	Perform RAMS analysis, incorporate exclusion zone constraints into simulations

6.4.2. Product Validation

To validate the product, multiple tests need to be performed to check if the product is working as intended. Several small scale tests can be performed by increasing the size of the test to reduce the cost of testing. For example, a small scale test of 1 kW power generation at 2 km altitude can be performed. After this test is successful it can be scaled up to 1.5 kW at 3 km altitude. This trend can be gradually built up till the intended end product is reached. Using this approach will result in lower costs needed for validation testing, but also for verification since this does not require making the final product yet. Data obtained with these small scale tests will be used to calibrate the design and software used in the design process.

Doing small scale tests will also be good practice for workers to practise the manufacturing of the product, improving the learning curve and eventually reducing manufacturing costs.

6.5. Performance Analysis

With the final balloon design parameters and preferred location, the operational performance of Skydancer can be provided. The main measure of performance is power generation, which flows directly from the project mission statement, and hence power will be further addressed in this section. The design parameters for power generation are applicable for 18 km altitude and are designed to comply with weather conditions on the 28th of February at the Pacific Asia location. At the design altitude of 18 km, the solar array should be able to generate 7287.6 kWh for BOL condition, which was presented as a power breakdown in section 5.3. The performance of the design degrades over its lifetime. Only a fraction of solar energy will be usable at the end of life. The breakdown of transmitted energies and efficiency losses are visually presented in Figure 6.8. Here it is shown that solar panels would generate 6353.8 kWh on the day of reference, at the end of life.

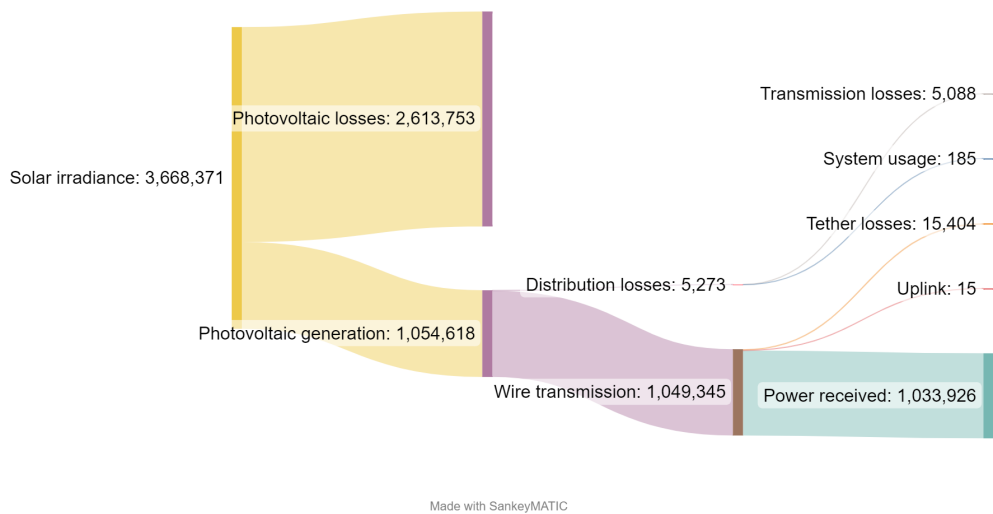


Figure 6.8: End-of-life power distribution for peak operating conditions (in Watts).

Starting at 18 km altitude, the wind profile model dictates that the balloon drifts 4.89 km away from starting position, as well as down to an altitude of 16.82 km. This can be seen in Figure 6.9.

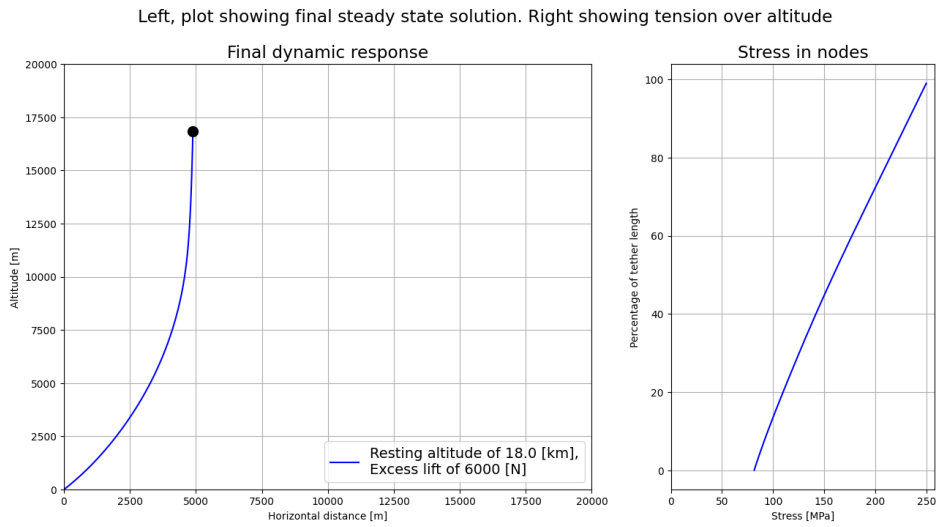


Figure 6.9: Dynamic response of the final design to incident wind profile

With the design parameters, the stress in the tether does not exceed $\frac{1}{4}$ th of the tensile strength. If such a downward drift were to occur for long periods of time, the power generation would not suffer much. A full day at 16.82 km still yields 7270.9 kWh for BOL conditions. At the design altitude, the temperature and power generation response is presented in Figure 6.10.

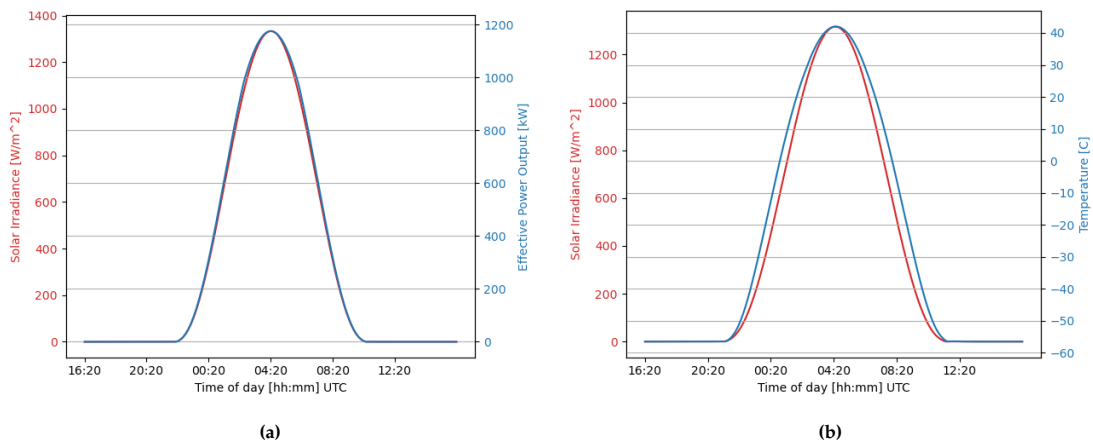
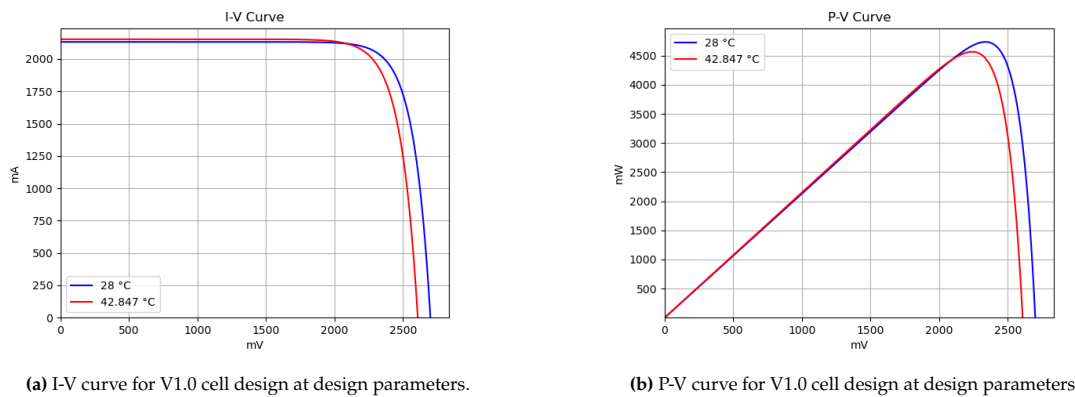


Figure 6.10: Temperature and power generation response at design parameters (wind speed of 5 m s^{-1}).

The electronic response of the solar cells is given below in Figure 6.11, where the influence of the cell temperature on the efficiency can be observed.



(a) I-V curve for V1.0 cell design at design parameters.

(b) P-V curve for V1.0 cell design at design parameters

Figure 6.11: Performance curves for the V1.0 cell design for peak operational conditions versus standard.

While the performance of the balloon depends on various varying factors, such as the wind profile, temperature (cooling capabilities), its life (degradation), date and time; the overall performance should remain satisfactory and steadily decrease throughout the years. Moreover, the life expectancy of the balloon should be taken into consideration, and possibly increasing the structural performance of the Skydancer would allow for a longer, but less efficient power generation, which would be profitable since the running costs are expected to be much lower than the development and deployment costs.

6.6. Reliability, Availability, Maintainability, and Safety

This section elaborates on the reliability, availability, maintainability, and safety considerations of the product. Collectively, they indicate the utility and life-cycle considerations of the system, and generally also with respect to the system's composing elements.

6.6.1. Reliability

Reliability represents the probability of a product performing its intended function, under operating conditions, without failure for a given period of time. With regards to the prospective components of the system, the onboard electronics and electrical components are well-defined examples which showcase the importance of being reliable, especially given the operational life-time.

Bypass Diodes

The SM74611 bypass diodes used, mentioned in subsection 4.1.2, are essential in maintaining the functionality of the photovoltaic array. Thus, their cumulative reliability should be acceptable for a system lifetime of at least 25 years. Considering that two diodes - with one being redundant - are used in each of the 22,493 panel elements, the probability of failure can be found, with $F(t) = 1 - e^{-\lambda t}$, where λ represents the constant failure rate over time. According to Texas Instruments' documentation for the SM74611KTTR⁴, λ^{-1} (mean time between failures) can be found to be 4.762×10^8 device-hours, for an estimated usage temperature of 55°C and activation energy of 0.7 eV. However, this reference value is higher than the expected operating temperature of 44.6°C, which according to the Arrhenius equation, a formula that correlates temperature to

⁴"Quality and Reliability". Texas Instruments. <https://www.ti.com/quality/docs/estimator.tsp?partType=tiPartNumber&partNumber=SM74611KTTR#resultstable>

the rate of an accelerant (seen in (6.1)), λ^{-1} should increase - thus increasing the overall reliability. Using the equation, the new estimate for λ^{-1} is $1.04 * 10^9$.

$$AF = \exp\left(\frac{E_a}{k} * \left(\frac{1}{T_{low}} - \frac{1}{T_{high}}\right)\right) \quad (6.1)$$

For attaining the probability of success of a redundant pair, $R_p = 1 - (F)^2$, where F represents the failure rate of the components. For a series, the equation becomes $R_p = 1 - N * F^2$, with N being the number of series elements and the quadratic relation coming from the additional redundant diode being used per panel. F can be found by the probability of failure equation with $t = 109500$, an approximate value of operational hours for 25 years of operation. This leads to $F = 1.053 * 10^{-4}$. For N being 22,493, as those are the number of panels in series in the entire solar array, the value of R_p is finally found to be 0.999751; which represents the reliability of the diode architecture of the entire photovoltaic array during the cumulative operation of 25 years.

Photovoltaic Array

The type of photovoltaic array used would also require a reliability assessment; since a lower than accepted value would mean a need for an improvement in operational durability and can help in identifying possible defects in certain components within the array.

To put the reliability of the array into light, the cell degradation can be used as a model parameter, this in turn can be characterised by the most demanding environmental contributors for the given stratospheric deployment case: temperature, solar irradiance, and especially, Ultra-Violet (UV) radiation. With the additional 2,975 panels used to account for UV radiation (subsection 4.1.5), the reliability of those panels can be found to be $e^{\frac{-1 * 109500}{2 * 109500 * 2975}}$ - or 0.999832. Note that the solar irradiance and temperature contributions are not considered vital in calculating the prolonged failure modes of the solar array.

Nevertheless, for more accurate means of evaluating the combined effect of environmental contributors, accelerated testing could replicate the normal degradation and stress/strain time conditions. Additionally, more elements within the entire photovoltaic system could be modelled; such as passive components, controllers, and individual layer performance. These can help to procure isolative measures to possible failures by cause-effect identification.

Structural Components

For structural components, their fatigue life is essential to understanding the reduction of strength over prolonged periods of time or usage. As an example, the variance in wind direction & magnitude and thermal loads define the cyclic nature of the loads generated by them and may be used as an input for a design and verification strategy to account for fatigue. The expansion and contraction cycle of the balloon due to equilibrium temperature change between days should be investigated, despite it being fractional. Its cycling is infrequent, due to being on a half-day order of magnitude, thus relaxing the accumulated fatigue stress.

6.6.2. Maintainability

Maintainability depicts the probability that maintenance for the system, under operating conditions and resources, can be performed within a defined time interval. Like most space systems, the SBD is designed to be autonomous in operation and service-free, unless unexpected scenarios and emergencies require maintenance to occur.

Despite this, the novelty of the system may give rise to the need for common checks during the initial stages. This will then give affirmation on the expected functionality of the system. The

status of subsystem components can be monitored on a daily basis to check for issues; such as gas leaks, panel performance, and electrical continuity; and can be done with sensor outputs. With emergencies due to weather or natural disaster complications being likely over the course of 25 years, the balloon would be retracted to a safer elevation or to ground. This would have to be done with a high level of certainty and numerous days in advance.

In subsection 5.1.5, an overview of the types of problems that may arise and methods for alleviating them are given.

6.6.3. Availability

Availability acts to consider both reliability and maintainability as a single metric, i.e. the system is operational and repairable within a set timeframe and environment. It is preferred to have as much up-time as possible, since this means actively contributing to the mission goals. Maximising availability could be done by finding the optimum of the product of maintainability and reliability. In subsection 6.6.2 and subsection 5.1.5, it has already been established that the system is intended to function without a regular maintenance cycle - thus reducing time where mission performance requirements are not being met, which would be otherwise considered for such a flight descent profile. Thus, the expected availability is set to increase over the mission duration, due to more certainty in system operation post-inspection checks carried out during the initial release stages.

By incorporating redundant architecture diodes and the means for easily shunting with the bypass diodes in case of string failures, the reliability of the overall electrical subsystem is able to go up significantly higher and also limits downtime. Additionally, as the solar array is also sized to accommodate for the possibility of failure due to UV degradation the prospect of needing maintenance decreases and the probability of meeting mission performance goals (i.e. reliability) increases.

Lastly, the use of safety factors in the structural design (section 4.6 and section 4.4) inherently increases the reliability of the components used and additional considerations in material properties - such as withstanding radiation or corrosion - makes them less prone to needing refurbishment over the mission's course. The low frequency of cyclic stresses also increases the mean time to failure, thus reducing failure rate F and increasing success rate P .

6.6.4. Safety

Safety represents the probability of staying within acceptable grounds of risk, which is a function of risk likelihood and magnitude. The mitigation to ensure system safety can be found using risk analysis techniques to keep risks within acceptance and under monitoring basis. The identification and control schemes for risks on critical subsystems and features of the system can be found in chapter 7. Some notable product-specific risks that are discussed in this chapter are hydrogen safety, operating environment dangers, material degradation, subsystem component failures, manufacturing & logistical issues, and reduction of mission performance.

With regards to the especially essential topic of hydrogen leakage minimisation and thermal stability for altitude safety and reduced ignition potential, the balloon skin permeability has been investigated and the skin thickness has been accordingly sized. Additionally, the photovoltaic arrays and tether have been designed such that internal losses due to impedance, corona and energy conversion - resulting in heat added to the rest of the balloon - are low. The balloon structural layout also allows for thermal relaxation and enables means of heat out-flux.

6.7. Sensitivity Analysis

To investigate the sensitivity of the design for a change in parameters, a sensitivity analysis is performed. This sensitivity analysis will first focus on the influence of certain parameters, mainly the parameters which are most driving for the design. This is done to test the robustness of the design and to see if a change in certain design parameters would still result in meeting the requirements. These considerations are listed in subsection 6.7.1. Afterwards, the possibility of sizing a single balloon for higher power outputs will be investigated in subsection 6.7.2.

6.7.1. Change in Customer Requirements

As select parts of the airspace have to be restricted, a requirement by local government or air authorities can be that this area needs to be further limited. In the current design, the worst case displacement is 5 km, which can be related to the area where a no-fly zone needs to be implemented for planes, depending on their cruising altitudes. If this worst case displacement has to be decreased, the excess lift needs to be increased to allow for more stability in the dynamic model, as described in section 4.4. Increasing the excess lift from 6 kN to 8 kN decreases this worst case vertical displacement to 4 km, decreasing the restriction area with 36%. As a result the tether will weigh 2200 kg instead of 1800 kg and the balloon volume will increase by 10%. This mainly results in a need for a re-designed and optimised supporting structure, but such a change is achievable. It is calculated that this change will result in increased systems costs, providing a total of 3.2 M€, which is mainly due to the increased tether costs.

A second change can be the operational altitude. As of now, the SBD is required to be above 15 km at all times, with a design altitude of 18 km. Increasing this design altitude will cause the balloon to expand further, due to the lower pressures, hence increasing the SBD's volume. This would lead to a larger structural & skin weight and a longer, thicker tether. The solar array weight will decrease a little bit, as the solar flux increases with increasing height, although this change is minor in the range of 0.4% per km. For a large increase in operational altitude, the required hydrogen volume and the tether strength can become limiting, but for a change in the range of kilometers the SBD will still be able to comply with the requirements, although an efficient redesign and re-evaluation is necessary.

Lastly, a change in the balloon gas is investigated. Due to requirements by local governments or safety concerns, it could be imagined that some parties would be interested in the SBD, without being fond of the hydrogen gas inside. Therefore, it is investigated what would happen if this hydrogen were to be replaced with helium. In the operational aspect, this would lead to larger transport and commissioning costs, as helium is way scarcer when compared to hydrogen. Because of the nature of helium, being an inert gas which is only produced as byproduct of natural gas refinement or due to decay of uranium, there is no way to argue that helium is a sustainable option. It also performs 8% worse in lifting capacity, meaning a larger SBD volume is required to lift the same weight of the ground. The configuration and exact sizing of a SBD designed for helium will hence be a bit altered, but no fundamental issues arise from this design change. Lastly, it should be noted that because of the scarcity, the costs of helium are a factor 70 higher when compared to hydrogen. This would lead to a larger system costs of 3.2 M€, decreasing the profitability.

For all three changes in requirements it can be concluded that the system is robust to these changes.

6.7.2. System Sizing

The top level input for the sizing of the SBD originates from the requirement on power delivery to ground. As of now, the SBD has been sized to deliver 1 MW of power to ground. In this part

of the sensitivity analysis, the effect of a change to 2 and 5 MW power delivered per balloon is investigated. The resulting mass budgets are shown in Table 6.5. In the following paragraphs the rationale behind these numbers is given.

Table 6.5: Mass budget for SBD sizing, all values are in kg

Component/subsystems	1 MW balloon	2 MW balloon	5 MW balloon
Solar cells + backplane integration	1600	3200	8000
Top structure	1200	3500*	12000*
Middle rod	80	120	200
Skin	160	340	1340
Payload	200	320	680
Electrical payload	85	210*	515*
Tether	1800	2000	2200
Total	5125	9690	24950

First of all, the area of the solar cells scales linearly with the power to be delivered. Hence, the weight of the solar cells, including the backplane, will also scale linearly. Because of the increase in total system mass, the volume of the SBD will also increase by a lot. Due to these increased loads on and lengths of the supporting structure, the mass of the top structure will massively increase. The 1200 kg found initially was the optimized value for the exact loads and distances of the current design. For these different sizes the structure has not been optimised due to time constraints. However, it is evident that the increase will be substantial, and was estimated to be around a factor 3 for a size increase of factor 2, based on the current structural model. For larger structures it should be researched whether a truss-like structure would be more weight effective than this current structure, which is based on two beams in bending and just one compression rod in between. This could potentially save a large part of the weight listed for the top structure in Table 6.5.

The new masses for the central rod were easily found based on the wire tension, payload weight and central rod length, which could all be estimated with good confidence. It can be seen that the increase of the weight for the middle rod is damped. Next up, the skin weight is related to the volume. Regarding the skin weight, this is related to the volume but also to one requirement on safety. It was established that the SBD should stay up in the air when one of the gas bags malfunctions. Because of this, more gas bags are needed for a larger balloon, as the fraction of excess lift over the total lift decreases. This causes the balloon skin to still boast a relatively large increase in weight.

The payload box at the bottom mainly depends on the transformer, which scales linearly with the power output. Furthermore, it was estimated that the structure of this payload box would increase by a bit as well, resulting in the provided weights. For the electrical payload, this consisted of the diodes and the wiring of the solar panels. The diodes scale linearly with the amount of cells, while the wiring scales at a larger rate. However, for larger solar arrays the wiring weight could be decreased by instead of wiring each chain to the transformer directly, multiple wires can already be combined by small converters.

Lastly, the tether is analyzed. Using the dynamic tether model described in section 4.4 and the new inputs for the different sizes, it was found that the tether was not increasing in weight by a significant amount. This is due to the tension in the tether, necessary for the positional stability, only increasing from 6000 N to 8000 N between the smallest and biggest SBD.

In conclusion, it can be seen that the difference in subsystem weight depends on the nature of

the subsystems. Combining all subsystems, it is concluded that the total weights scales close to linear to the power output. The structures and the skin have a large relative increase, while the relative weight of the tether decreases from 35% to 9%. In this mass budget the items indicated with a star also denote where weight reduction can be achieved rather easily, by implementing the design changes described before.

The dimensions of the SBD for these three power outputs are shown in Table 6.6. The last column, the air gap, is the gap between the solar array and the balloon. It should be noted that the dimensions of the balloon are based on a 1:4 ratio, as this was used in the drag and stability calculations. Because of this, the solar array for the biggest 5 MW SBD has a larger radius than the balloon radius, which would pose structural challenges. Therefore, the SBD would need to be flattened, making the spheroid more oblate. This change will result in changes in drag coefficient, stability characteristics and tether, skin & structural weights. Therefore, further calculations and iterations would need to happen to thoroughly investigate the effects of this size mismatch. However, the figures provided in Table 6.5 and Table 6.6 give an initial estimation and conclusions can be drawn from them.

Table 6.6: Size budget for SBD sizing

Dimensions	1 MW balloon	2 MW balloon	5 MW balloon
Solar array (m ²)	2665	5330	13325
Volume (m ³)	50557	91593	227176
Solar array radius (m)	29.1	41.2	65.1
Balloon diameter (m)	72.8	88.8	120.2
Balloon height (m)	18.2	22.2	30.0
Air gap (m)	3.0	4.0	5.0

In conclusion, scaling the balloon from 1 MW to 2 MW seems like a viable option and there are no fundamental issues that arise. The weight of the structure in this case can probably be decreased by a more thorough analysis or with a truss-like structure. For the 5 MW SBD, not only the structure, but also the balloon itself should be reshaped. This structure would also start the approach of the megastructure scale.

Drawbacks of increasing the scale are the increase in risk and severity of the damage when something goes wrong. Furthermore, a further increase in the size would make the SBD more unpractical and harder to manufacture and commission. However, increasing the scale would also come with some big benefits. First of all, one SBD can serve more households and therefore have a stronger market position. Furthermore, although the manufacturing costs are higher, the commissioning and maintenance costs will see a steep drop when the full constellation changes from 100 to 50 or 20 balloons. This also results in a lower interference with airspace, which could be a requirement or an issue raised by local governments.

Furthermore, the material use of the total constellation will shift. The material used for the solar cells is the same, as the total amount of solar area is designed for 100 MW, but the materials used inside the SBDs and especially the materials used for the tether are decreasing for a decrease in the amount of SBDs. All in all, this sensitivity analysis has shown that it is worthwhile to further investigate the scaling up of the SBD and that no fundamental issues are present for a scale increase in this order. This is mainly due to the lower material usage and the more convincing business case, due to the lower airspace occupation and the greater amount of households that can be powered by one SBD.

7 | Technical Risk Assessment

This chapter covers the technical risk assessment. It is used to have an overview of risks that could rise during the duration of the project. The first step in this assessment is the identification of risks, which is done in section 7.1. Afterwards, the risk mitigation strategies are presented in section 7.2, which also shows the risk maps before and after mitigation.

7.1. Risk Identification

A risk is defined as the possibility that an event occurs which has a negative impact on the project. Assessing and mitigating these risks forms a crucial part of big design projects like this. The technical risks are split up into the following categories:

- **REQ** - *Requirements* - Risks of not meeting the established design requirements.
- **PER** - *Performance* - Risks of not meeting satisfactory performance characteristics
- **RES** - *Resources* - Risks related to not having sufficient resources available.
- **COM** - *Complexity* - Risks due to underlying project complexity.
- **QUAL** - *Quality* - Risks endangering the quality of design

Technical risks have been identified and assigned for each of the above mentioned categories. A risk label has been assigned for each risk, where "TR" stands for "Technical Risk", and letters following after the dash indicate a technical risk category that risks belongs to. The list of risks including their labels and descriptions are listed below. Compared to the Midterm Report [1], the risk TR-PER.11 regarding the tandem balloon failure has been deleted, as it was decided to not use tandem balloons. Furthermore, risk TR-QUAL.01 regarding unsatisfactory communication has been deleted as this was deemed a redundant risk, taking into account the risk regarding communication system failure TR-PER.04. Furthermore the risks TR-PER.07 and TR-RES.06 have been further defined.

Requirements Risks

- **TR-REQ.01** *System cannot deliver 100MW of power*: Since a system of this size is completely novel, there is a possibility of underestimating the project's feasibility and failing to design a system of this size. This could result in a need for integral redesigning of the SBD system which could result in loss of project value, schedule delay and increase in project expenses.
- **TR-REQ.02** *System cannot operate for 25 years*: Due to the lack of past experiences with SBD systems operating for long periods, the design requirement might not be possible to incorporate. Operating for a shorter time-frame would result in lost value of the final design.
- **TR-REQ.04** *System cannot achieve market compliance*: Due to the novelty of this project and the lack of available knowledge, it is difficult to provide an accurate estimate of the project's initial and running costs. On top of that, it is necessary to have an accurate global market prediction, which adds complexity to meeting this project requirement.

Performance Risks

- **TR-PER.01** *Structures failure*: The chosen SBD material shall be "green", which might be more prone to failure compared to traditional structural materials. Damage to the structure can result in the loss of critical elements, resulting in project failure.
- **TR-PER.02** *Attitude and altitude control system failure*: Due to non-functioning sensors (e.g. sensors that cannot work in the provided environment or get smudged / covered), attitude and altitude control might be performed incorrectly. Fixing would require time and budget, and could result in project failure in exceptional cases.

- **TR-PER.03** *Energy collection system failure:* Energy collection system need to harvest solar energy, process, transmit and receive it on the ground. Malfunction of the energy transfer instrument would trigger energy transmission, and hence energy collection system would be nonfunctional. Fixing would require time and budget, and could result in project failure in exceptional cases.
- **TR-PER.04** *Communication system failure:* Broken parts in communication system and network overload or congestion could cause communication system failure. Fixing would require time and budget, and could result in project failure in exceptional cases.
- **TR-PER.06** *Electrical payload failure:* Ruptured internal wire would cause an electrical system malfunction. Fixing would require time and budget, and could result in project failure in exceptional cases.
- **TR-PER.07** *Thermal control failure:* Excessive internal forces can cause a failure in the thermal control subsystem, causing the battery to malfunction, making communications overnight impossible. Fixing if would be difficult, if not impossible, and would require a lot of time and budget.
- **TR-PER.08** *SBD collision with other bodies:* Balloon segments of the SBD might collide with other objects such as planes, drones, birds or other balloons, which must be avoided. Collision would either damage the SBD itself, cause harm to property of other companies, endanger people's lives or make harm to the environment, none of which shall be tolerated.
- **TR-PER.09** *Wire failure:* A torn wire will result in a unrestrained balloon, which would make power transfer an station keeping impossible, hence leading to project failure.
- **TR-PER.10** *Main balloon failure:* A ruptured balloon in operational stage would mean the end of the project, causing the whole structure to crash down to Earth.
- **TR-PER.11** *Tandem balloon failure:* A ruptured tandem balloon will degrade the station keeping performance and increase the stresses in the wire, which could result in project failure.
- **TR-PER.12** *Hydrogen leakage:* Due to the inherent leaking the SBD will have a lower buoyant force over time, causing a force imbalance and loss of altitude.
- **TR-PER.13** *Balloon drifting:* Due to high velocity atmospheric winds and gusts, the system may start drifting away from its intended position, causing extra stresses in the wire.
- **TR-PER.14** *Critical lightning damage:* Lightning impacts can be destructive for the SBD, due to the electronics on-board. Furthermore, upper atmosphere lightning, such as sprites and blue jets can negatively affect the SBD due to the plasma they create in the atmosphere.
- **TR-PER.15** *Material degradation:* The high intensity of UV radiation can have negative effects on material performance. Especially for polymers, photo oxidation makes the material brittle as it causes the chains in this polymer to break.
- **TR-PER.16** *Hydrogen explosion:* Due to the huge amounts of hydrogen being used to lift the design a combustion of a small amount of hydrogen can lead to giant explosion. Resulting in failure of the design or project.
- **TR-PER.17** *Extreme weather:* Extreme weather like hurricanes and storms make it impossible to stay operational.

Resources Risks

- **TR-RES.01** *Inaccurate simulation results* Having inexperienced engineers run the simulations or using a flawed simulation software could lead to inaccurate simulation results. Inaccurate design properties might be translated into the project, which would endanger the functionality of final design.
- **TR-RES.02** *No commercially available simulation/design software:* If existing software is too limited to use for design simulations, then unique software should be developed, resulting in additional expenses and project delay.
- **TR-RES.03** *Receiving flawed components:* Due to unreliable suppliers and manufacturers, critical system components might be delivered untested and in poor quality. Using them could result in design failure.
- **TR-RES.04** *Canceled SBD launching operation:* The launching operation might be canceled due to weather conditions, detected SBD flaws at a pre-launch stage or mistakes of third parties, which would result in a project delay and increased project costs.

- **TR-RES.05** *Unrevealed design flaws*: Due to insufficient verification, validation and limitation in testing facilities (testing is preferred to be performed on the ground due to high costs), some design flaws might be unnoticed. Depending on the flaw, it can both be negligible or catastrophic to the project development.
- **TR-RES.06** *Accumulation of project losses*: As the SBD will be launched from a sea platform, an unsuccessful launch can cause damages to the full sea platform and commissioning boats and cranes. This results in a setback of the project, meaning increase of expenses and a project delay.

Complexity Risks

- **TR-COM.01** *Poor integration of subsystems*: Due to poor management of integration of multiple subsystems and their parameters, the end system might not be functional.
- **TR-COM.02** *Unmet certification criteria*: Due to uniqueness of the project, it does not fit into the standard certification categories.
- **TR-COM.03** *Unmanufacturable parts*: Due to the uniqueness of the project and lack of available manufacturing equipment, manufacturing process might be complicated and costly if there will arise a need to develop new manufacturing equipment or if preferred manufacturing method will be labour-intensive.
- **TR-COM.05** *Poor project acceptance*: The project might not be well-received due to its unclear negative influence regarding sustainability. Since no similar project has been done in the past, is difficult to predict how exactly it could affect global warming, natural habitats and local societies during the operational project phase.

Quality Risks

- **TR-QUAL.01** *Unsatisfactory communication between ground and SBS*: Due to bad weather conditions communication between ground and SBS segment can be difficult for an unforeseen amount of time. This results in the system being unable to receive new commands and send status updates, which could result in system failure.
- **TR-QUAL.02** *Harmed components*: Carefree handling and transportation can harm crucial components. In that case new components would be purchased, leading in extra project costs.
- **TR-QUAL.03** *Balloon degradation to an unacceptable extent*: Balloon can degrade due to the long and cyclic exposure to the sun and influence of external forces (e.g. gusts). That would lead to reduced lifespan of the balloon, hence a loss of project value.
- **TR-QUAL.04** *Engineering/design mistakes*: Due to human error, engineers could make mistakes such as miscalculations or usage of inconsistent values/units. Depending on the severity of a mistake, the negative influence on the project could vary anywhere between negligible to catastrophic.

7.2. Risk Map and Mitigation

To organise these risks, they are presented in a risk map. This map indicates the probability of occurrence and the severity of risk impact. The following risk severity definitions have been used for the different metrics with the risk map [63, 64]:

- **A**: Negligible: Inconvenience or non-operational impact
- **B**: Low: Small reduction of technical performance
- **C**: Moderate: Some reduction in technical performance, impact on mission is manageable.
- **D**: Critical: Mission success is questionable
- **E**: Catastrophic: Mission failure

On the horizontal risk map axis, risk probabilities are indicated. These are the probabilities of the risk occurring throughout the lifetime of 25 years [63]. For the purpose of SBD risk management procedures, the risk probabilities have been defined as follows:

- **1**: Improbable: < 2 %

- 2: Remote: 2-20 %
- 3: Occasional: 20-50 %
- 4: Probable: 50-80 %
- 5: Frequent: > 80 %

This risk map is shown in Figure 7.1. The risks should be moved towards the left-down corner of the risk map by the means of mitigation. Different mitigation strategies can be implemented for each risk. They are presented in Table 7.1 together with estimated post-mitigation risk rank. Risks after mitigation are illustrated in an updated risk map, shown in Figure 7.2.

Table 7.1: Risk mitigation and rankings

Risk ID	Risk	Rank	Mitigation	New rank
TR-REQ.01	<i>System cannot deliver 100MW of power</i>	D4	Design for a constellation of 1 MW balloons which allows for ease of scalability.	B2
TR-REQ.02	<i>System cannot operate for 25 years</i>	D4	Perform extensive literature study, set up strategy for inspection and maintenance every five years and design for EOL.	B4
TR-REQ.04	<i>The system cannot achieve market compliance</i>	C4	Perform an extensive market analysis and an expenditure plan, which would allow to foresee the investment feasibility.	C3
TR-PER.01	<i>Structures failure</i>	E3	Incorporate sufficient safety factors of 20%.	E2
TR-PER.02	<i>Attitude and altitude control system failure</i>	C3	Perform occasional attitude and altitude control checks during operational phase. Indicate and improve the weaknesses during the detailed design stage.	C2
TR-PER.03	<i>Energy collection system failure</i>	E3	Design for redundancy using bypass diodes and blocking diodes in the solar array wiring.	D3
TR-PER.04	<i>Communication system failure</i>	D3	Bring additional communication subsystem.	B2
TR-PER.06	<i>Electrical system failure</i>	C4	Use only certified electrical wires and devices. Ensure that operating conditions (e.g. temperature, humidity) are fulfilled.	C3
TR-PER.07	<i>Thermal control failure</i>	D3	Perform extensive research about the tooling used in the thermal control system. Indicate and improve the weaknesses during the detailed design stage.	D2
TR-PER.08	<i>SBD collision with external bodies</i>	E2	Keep external stakeholders well informed about launching procedures. Design for minimal tether diameter and limited horizontal displacement.	C1
TR-PER.09	<i>Wire failure</i>	E3	Investigate creep and other failure modes, incorporate high safety factors.	E1
TR-PER.10	<i>Main balloon failure</i>	E2	Use 12 gas bags and have the lift of one gas bag be lower than the excess lift.	C2
TR-PER.12	<i>Hydrogen leakage</i>	C4	Use PVDC for the balloon skin as this boasts a very low permeability.	A4
TR-PER.13	<i>Balloon drifting</i>	D4	Design for worst case displacement.	B2

TR-PER.14	<i>Critical lightning damage</i>	E4	Set up an emergency protocol which brings the SBD down to the sea platform within 24 hours. Deploy in locations with lower annual lightning rates. Allow for cloud discharge by the conducting outer tether casing.	D3
TR-PER.15	<i>Material degradation</i>	C5	Set up a strategy for inspection and maintenance every 5 years. Use UV coating or polymer stabilisers	B5
TR-PER.16	<i>Hydrogen explosion</i>	E2	Limit electrical components very near the balloon and decrease any static electricity build-up.	E1
TR-PER.17	<i>Extreme weather</i>	E4	Set up an emergency protocol which brings the SBD down to the sea platform within 24 hours.	B4
TR-RES.01	<i>Inaccurate simulation results</i>	C3	Use only verified and validated simulation software, ensure that it is used as intended by software producers.	C2
TR-RES.02	<i>No commercially available simulation/design software</i>	D2	Research availability of useful software. If it is not accessible, assign resources on creating, verifying and validating in-house software in early design stages	B2
TR-RES.03	<i>Receiving flawed components</i>	D3	Inspecting received components visually as soon as they are delivered.	C2
TR-RES.04	<i>Canceled SBS launching operation</i>	A3	Rescheduling launch date as soon as possible.	A2
TR-RES.05	<i>Unrevealed design flaws</i>	E3	Making and following a detailed verification and validation plan adapted for testing on ground.	C3
TR-RES.06	<i>Accumulation or project losses</i>	D3	Consider launching balloons individually or in small groups.	D1
TR-COM.01	<i>Poor integration of sub-systems</i>	D3	Provide training for system engineers.	D2
TR-COM.02	<i>Unmet certification criteria</i>	D4	Research certification criteria and be aware of it.	D2
TR-COM.03	<i>Unmanufacturable parts</i>	C2	This risk has to be accepted.	C2
TR-COM.05	<i>Poor project acceptance</i>	D3	Provide clear communication to external parties and end users, supported with independent research.	D1
TR-QUAL.02	<i>Harmed components</i>	C2	Implement internal regulations for safe transportation of system components.	C1
TR-QUAL.03	<i>Balloon degradation to an unacceptable extent</i>	C4	Set up a strategy for inspection and maintenance every 5 years. Design the solar panels for EOL performance. Furthermore account for degradation using safety factors in balloon sizing.	B4
TR-QUAL.04	<i>Engineering/design mistakes</i>	C3	Occasionally performed peer-reviews, making and implementing a verification and validation plan.	C2

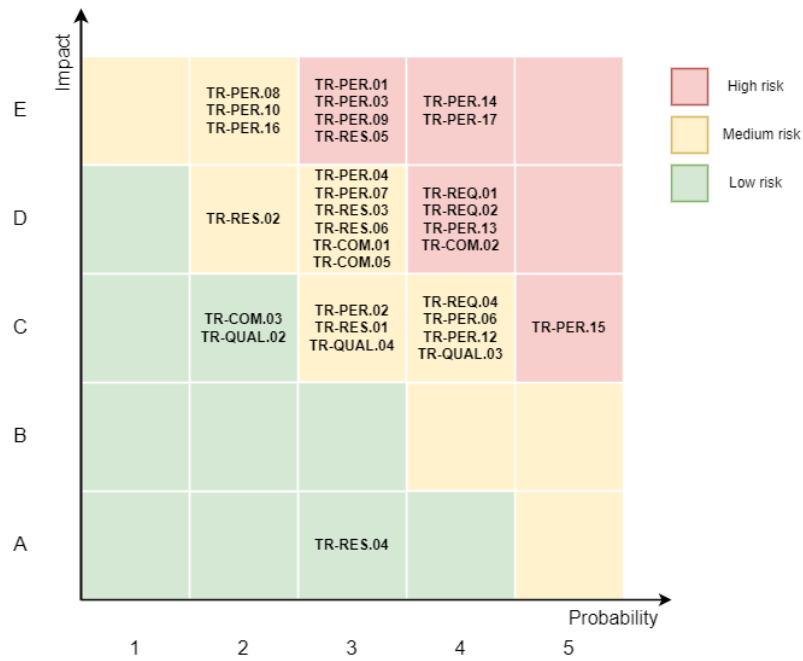


Figure 7.1: Technical risks before mitigation

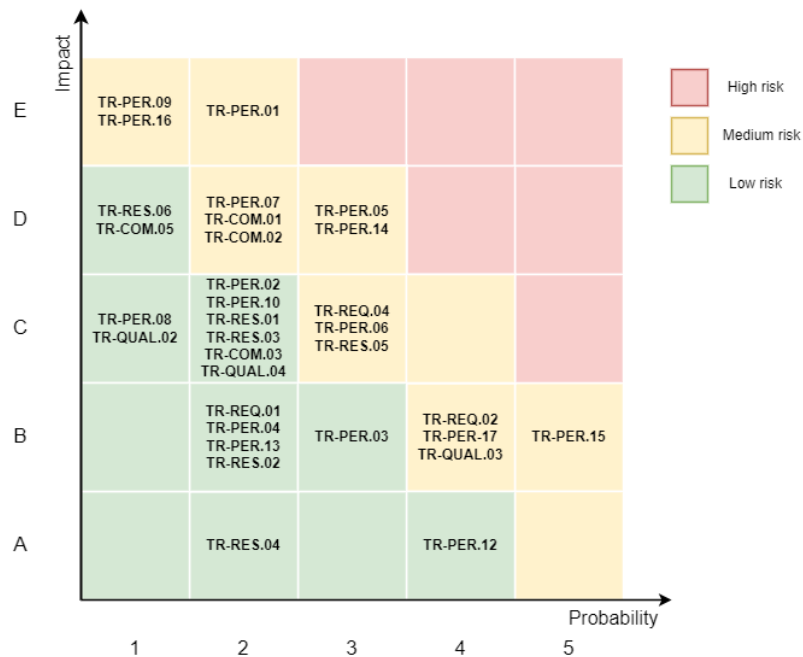


Figure 7.2: Technical risks after mitigation

8 | Market Review

This chapter will evaluate the position of the proposed SBD system within the electricity market. Considerations will be given to the location selection in order to make more specific predictions about a more local energy market rather than the broad global market. This selection of non-tangible benefits of the system will be discussed and a cost breakdown will be performed. Using this, a return on investment calculation will be made and the metric of market compliance is analyzed.

In section 8.1 target market and competitiveness are analyzed. After this, the system costs are analysed in section 8.2. The concluding section will look at the return on investment and determine whether the market appliance is achieved in subsection 8.3.3.

8.1. Market Analysis

There are large differences between regions in the state of their energy market, with some areas proving to be more promising than others due to for example an increasing demand for power. In this section, the location selection is performed and the benefits of the system are discussed together with the challenges and opportunities of the local energy market.

8.1.1. Location Selection

A set of locations was analyzed which were representative of the diverse biomes and weather situations that the surface of the Earth contains. Locations included equatorial areas, deserts or high latitudes. These locations were rated on factors that were considered relevant to the viability of a high altitude solar system and the competitiveness in the local market. The ranking of these locations is tabulated in Table ???. Here the solar flux at 0 and 18 km height are reported. Derived by the program described in section 4.2. These solar fluxes are the average over a year, so the day and night and seasonal cycles are included.

Initially, northern latitudes seemed promising due to the poor performance of conventional solar in such locations. Locations which were located at high latitudes have a high amount of wind potential due to polar vortex or hydropower potential due to elevation differences. These latitudes are also heavily used by airlines, especially in Europe. With a necessary kilometres-wide exclusion zone around the system, this would prove impractical. This viability of other renewable energy sources is an important metric. The fact that the system is not affected by weather patterns as much as ground based solar drove the location analysis as well. In places such as the Sahara desert or Australia, the solar potential is high and the additional cost of an SBD does not weigh up to the marginally higher power production due to less atmospheric attenuation. In these places, the weather is basically of no concern, and thus no large benefit is gained here with a high altitude solar system. The amount of land available in these places also means that the cost of the area for solar panels is a small factor in the total cost, whereas the SBD has a stronger business case where land is scarce.

Shifting the focus to equatorial regions such as Pacific Asia or the Gulf of Guinea an opportunity can be identified. These countries have a limited area which is needed for local food production and living spaces, moreover is filled with valuable rainforests. Furthermore, their economies are developing, which comes with increasing use of energy and thus also renewable energy. Wind potential close to the equator is relatively low due to the lower winds achieved and the cut-in

Table 8.1: Location selection for different regions

Country/region	At sea?	Solar flux at 18 km (W/m ²)	Solar flux at 0 km (W/m ²)	Increase in flux (%)	Hydro?	Wind? ^a	Lightning?	Air traffic? ^b	Share renewable energy (%) ^c
Netherlands	Yes	150	90	67	No	Yes	No	Yes	20 to 40
Mediterranean	Yes	210	140	50	Some	Yes	Some	Yes	10 to 60
Sahara	No	260	175	49	No	Yes	No	Little	Below 10
Caribbean East	Yes	300	210	43	No	No	Some	Some	Below 10
Argentina	Yes	175	110	59	Yes	Yes	Some	Little	20 to 40
Pacific Asia	Yes	300	210	43	Some	No	Some	Some	10 to 20
Gulf of Guinea	Yes	300	210	43	Some	No	Some	Some	Below 10
Northern Australia	Yes	290	190	53	No	Some	No	Little	40 to 60

^aGlobal Wind Atlas'. Last accessed on 24-01-2023. <https://globalwindatlas.info/en>

^b'Proba-V maps world air traffic from space'. Last accessed on 24-01-2023. https://www.esa.int/Enabling_Support/Space_Engineering_Technology/Proba-Missions/Proba-V_maps_world_air_traffic_from_space

^c'Share of renewables in electricity production'. Last accessed on 24-01-2023. <https://yearbook.enerdata.net/renewables/renewable-in-electricity-production-share.html>

speed of these turbines. This, in combination with a small amount of hydropower potential, leaves a gap in a future renewable energy mix which can be filled with high-altitude solar. Although air traffic is present almost everywhere in the 21st century, it is very much manageable at these locations compared to the busy aviation hubs of Europe, North America and Asia. Due to these reasons, the main market that is considered to be entered will be these equatorial markets.

An additional, similar opportunity is that of small islands within the ocean. These islands are often still dependent on imported diesel fuel generators and have little space available. The need for renewable energy will both be an economic and ecological improvement. Due to their remote nature air travel is the least of concern compared to the locations analyzed. Operating Skydancer on these remote islands is financially challenging though. It is determined that the first focus of deployment possibilities are those around the equator for the mainland and only once financially practical, Skydancer can be used for small islands.

8.1.2. System Benefits

The system comes with many advantages over conventional energy sources which will aid the system in achieving market compliance. Some of these are quantifiable but there will be non-tangible effects on the environment in addition to this. These will be discussed in the following section.

Reduction of Pollutants

Conventional thermal power plants are a large emitter of pollutants, both in the form of direct pollutants such as NO_x and SO₂ gasses and also in CO₂ emissions, causing climate change. It is already shown that Skydancer has a significantly lower carbon footprint than other conventional renewable energy sources, as shown in Figure 2.4.

NO_x and SO₂ gasses are harmful to human health and nature. Aside from the implicit cost of these pollutants which are normally not represented in the price of the electricity generated by these fuels, they sometimes lead to actual issues. From 2019 onwards the Dutch government has been in a nitrogen crisis, caused by excessive emissions of nitrogen compounds, which has a negative impact on the natural nitrogen cycle and exceeds the regulations set up by the European Union. The situation is ongoing and there have been emergency laws and tens of billions of euros set aside in order to tackle the crisis. In general, pollutants such as SO₂ and particulate matter will harm human health. This is especially pronounced in cities with heavy smog cover, the incidence of lung disease is much higher than in less polluted rural areas. It is these effects of pollutants on the environment and human health that are not taken into account in the price of polluting fuels. This causes the price to not reflect the negative externalities, which makes for an inefficient market. Quantifying the exact costs is a difficult task as it is nigh impossible to trace back the exact cause of damage caused. Through the statistical analysis, an estimate can be made, although with large margins due to the inherent uncertainties in models. Figure 8.1 shows that the European Environmental Agency provides high and low estimates for the external costs of energy sources, and it illustrates the target consumer base, i.e. those who rely on the relatively more costly sources of generated energy. Skydancer will have a comparable range for the external cost, so very low in contrast with coal, oil and other non-environmentally friendly sources of fuel.

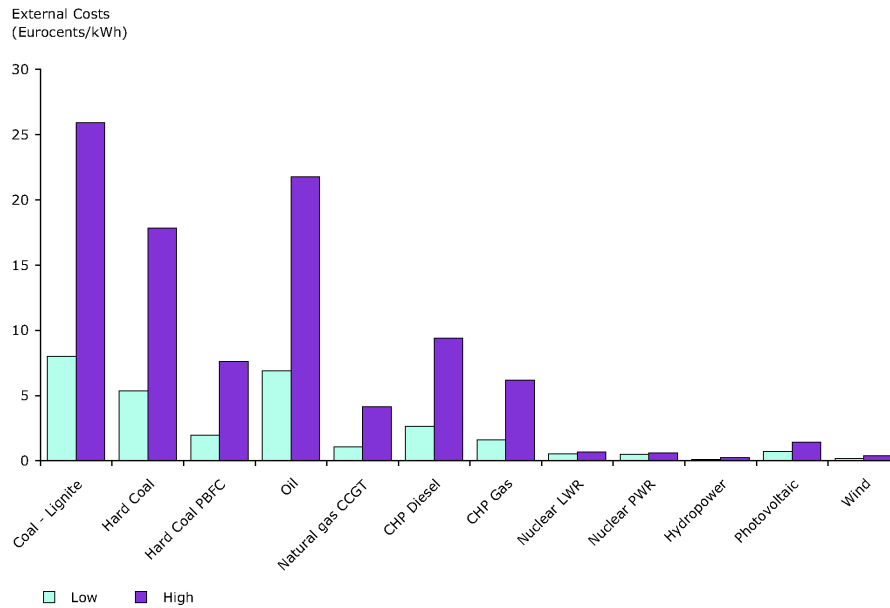


Figure 8.1: Estimated average EU external costs for electricity generation technologies [65]

As expected energy sources that are considered "polluting" have the highest externalities. In addition to the highest carbon emissions per unit of energy coal also produces the most pollutants. An interesting note is that even the lowest estimates for the external costs of fossil fuels exceed the price of new solar and wind constructions throughout the world. This implies that the business case of these energy sources is actually quite poor when looking at the full-system costs and that society indirectly subsidizes it by bearing the negative effects for free. The external costs can be viewed as an additional cost of the fuel or a subsidy for renewable sources which have nearly 0 external costs. This is for comparison purposes only, as the exact implementation of the subsidy or additional cost does affect the economics in the real world.

The aforementioned external costs have already seen a large decrease, due to the increased attention to the influence of these types of electricity generation on climate change. Mainly due to additional legislation on the maximum emissions of gasses and particulate matter a large push has taken place to make the combustion of fuels more efficient and clean. However, these improvements have mainly been implemented in the most developed countries, whereas upcoming economies lack behind in these improvements. Since the location of interest for the system is developing economies near the equator these externalities are assumed to be significantly higher due to the older and less efficient and clean infrastructure in place. It is therefore even more appealing to install the proposed SBD system there than it would be to install it in Europe, should you take the full external costs into account.

Ground Usage and Ridesharing

A big benefit of this system is the low ground usage of this system. This is mainly appealing for archipelagos and areas with the limited ground area, where there is no unused space for solar farms. As the proposed system is sea-based, the ground use is minimal. This also has the benefit of a decrease in visual pollution, which is a major problem for wind turbines but also for conventional solar. Furthermore, as the proposed system can come back down to Earth relatively easily, this design makes the stratosphere easy to reach. Ridesharing can be an additional source of income, but can also prove beneficial for Earth observation and other research regarding the

stratosphere or for long distance research areas.

Energy Independence and Geopolitical Implications

Energy independence is a goal for a large number of countries, as modern economies and industries cannot freely function without a consistent electricity supply. The need for this independence has become increasingly visible due to the large energy crises caused by the Russian invasion of Ukraine at the start of 2022. With the pivot to renewable energy in full force with natural gas as a backup, the prices have skyrocketed due to gas embargos [66]. Due to these price hikes, inflation is rampant and economic growth is stunted as manufacturing is unprofitable. Governments have spent large amounts of money on easing the effects of this crisis and finding other sources of energy. This is just one recent example of the danger of being dependent on other countries for energy. Energy independence would increase price stability and guarantee a supply of energy improving the economic climate within countries. In 2022 Germany alone spent 264 billion euros to shield customers from the big increase in energy costs ¹. Combining this with the annual total energy consumption, this yields a figure of 8 cents per kWh or €80/MWh which was spent to lower the energy price at the customers' end. This figure is higher than the price of electricity in the years prior to the energy crisis. It is nigh impossible to quantify what the effect of additional renewables would be, but it is an example of the potential repercussions of not having a diversified and independent energy system. This is in addition to the political leverage that energy-exporting countries have over the importing countries or regions.

Grid Stability and Weather Independence

A well identified problem with conventional renewables is the intermittency and dependency on the weather. Cloud coverage and wind speeds have large impacts on electricity production that day. The large peaks and troughs associated with renewables mean that the grid has to be able to handle everything from 0% to 100% production, which makes for an expensive grid reinforcement operation. Conventional levelized cost of electricity (LCOE) calculations simply divides the total energy produced by the total cost of the lifetime. This assumes a perfect electricity market where the grid is always balanced. In reality, the addition of renewables requires backup in the forms such as natural gas peaker plants or battery storage. This can cost considerable amounts of money and is not encompassed by the LCOE. The so called levelized full system cost of electricity (LFSCOE) is a metric which does take into account the cost of grid balancing and stability. In Figure 8.2 it can be seen that the true cost of intermittent energy sources becomes very large as the grid penetration approaches 100%, with 95% penetration being significantly less costly as there is still some dispatchable power left which helps stabilize the grid [67].

Although equatorial areas in theory have the largest amount of sun due to the least atmospheric attenuation, in practice their solar power potential is actually quite poor. This is due to the tropical climate caused by the updraft of the atmosphere caused by a large amount of solar energy, pulling in winds with moisture. This causes extensive cloud coverage which blocks a lot of the sunlight for land based solar PV. The highest land based PV potential is actually slightly above and below the equator, where the climate is dry and cloud coverage is low ². This causes the equatorial region to be a prime option due to the low wind and conventional solar power potential.

¹<https://www.bruegel.org/dataset/national-policies-shield-consumers-rising-energy-prices>

²<https://globalsolaratlas.info/map?c=21.125498,11.794173,2>

Technology	LCOE [USD/MWh]	LFSCOE	
		Germany [USD/MWh]	Texas [USD/MWh]
Biomass	95	103	117
Coal (USC)	76	78	90
Natural Gas CC	38	35	40
Natural Gas CT	67	39	42
Nuclear	82	105	122
Solar PV	36	1380	413
Wind	40	483	291

Figure 8.2: Estimated levelized full system cost of electricity for multiple energy sources. [67]

The advantage of the high-altitude solar system is that the electricity production is incredibly predictable. Although it still deals with the day-night cycle, the location above the clouds and weather means that the daily production is merely a function of the seasons. Some months will have longer daylight or a higher sun, increasing the solar flux and production. These effects can be calculated far in advance with very high confidence and can be anticipated upon. Because of this, the LFSCOE of high-altitude solar is expected to be considerably lower than conventional renewables. These also have predictable seasonal variations but there is still the inherent uncertainty of weather within these calculations, which is not present for the Skydancer. Note that the LFSCOE is about the grid only, and does not take into account the cost of carbon or other externalities discussed in subsection 8.1.2.

8.2. Cost Break-Down Structure

In this section, the costs of the individual system components are analyzed. In addition to this, the costs of operations such as maintenance are estimated in order to provide a complete figure for the total cost of the Skydancer system.

8.2.1. Tether materials

The main materials of the tether are the UHMWPE and the aluminium conductor. The material costs can trivially be calculated, but due to the special nature of the production process of UHMWPE and the geometry of the fibre, this would result in an underestimation of the cost, which should be compensated for. UHMWPE is commercially available in the form of Dyneema. This is sold for purposes such as ship mooring and climbing ropes to individuals, and to commercial entities for offshore mooring or other industrial activities. Available ropes are expensive on a by kilo basis: approximately €250 per kilogram³. This is the price for individuals with an order size of mere meters. Economies of scale would cut this number at least in

³<https://rwrope.com/products/amsteel-blue-12-strand-dyneema-rope?variant=31678616698982>

half, using a conservative estimate. This would yield a price of 125€ per kilogram, using the conservative estimate to account for the added manufacturing complexity of the incorporation of the aluminium conductors. The total weight of UHMWPE used in the wire is 1612 kilograms according to the wire structural model. Together with an aluminium weight of 187 kilograms as mentioned in section 4.3 the total costs of the tether can be calculated with a price of aluminium of €2500 per metric tonne ⁴. This total amounts to approximately €200.000

8.2.2. Balloon

The balloon segment consists of two materials, UHMWPE and PVDC. UHMWPE has been discussed in the above section and its costs are well known, PVDC is a new material in addition to significant manufacturing costs for the balloon shape compared to the number of raw materials. PVDC is a relatively simple polymer which is available in film form for prices around €1.20 per kilogram ⁵. Since the amount of PVDC used in the balloon is 23.7 kg this will not contribute to the cost greatly compared to the 135 kilograms of UHMWPE with a considerably higher kilogram price. Combining these prices yields a raw material cost for the balloon of €17.000, excluding the manufacturing costs. As quality manufacturing is an integral part of a balloon that must be absolutely airtight and resistant to environmental factors, factor three was estimated with respect to material costs. This puts the total cost of the balloon skin at €68.000 The balloon is also filled with hydrogen, which can be produced using low-carbon electricity or using fossil fuels, with the latter being considerably cheaper. In accordance with the sustainability purpose of this project, renewable hydrogen was chosen with an average price of €5 per kilogram [68]. From subsection 4.5.1 a hydrogen weight of 358 kilograms is obtained, yielding a cost of €1800 and a total balloon cost of €69.800

8.2.3. Structures

The structures section consists of the top section, the central rod and the payload box. The payload box is assumed to be 150 kg in 4.6. The middle rod makes use of the mechanical strength of the tether to reduce the weight to only 78 kg. The top structure, responsible for supporting the solar panels and distributing the load to the lifting force of the balloon will be the most mass-intensive. The modular structure consists of 12 branches with a bottom, top and connecting rod with respective weights of 49.2, 42.1 and 6 kg respectively. The material is assumed to be aluminium for all sections. This leads to a total weight of approximately 1400 kg of aluminium. The structure itself consists of relatively simple elements, such as rods and I-beams, all commercially available. The complex aspect comes from the connecting rods, which will have a gyroidal shape. This has to be specially manufactured with additional costs due to complex tooling. Luckily this is a small aspect of the total structure, but it will increase the costs regardless. Due to this additional complexity, the manufacturing cost is estimated to be 2.5 times the raw material cost. With a weight of 1400 kg, this yields a cost of €12.250

8.2.4. Solar Array

A consideration made in the design of the solar array is the cost of manufacturing. In 2018 the direct manufacturing cost of such triple junction solar cells was estimated at $\$70W^{-1}$ for relatively large runs of $200 kW yr^{-1}$ [69]. The step-by-step breakdown can be seen in Figure 8.3. The largest contributors to overall costs are the substrate and epitaxial growth costs. The authors find that there is ample opportunity to reduce the costs in these areas significantly. Besides reducing these costs directly, also the cost of metallization and the scaling up of production volume contributes to much lower predicted costs.

⁴<https://markets.businessinsider.com/commodities/aluminum-price>

⁵<https://www.indiamart.com/proddetail/pvdc-clear-film-21691330697.html?pos=4&pla=n>

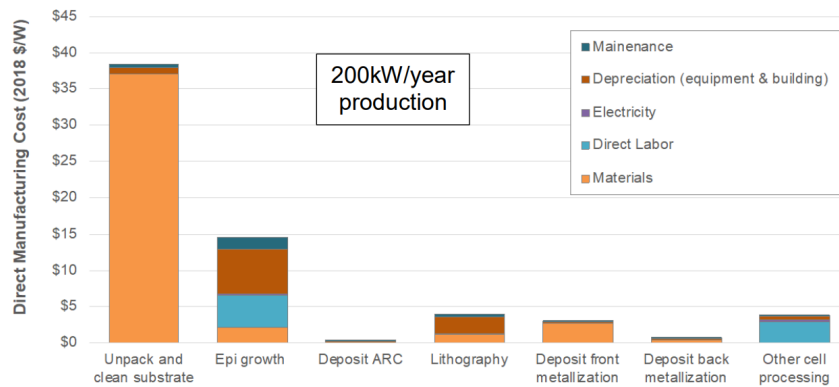


Figure 8.3: Direct manufacturing cost breakdown for 3J III-V solar cells [69].

The cost nearly halves by increasing the production volume to order 50MW yr^{-1} , which is achievable for our required 100MW system. Even with scaling the production, the epitaxial growth (MOCVD) equipment costs are still significant due to the tool price and long cycle times. Exact numbers for such scaling are difficult to predict, given the small scale of current production. Due to the required production of scale, a continuous, in-line MOCVD reactor could be built in the near future. Alternatively, the dynamic hydride vapour phase epitaxy (D-HVPE) method has demonstrated increased deposition rates, but is not as proven on large scales as MOCVD.

Improvements to the substrate costs can be made by reusing the growth substrate, reducing polishing and minimising the material required. the reuse of substrates can be implemented currently while minimising material requires adjusting of current MOCVD gas delivery systems and delivery chambers. Especially D-HVPE is expected to decrease material use significantly. The authors estimate that by implementing these improved growth methods and several substrate reuses for a high volume production, the total costs reach $\$2\text{W}^{-1}$ [69]. It should be noted that these estimations are not perfect. Similar industries such as c-Si solar and displays have seen larger reductions in cost with scale, than was anticipated.

Other costs for the solar array are the wiring and diodes. The wiring as sized in subsection 4.1.5 requires 8.3 kg of aluminium and 32.3 kg of PVC. The cost of these wires is insignificant to the rest of the system. Components that do contribute to the overall cost are the blocking and bypass diodes. The cost of a diode is derived from the SM74611, which was chosen as a representative component⁶ in subsection 4.1.2. These are commercially available at less than $\$1.3$ per piece. According to the production scale and exact implementation, a price of $\$1$ per diode is estimated. This results in a cost of $\text{€}44\,932$ for diodes plus $\text{€}2\,410\,556$

8.2.5. Electronics

Aside from the components mentioned in the previous section, the system also contains significant amounts of miscellaneous electronics such as sensors, data handling, processors and the transformer. These components vary wildly in function, size and thus cost. For these components a general estimate for cost is made, bearing in mind that this is with a large margin due to the high design fidelity necessary to accurately determine the cost. The figure estimated amounted to a total cost of $\text{€}20\,000$

⁶"SM74611". Texas Instruments. Last accessed on 23-01-2022. <https://www.ti.com/product/SM74611>

8.2.6. Commissioning, Maintenance and Decommissioning

The current maintenance profile revolves around lowering the system once every five years. Due to this, maintenance is not often and will thus not constitute a large fraction of the total cost. Conventional solar farms have maintenance costs of 1% per year, for a 25 year lifetime cost of 25% of the initial project cost⁷. Taking into account the reduced maintenance schedule compared to conventional PV and the use of higher quality solar cells, an estimate of 20% of the total cost of the project is made for commissioning, maintenance and decommissioning.

8.2.7. Total System Costs

With the analyses performed in the previous sections a total estimate can be made. The totals are added up with the maintenance, decommissioning and commissioning factor (C&M&D Factor) multiplied by this number to generate the total. This is given in Table 8.2.

Table 8.2: The cost breakdown of the system per component.

Category	Value
Tether	€ 200,000
Balloon	€ 698,00
Structure	€ 12,250
Solar Array	€ 2,257,600
Electronics	€ 20,000
C&M&D Factor	1.2
Total:	€ 3,071,580

8.3. Market Compliance

In this section, the market compliance of the Skydancer system is evaluated, both in purely financial terms as well as the broader meaning of market compliance, such as societal and economical effects.

8.3.1. Revenue Analysis

Electricity prices in equatorial countries such as Indonesia and Nigeria are around the €80-100 per MWh. More developed nations such as Rwanda or Costa Rica have higher prices, around €150⁸. It appears this trend holds for the rest of the world, with development being correlated with a higher electricity price. This price is the household price and includes distribution and fees such as taxes, and therefore a reference price for the producer is chosen of €70 per MWh as an estimated average, accounting for the increased demand for power in developing regions.

The thermal model described in subsection 4.1.3 can provide the expected power generated. Using the representative solar incidence of the chosen Pacific Asia location in subsection 8.1.1, the exact response of the solar array can be calculated. The integral of the electricity response provides the total power generated. At BOL the power generated over an entire year amounts to 2,185 MWh when accounting for the predicted transmission losses. At EOL this drops to 1900 MWh. With an assumed linear deterioration of the production capacity, this yields an average production of 2042 MWh over the expected lifetime of a 1 MW balloon. The expected revenue is therefore approximately €3.6 million dollars over the life, or €143 000 annually.

An additional source of income can be that of rideshare payloads which need to operate within

⁷<https://www.solarmango.com/2016/08/07/cost-maintaining-solar-panels-25-years/>

⁸https://www.globalpetrolprices.com/map/electricity_average/

stratospheric conditions. These can include but are not limited to research experiments, earth observation instruments or data transmission. As these are not the focus of the design, they are neglected for further financial analysis, but the future expectations are that they will contribute to the system revenue.

8.3.2. Return on Investment

The total amount of electricity produced over 25 years is 51 000 MWh, dividing the total cost from Table 8.2 by this number yields the levelized cost of electricity, allowing comparison with other energy sources. Calculating the value of the LCOE of the system yields €60.2 per MWh.

The profit margin is thus €9.8 MWh assuming an electricity price of €70 per MWh. This yields a return on investment of 17.2% at the end of the 25 years, or €528 432 Over 25 years, taking into account compound interest, this results in a yearly RoI of 0.64%. An important side note is that this result is for the market which does not take into account non-tangible benefits such as offset carbon emissions.

If government subsidies or policies were in place that put a price on negative external effects which are used to subsidise renewable energy the profitability would vary greatly. In Figure 8.1 external costs for EU electricity generation sources are given, which vary from €20 to €250 per MWh. In equatorial regions with less modern technology, these external effects will be even more pronounced.

In Figure 8.4 the projected revenue and costs are plotted over time, with the costs increasing over the years due to the maintenance cost and the subsidies being €10, €30, €50 and €100 respectively. Revenue reduces over the years due to the decrease in production as the cells deteriorate.

It can be seen that subsidies greatly improve profitability compared to the lower, unsubsidized line. The €100 MWh subsidy even reduces the break-even period to a mere 7 years, increasing the return on investment to over 200% after 25 years. The return on investment is non-zero and positive without subsidies, albeit low compared to other investments. Governmental environmental and energy policies greatly affect the profitability of the system as a whole.

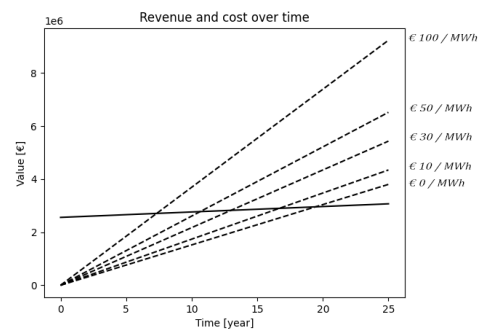


Figure 8.4: Revenue and costs over time, steeper lines have higher subsidies - which are based on energy produced.

8.3.3. Market compliance

Although the numbers mentioned in subsection 8.3.2 imply a positive return on investment, this does not necessarily imply a positive business case. Without subsidies, the system yields 0.6% return on investment a year, which historically will not outperform inflation. Compared to other investments, such as real estate or even other renewables the return is low and dissuading to potential investors. This has to do with the way the price of electricity is established. Apart from some regions in the world which have a form of carbon pricing, the price of electricity is related to the costs of production and the demand.

External effects also having an influence on the market position are depicted in Figure 8.5, illustrating the positive and negative effects that the high-altitude system has on its environment and society as a whole. They are not quantified, as putting a number on these factors cannot be done with an appreciable degree of certainty. A positive or negative impact can be determined

though, along with the relative magnitude. The rankings are derived from the analysis in section 8.1. The largest positive externality is the low carbon emission and the largest negative externality is the interruption of airspace by the tether. A no-fly zone would have to be implemented surrounding it, but this is hard to put an exact price figure on. Moreover, geopolitical and geo-engineering considerations are beneficial externalities.

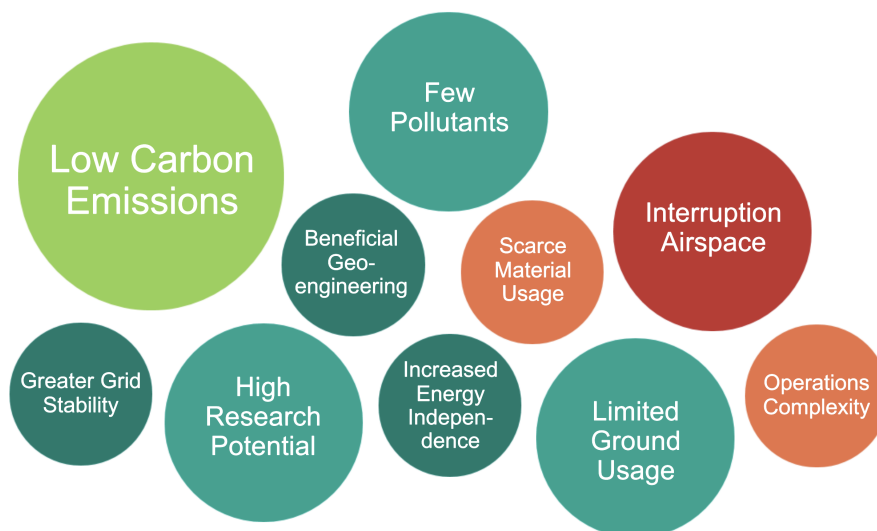


Figure 8.5: External Effects Skydancer.

Considering the lack of wind and conventional solar PV potential around the equator, and hydropower being limited by geography, the high-altitude system has an edge. This increases the levelized cost of electricity of the other sources which decreases their return on investment, making the system more attractive as an investment. Another option for energy production with a low external cost is nuclear power. This energy source has the disadvantage of being subject to politics, rigorous legislation and high capital investment needs. A country in equatorial Africa will not have an easy time obtaining the technology or approval to build a nuclear plant, considering the stringent safety regulations from worldwide regulators due to the potentially disastrous consequences. As this analysis transcends economics into politics and law, it was left out of this market analysis, focusing mainly on "conventional" low carbon electricity sources.

It is important to note that the cost analysis was done with broad margins due to uncertainty caused by the level of fidelity in this design. From a purely financial perspective, the system is slightly profitable, albeit not a particularly attractive investment. Due to the margins, the system could turn out slightly unprofitable or even more so. Assuming an even distribution there is a slight bias toward profitability. The most important metric for achieving market compliance is the development of policies from governmental institutions in order to promote carbon-free energy sources or at least to let energy sources have a fair price. As illustrated in Figure 8.1 some energy sources have negative externalities many times bigger than the price of the electricity produced by these sources. In a perfectly efficient market, these have no right to exist. Although the Skydancer system has considerable challenges, the advantages will outweigh these. It is difficult to overstate how important the rapid rollout of low-carbon energy sources is for not only human and economic development but also for the well-being of the Earth's ecosystem.

8.3.4. Comparison to Competitors

To complete the market analysis, the proposed system is compared to the main competitors on six different metrics. These are grid stability, deployment time, system costs, technology readiness level, ecosystem impact and visual pollution. This comparison is shown in Figure 8.6.

Regarding the grid stability, the Skydancer concept is outperforming most competitors, as the power output is very predictable and follows the day and night schedule. This makes the grid stability way better when compared to ground or ocean based solar, which are both influenced by cloud coverage. Furthermore, the grid stability of wind energy is dependent on the wind speed and cut-in speed and the rated power of the turbine. The only renewable source which outperforms the Skydancer with regards to grid stability is Nuclear power, as this can provide a constant energy production but can also ramp up or down depending on the grid's need [70].

Regarding the deployment time, the Skydancer performs similarly to offshore solar, with a deployment time of 3-6 months, which is better compared to offshore wind, for which construction can take two to five years⁹. The deployment time for nuclear energy is in the magnitude of 10-20 years, while for space based solar power (SBSP) this is at least doubled. Furthermore, the technology readiness level (TRL) of the different systems can be compared. Only four out of these seven renewable sources are used on large scale at this point in time. The TRL of SBSP is at 2, while the Skydancer is at 3. Lastly, offshore solar is at TRL 7 at the time of writing, as floating platforms are being demonstrated at the time of writing¹⁰

The system cost can be compared based on the LCOE, which are readily available for the majority of the competitors [71]. The two missing LCOE are the ones for the Skydancer concepts, which are calculated to be 0.60 €/kWh and the one for SBSP, which is unarguably the highest of all.

The last two metrics, cover the sustainability aspects. On both ecosystem impact as visual pollution, the Skydancer concept scores the highest out of all competitors. Regarding ecosystem impact, it was explained in subsection 2.2.1 how the Skydancer concept contributes to life on land and life on water. For visual pollution, this outperforms all competitors as the tether is not visible from great distances and as only the sea platform is the polluting factor. SBSP is the option scoring the second best, as the microwave or infrared waves have a pronounced effect on the ecosystems and as the visual pollution of this system is still prevalent. Although only one receiving station is needed, such a ground station will be a few square kilometers big [sbsp]

⁹"Everything you'd like to know about offshore wind farm construction", Iberdrola, Accessed on 30-01-2023, <https://www.iberdrola.com/about-us/our-activity/offshore-wind-energy/offshore-wind-park-construction>

¹⁰"A world's first: offshore floating solar farm installed at the Dutch North Sea", Oceans of Energy, Accessed on 31-1-2023, <https://oceansofenergy.blue/a-worlds-first-offshore-floating-solar-farm-installed-at-the-dutch-north-sea/>

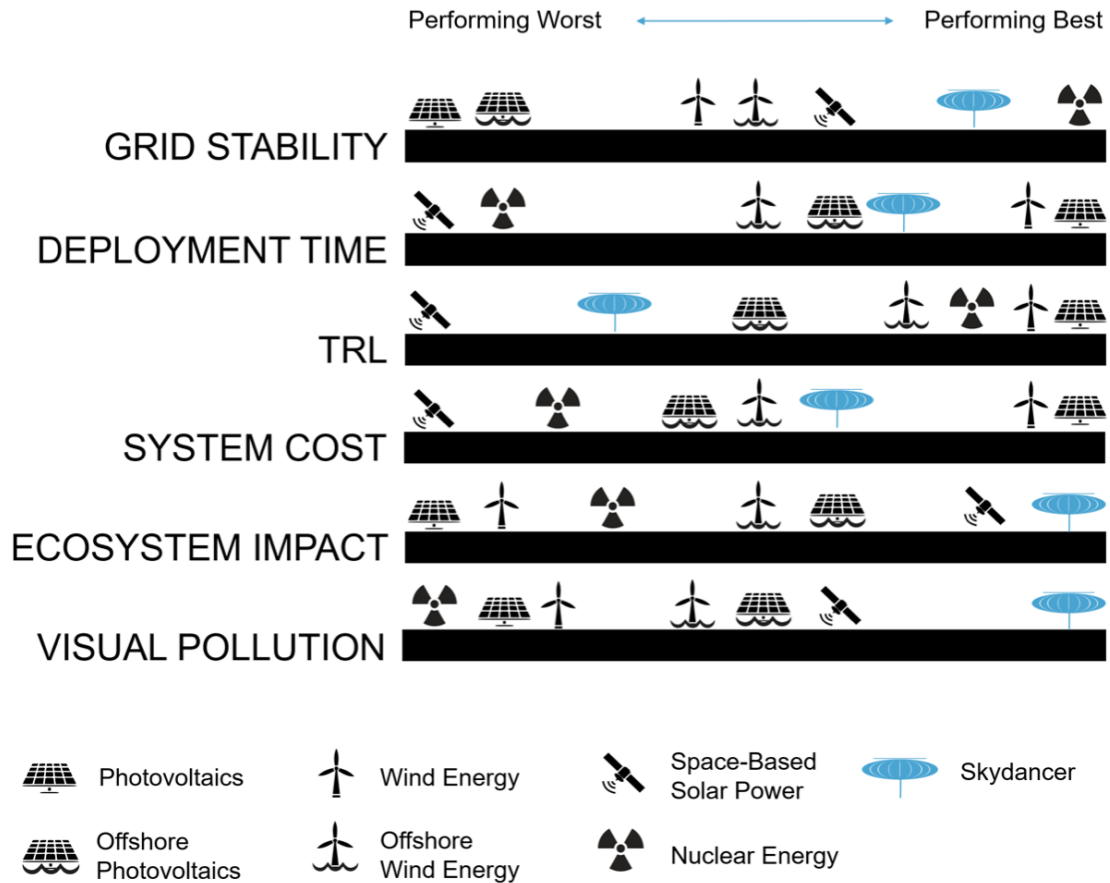


Figure 8.6: Competitiveness Skydancer

8.3.5. Concluding remarks on market compliance

Whether the system has achieved market compliance is a difficult question to answer. The viability is dependent on how governments will develop their policy in light of the daunting task of the transition to low-carbon energy sources. Depending on the subsidies and the efficiency of the market the Skydancer system can either be a terrific investment with a payback period of less than a decade or an investment that will have trouble outperforming inflation. In competition with solar and wind, the system does have tangible benefits and advantages targeted for specific, previously overlooked locations. Along the equator, the Skydancer system experiences a perfect storm of circumstances and with the right policies can make a market compliant difference, both for the country it is deployed in, and the world. Nevertheless, with the indirect value Skydancer can provide in the form of contributing to local economies, fostering developing nations, and enabling the hosting of scientific payloads, the positive externalities summed with liquid assets would likely be able to meet the market compliance goals of the mission.

9 | Requirement Compliance

This chapter discusses the system requirements and presents a compliance matrix showing compliance with the set requirements. It shows the identifier, requirement description, if there is compliance with this requirement and if so where there is proof of this. If there is no compliance, a description is given of how the requirement will be achieved in the future. First, requirements are reviewed in section 9.1, then the compliance matrix is shown in section 9.2 and lastly, section 9.3 considers how the requirements that are not yet complied with will be met in the future.

9.1. Requirements Review

The full set of requirements was reviewed before examining compliance. A few requirements were removed, changed and added due to a change in the relevance of the requirements because of some design choices.

Firstly, requirements SBD-COM-01 and SBD-COM-02 were removed as it was determined that the power for the communication subsystems will be dependent on the data rate. It needs to be minimized and designed for, hence a requirement on it is obsolete.

Second, requirement SBD-SUS-01 about the Dutch government's 'Klimaatakkoord'¹ is removed because the SBD will no longer be operated in the Netherlands. It is in turn replaced with the new requirement SBD-SUS-07 which states that the system shall have a carbon footprint lower than conventional solar energy, at 40 g CO₂/kWh.

Due to the choice to design for 100 balloons, each producing 1 MW of power, the value 'TBD' in requirements SBD-PWR-01, SBD-PWR-02 and SBD-PWR-05 has been replaced with 1 MW.

Requirement SBD-REG-03.01 has been added as a sub-requirement of SBD-REG-03 about operations regulations, stating the maximum voltage in the solar array to stay under regulatory high-voltage, this is a world wide regulation. Requirement SBD-SFT-01.01 has been added as a sub-requirement of SBD-SFT-01 about reliability, stating the minimum required reliability of the photovoltaic system. A summary of the reviewed requirements is added below.

SBD-STR-04 and SBD-STR-05 have to be reworded to fit better with the design. Same holds for SBD-SUS-04.

Removed Requirements

SBD-COM-01	The balloon segment communication subsystem shall use a maximum of TBD power.
SBD-COM-02	The G/S segment communication subsystem shall use a maximum of TBD power.
SBD-SUS-01	The project shall contribute to obtaining the Dutch government's goals defined in the 'Klimaatakkoord'.
SBD-STR-04	The structure shall protect all subsystems from the environment.
SBD-STR-05	subsystems shall be kept at a temperature range of TBD.
SBD-SUS-04	The system's waste shall be recycled whenever economically viable.

¹"Wat is het Klimaatakkoord?". Rijksoverheid. 20<https://www.rijksoverheid.nl/onderwerpen/klimaatverandering/klimaatakkoord/wat-is-het-klimaatakkoord>

Changed Requirements

SBD-PWR-01	One balloon segment shall harvest at least 1 MW of solar power.
SBD-PWR-02	One balloon segment shall transmit at least 1 MW of power.
SBD-PWR-05	One ground segment shall be able to receive at least 1 MW of power.
SBD-COM-03	The balloon segment communication system shall have a minimum data rate of 51.86 Mbps.
SBD-COM-07	The communications shall use the X band.

New Requirements

SBD-SUS-07	The system shall have a carbon footprint of less than 40 g CO ₂ /kWh.
SBD-POS-12	The balloon segment shall be able to land within 24 hours.
SBD-REG-03.01	The DC voltage of the solar array shall stay below 1500 V ²
SBD-SFT-01.01	The photovoltaic systems shall at least have a reliability level of 0.98 throughout mission duration
SBD-STR-06	The structure should protect all subsystems from the environment.
SBD-STR-07	Components shall be kept at a temperature range of TBD.
SBD-SUS-08	Recyclable waste from the system shall be recycled.

9.2. Compliance Matrix

This section presents the compliance of the system to the requirements, presented in the compliance matrix in Table 9.4.

It can be observed that quite a few requirements have TBD for unknown/unset values. It was expected that these requirements were necessary up until this design stage. It was concluded that these can however be better situated in the future. Instead of removing them and adding them later with values, it has been decided to keep them and the TBD values will be filled in later. It might be possible that multiple sub-requirements flow from these.

Table 9.4: Compliance Matrix

ID	Description	Compliance?	Section
SBD-PWR-01	The balloon segment shall harvest at least 1 MW of solar power.	Yes	4.1
SBD-PWR-02	The balloon segment shall transmit at least 1 MW of power.	Yes	5.3.2
SBD-PWR-05	The total ground/space (G/S) segment shall be able to receive at least 100MW of power.	Yes	4.1
SBD-PWR-06	The G/S segment shall be able to convert received power to usable electrical power.	Yes	5.1.1
SBD-POS-01	The balloon segment shall be able to determine its attitude with a precision of at least TBD.	TBD	
SBD-POS-03	The balloon segment shall be able to determine its altitude with a precision of at least TBD.	TBD	

²"IEC 61140:2016". International Electrotechnical Commission. Last accessed on 10-01-2022. <https://webstore.iec.ch/publication/23997>

SBD-POS-05	The balloon segment shall be able to determine its velocity with a precision of at least TBD.	TBD	
SBD-POS-06	The balloon segment shall be able to determine its acceleration with a precision of at least TBD.	TBD	
SBD-POS-08	The balloon segment shall operate in an altitude range of 15 - 45 km.	Yes	4.4.3
SBD-POS-09	The balloon segment shall be able to endure trajectory drifts due to stratospheric winds up to 30 m/s.	Yes	4.4.1
SBD-POS-12	The balloon segment shall be able to land within 24 hours.	Yes	5.1.4
SBD-POS-13	The balloon segment shall be able to determine its latitude with a precision of at least TBD.	TBD	
SBD-POS-14	The balloon segment shall be able to determine its longitude with a precision of at least TBD.	TBD	
SBD-COM-02	The balloon segment communication subsystem shall have a minimum pointing accuracy of TBD.	TBD	
SBD-COM-03	The balloon segment communication system shall have a minimum data rate of 51.86 Mbps.	Yes	4.8.2
SBD-COM-05	The G/S segment communication subsystem shall have a minimum pointing accuracy of TBD.	TBD	
SBD-COM-06	The G/S segment communication system shall have a minimum data rate of TBD.	TBD	
SBD-COM-07	The communications shall use the X band.	Yes	4.8.2
SBD-COM-08	The communication antenna at G/S should have a gain of at least TBD.	TBD	
SBD-STR-01	The balloon segment shall not plastically deform in normal operational conditions.	Yes	4.5.1, 4.6
SBD-STR-02	The design of the balloon segment shall account for material degradation due to cyclic solar exposure.	Yes	4.5.1, 4.6.4, 5.3.2
SBD-STR-03	The structure shall house all necessary subsystems.	Yes	4.6.1
SBD-STR-06	The structure should protect all subsystems from the environment.	Yes	4.6.2
SBD-STR-07	Subsystems shall be kept at a temperature range of TBD.	TBD	
SBD-SUS-02	The system's energy intake during the operations phase shall be fully covered by renewable energy.	Yes	5.1.3
SBD-SUS-03	The system shall leave no debris in the atmosphere or on Earth during the decommissioning phase.	Yes	5.1.4
SBD-SUS-05	Cradle-to-cradle materials shall be used.	Yes	4.6.5

SBD-SUS-06	The system shall be upgradeable to comply with future technological developments.	Yes	6.5
SBD-SUS-07	The system shall have a carbon footprint of less than 40 g CO ₂ /kWh.	Yes	6.3
SBD-SUS-08	Recyclable waste from the system shall be recycled.	Yes	5.1.4
SBD-COS-01	The system shall have a minimum return on investment of 10% over 5 years.	No	8.3.2
SBD-COS-02	The system shall deliver energy at market compliance or better.	Yes	8.3.3
SBD-SCH-01	The system shall be delivered within 5 years.	Yes	5.5
SBD-SCH-02	The system shall have an operational lifetime of at least 25 years.	Yes	4.1.4
SBD-SCH-03	The system shall be designed with a resource constraint of 9 students.	Yes	-
SBD-SCH-04	The system shall be designed with a time constraint of 10 weeks.	Yes	-
SBD-REG-01	The manufacturing process shall comply with TBD regulations.	TBD	
SBD-REG-02	The launch of the balloon shall comply with TBD regulations.	TBD	
SBD-REG-03	The operation of the balloon shall comply with TBD regulations.	TBD	
SBD-REG-03.01	The DC voltage of the solar array shall stay below 1500 V ³	Yes	4.1.2
SBD-SFT-01	The system shall have a reliability level of TBD.	TBD	
SBD-SFT-01.01	The photovoltaic systems shall at least have a reliability level of 0.98 throughout mission duration	Yes	7.11
SBD-SFT-03	System failure shall not result in the loss of life.	Yes	4.1.4, 4.4.2, 4.6.4, 4.8.1, 6.4.2

9.3. Feasibility Analysis

For many of the requirements, compliance is still to be determined. This section will discuss what these requirements are still dependent on and what needs to be done to make sure they are met in the future.

Regarding the positioning requirements that are still TBD, they need extra research into the specific precision required for the system and for possible future payloads. Furthermore, the movement of the system itself demands more simulations on the limits of the tether and the connection points to the balloon.

Concerning the communications requirements need more analysis of the precision of both the

³"IEC 61140:2016". International Electrotechnical Commission. Last accessed on 10-01-2022. <https://webstore.iec.ch/publication/23997>

ground system and the antenna on the balloon. Moreover, the data rate and the gain from the ground station use more investigation for specifics.

The requirement on subsystem temperature range depends on the type of payload to be used in the future. It is possible that no additional temperature management has to be done, although it might be needed for some specific measurement payload.

The regulations' requirements that are still TBD need extra research into regulations at the locations where the high altitude solar farm will be deployed. These can differ a lot per country and thus need to be examined further

Requirement SBD-COS-01 about the minimum RoI after five years is not met technically, as the RoI is now lower although positive. However, depending on government policy and the inclusion of non-tangible benefits, the system is considered market compliant and will have a large enough RoI depending on possible subsidies which in the past have been used to develop for example wind and solar energy to be profitable investments. More information on this requirement is presented in chapter 8.

10 | Conclusions

This paper's focus is on the detailed design of the stratospheric balloon design concept generated previously. The steps taken comprise the determination of operational location and height, with the design done on the solar array, tether, structure and additional payload elements.

A dynamic model was set up to study the response of varying design parameters to a representative incident wind profile. Besides the aerodynamic characteristics, the net excess lift and tether radius proved influential for the final state. After weighing the difficulty in providing excess lift for higher altitudes and lower solar irradiance for lower altitudes, an operational altitude of 18 km was chosen. The corresponding preferred operational location is around the equator, such as Pacific Asia and the Gulf of Guinea. This was concluded from the multitude of drawbacks when it comes to deploying at high latitudes. These locations carry high wind potential due to the polar vortex and the potential of hydropower due to elevation differences. Around the equator, conventional renewable energy methods are more disruptive to the local environment. The area is limited due to large valuable rain forests, other available space would rather be used for food production and habitation.

The photovoltaic array was sized in accordance with a thermal model to minimise the losses due to thermal inefficiency. High efficiency cells on a raised backplane achieve 32.9% conversion at peak intensity and temperature. The array is sized in accordance with the 1 MW of power production requirement. At peak incidence for predicted end-of-life conditions, this requires approximately 2665 m². The array incorporates a proper electrical layout and redundancy. It consists of 478 parallel chains of 46 panels in series to achieve the desired voltage and corresponding current.

The tether must be able to transmit the power generated across this 18 km. For the electrical design, it was sized by evaluating the losses found in high voltage transmission, being inductive, Ohmic and corona. An aluminium core of 1.9 mm² under 130 kV is optimal to carry the current with minimal losses. The insulation and structural support of the tether is to be constructed of UHMWPE (ultra-high-molecular-weight polyethylene), filament wound with the aluminium for a total radius of 5.6 mm. This combination is predicted to be capable of handling the loading expected from the dynamic model by a factor of four.

The structural configuration of the balloon itself must carry the raised solar array while being light enough to provide excess lift efficiently. The shape is pumpkin-like, comprising 24 legs interconnected with 12 gas bags. The solar array is supported by 12 aluminium I-beams and suspended by a central rod of CFRP running through the balloon. An additional 12 compression rods connect the bottom of the solar array to the top of the balloon. A small platform is attached to the bottom of the rod which houses the other subsystems. The balloon itself is made of UHMWPE 9.4 µm to keep the required 50 600 m³ of hydrogen.

Additional subsystems required for a functioning system include the distribution and conversion of the power, communications array and data handling as well as sensors and meters. A full sensor package is described consisting of both critical and additional components. The communications array is sized according to data handling requirements. Other subsystems such as a battery and electrical heater are included in the design. The power distribution module is described as to the functionality required. The largest contributor to mass is the transformer.

Table 10.2: Mass breakdown of the final design

Component	Value (kg)
Solar array	1685
Top structure	1200
Support rod	80
Skin	160
Payload	200
Tether	1800
Total	5125

Table 10.1: Dimensions of the final design

Dimension	Value	Unit
Solar array	2665	m^2
Volume	50600	m^3
Balloon diameter	72.8	m
Balloon height	18.2	m

The balloon design has been evaluated for its position within the electricity market. The main benefits it can provide are that fact that it allows for grid stability and has a significantly lower carbon footprint compared to conventional renewable energy sources. The total system costs of the system have also been established and come to €3.1 million per balloon. Leading to a levelized cost of electricity of 60 cents per kWh. Lastly, a conclusion is drawn with regard to market compliance. Compliance is dependent on the subsidies, efficiency of the market and the policies governments are developing. However, Skydancer has non-tangible benefits compared to the competition. Based on the estimated 52.1 GWh it is predicted to produce, the return on investment is non-zero and positive without subsidies, albeit low compared to other investments.

The sustainable approach was an important aspect in regard to the design and functioning of the system. In specific, environmental, social and economical sustainability is taken from the United Nation's Sustainable Development Goals (SDG), where there should be a balance between these three facets. Moreover, a carbon footprint analysis has been performed, which concluded 270 000 kg CO₂ for 1 MW of power for 25 years and a footprint of 5.4 g CO₂/kWh.

Recommendations for the continuation of the Skydancer concept

The research performed showed that a stratospheric balloon design for harvesting solar energy has potential within the energy market. More research is required to move the Skydancer concept beyond this conceptual design stage. Many aspects may prove valuable to investigate as some aspects are first of a kind. In particular, the response of a tethered high-altitude balloon to a complex atmospheric environment has a high impact on the possibilities. The modelling of such a system requires many specific datasets, and the validation of which various large scale tests. Additionally, another look should be taken into the scaling of such a balloon. A larger design is preferred for cost and effectiveness, however the complexity of operating and manufacturing may outweigh the potential benefits. The weight of the total product can also be optimised to lower the cost even further. This could be for example achieved by cut-outs in the support structure.

Furthermore, the design requires a closer look at current regulations. The aspect of air restrictions through the traffic of aircraft and the procedures of having an offshore platform is limiting. Other regulations may need to be set up for the actual operation of such a balloon. As with many first of its kind concepts, the impact is not yet understood. Other integration effects such as the connection to the local energy grid, which were beyond the scope of this project, should also be taken into account.

Lastly, research should specifically be put towards the verification and validation of the full system. To verify the balloon, smaller systems can be either analysed, reviewed or tested to comply with the requirements set. Multiple tests should be performed to verify the product works as intended. Especially the tether requires large scale testing. Without a doubt, the system can be improved by future technology improvements and refinements.

Table 10.3: Work Division for Final Report

Name	Worked on
Digna	Front page, Ch 4 (section 6), Ch 6 (section 2 and 5)
Jelte	Ch 3, Ch 4 (Sections 1, 8), Ch 5 (Sections 2, 4), Ch 6 (Sections 1, 5), Ch 8 (Section 2), Conclusions
Joep	Summary, Ch 4 (Sections 3, 4, 6, 8), Ch 8.
Matthijs	Ex. Overview, Ch 3, Ch 4 (Sections 4, 7), Ch 5 (Sections 4,5), Ch 9
Niek	Ch 4 (Sections 4, 5, 6), Ch 5 (Section 1, 3), Ch 6 (Sections 2, 5), Ch 9, Ch 10
Niels	Nomenclature, Ch 2 (section 1), Ch 4 (section 4), Ch 5 (section 1, 2), Ch 6 (section 4), Ch 7
Sahir	Ex. Overview, Ch 4 (Sections 2, 5), Ch 6 (Sections 4, 6)
Stella	Summary, Ex. Overview, Ch 2 (Section 2), Ch 4 (Sections 1, 6), Ch 5 (Section 1), Ch 6 (Section 3), Ch 8 (Sections 1, 3)
Wouter	Summary, Ex. Overview, Ch 1, Ch 4 (Sections 1, 6, 7), Ch 6 (Section 7), Ch 7, Ch 8 (Sections 1, 3)

References

- [1] DSE Group 3. *Midterm Report - Sustainable Energy from Pseudo Satellites*. Tech. rep. TU Delft, Dec. 2022.
- [2] Emily C. Warmann and Pilar Espinet-Gonzales. “An ultralight concentrator photovoltaic system for space solar power harvesting”. In: *Acta Astronautica* 170 (2020), pp. 443–451. issn: 0094-5765. doi: 10.1016/j.actaastro.2019.12.032.
- [3] K Hyung Chul et al. “Life Cycle Greenhouse Gas Emissions of Thin-film Photovoltaic Electricity Generation”. In: *Journal of Industrial Ecology* 16.s1 (2012), S110–S121. doi: <https://doi.org/10.1111/j.1530-9290.2011.00423.x>. url: <https://onlinelibrary.wiley.com/doi/abs/10.1111/j.1530-9290.2011.00423.x>.
- [4] S. Schlömer et al. “Annex III: Technology-specific cost and performance parameters”. In: *Climate Change 2014: Mitigation of Climate Change. Contribution of Working Group III to the Fifth Assessment Report of the Intergovernmental Panel on Climate Change* (2014).
- [5] Omar Saif et al. “On the optimization of InGaP/GaAs/InGaAs triple-junction solar cell”. In: *IOP Conference Series: Materials Science and Engineering* 446.1 (Dec. 2018), p. 012010. doi: 10.1088/1757-899X/446/1/012010.
- [6] Tatsuya Takamoto, Hidetoshi Washio, and Hiroyuki Juso. “Application of InGaP/GaAs/InGaAs triple junction solar cells to space use and concentrator photovoltaic”. In: *2014 IEEE 40th Photovoltaic Specialist Conference (PVSC)*. 2014, pp. 0001–0005. doi: 10.1109/PVSC.2014.6924936.
- [7] E. Hulicius and V. Kubeček. “Semiconductor lasers for medical applications”. In: (2013), pp. 222–250. doi: 10.1533/9780857097545.2.222.
- [8] Ryan M. France et al. “Triple-junction solar cells with 39.5% terrestrial and 34.2% space efficiency enabled by thick quantum well superlattices”. In: *Joule* 6.5 (2022), pp. 1121–1135. issn: 2542-4351. doi: 10.1016/j.joule.2022.04.024.
- [9] T.L. Bergman et al. *Fundamentals of Heat and Mass Transfer*. Wiley, 2011. isbn: 9780470501979.
- [10] Marios Theristis and Tadhg S. O’Donovan. “Electrical-thermal analysis of III–V triple-junction solar cells under variable spectra and ambient temperatures”. In: *Solar Energy* 118 (2015), pp. 533–546. issn: 0038-092X. doi: <https://doi.org/10.1016/j.solener.2015.06.003>. url: <https://www.sciencedirect.com/science/article/pii/S0038092X15003059>.
- [11] Jiangtao Wu et al. “Thermal modeling of stratospheric airships”. In: *Progress in Aerospace Sciences* 75 (2015), pp. 26–37. issn: 0376-0421. doi: 10.1016/j.paerosci.2015.04.001.
- [12] Jun Li et al. “Output performance analyses of solar array on stratospheric airship with thermal effect”. In: *Applied Thermal Engineering* 104 (2016), pp. 743–750. issn: 1359-4311. doi: 10.1016/j.applthermaleng.2016.05.122.
- [13] E. Normand and T.J. Baker. “Altitude and latitude variations in avionics SEU and atmospheric neutron flux”. In: *IEEE Transactions on Nuclear Science* 40.6 (1993), pp. 1484–1490. doi: 10.1109/23.273514.
- [14] Dirk C. Jordan et al. “Compendium of photovoltaic degradation rates”. In: *Progress in Photovoltaics: Research and Applications* 24.7 (2016), pp. 978–989. doi: 10.1002/pip.2744.
- [15] M. Collins, S. Tett, and C. Cooper. “The internal climate variability of HadCM3, a version of the Hadley Centre coupled model without flux adjustments”. In: *Climate Dynamics* 17 (Jan. 2001), pp. 61–81. doi: 10.1007/s003820000094.

- [16] Greg Kopp. "Daily solar flux as a function of latitude and time". In: *Solar Energy* 249 (2023), pp. 250–254. ISSN: 0038-092X. DOI: 10.1016/j.solener.2022.11.022.
- [17] Jean H. Meeus. *Astronomical Algorithms*. Willmann-Bell, Incorporated, Jan. 1991. ISBN: 0943396352.
- [18] Ibrahim Reda and Afshin Andreas. "Solar position algorithm for solar radiation applications". In: *Solar Energy* 76.5 (2004), pp. 577–589. ISSN: 0038-092X. DOI: 10.1016/j.solener.2003.12.003.
- [19] P. Bretagnon and G. Francou. "Planetary Theories in rectangular and spherical variables: VSOP87 solution". In: *Astronomy and Astrophysics* 202 (Aug. 1988). Provided by the SAO/NASA Astrophysics Data System, p. 309.
- [20] Xiaojian Li et al. "Modeling and analysis of floating performances of stratospheric semi-rigid airships". In: *Advances in Space Research* 50.7 (2012), pp. 881–890. ISSN: 0273-1177. DOI: 10.1016/j.asr.2012.05.022.
- [21] Frank Kreith and Jan F. Kreider. *Numerical Prediction of the Performance of High Altitude Balloons*. Tech. rep. 2. University of Colorado. Boulder, Colorado. The United States: University Corporation for Atmospheric Research, July 1974. DOI: 10.5065/D64X55SR.
- [22] Greg Kopp and Judith L. Lean. "A new, lower value of total solar irradiance: Evidence and climate significance". In: *Geophysical Research Letters* 38.1 (Jan. 2011). DOI: 10.1029/2010GL045777.
- [23] W. M. Smart. *Textbook on Spherical Astronomy*. Ed. by R. M. Green. 6th ed. Cambridge, England: Cambridge University Press, 1977. DOI: 10.1017/CB09781139167574.
- [24] Institute of Electrical and Electronics Engineers. "IEEE Standard for Floating-Point Arithmetic". In: *IEEE Std 754-2019 (Revision of IEEE 754-2008)* 2019.754 (July 2019), pp. 1–84. DOI: 10.1109/IEEESTD.2019.8766229.
- [25] Charles R. Harris et al. "Array programming with NumPy". In: *Nature* 585.7825 (Sept. 2020), pp. 357–362. DOI: 10.1038/s41586-020-2649-2.
- [26] Wes McKinney. "Data Structures for Statistical Computing in Python". In: *Proceedings of the 9th Python in Science Conference*. Ed. by Stéfan van der Walt and Jarrod Millman. 2010, pp. 56–61. DOI: 10.25080/Majora-92bf1922-00a.
- [27] W.-J. Gu and R. Liu. "A study of volume and weight vs. frequency for high-frequency transformers". In: *Proceedings of IEEE Power Electronics Specialist Conference - PESC '93*. 1993, pp. 1123–1129. DOI: 10.1109/PESC.1993.472059.
- [28] *Dyneema fact sheet*. Tech. rep. P.O. Box 559, 6200 AN, Maastricht, The Netherlands: Eurofibers, Jan. 2008.
- [29] Slobodan Cuk and R. D. Middlebrook. "Advances in Switched-Mode Power Conversion Part I". In: *IEEE Transactions on Industrial Electronics* IE-30.1 (1983), pp. 10–19. DOI: 10.1109/TIE.1983.356697.
- [30] D. Zhang et al. "Tandem, long-duration, ultra-high-altitude tethered balloon and its system characteristics". In: *Advances in Space Research* 66.10 (2020), pp. 2446–2465. ISSN: 0273-1177. DOI: 10.1016/j.asr.2020.08.006.
- [31] Daisuke Akita. "Feasibility study of a sea-anchored stratospheric balloon for long-duration flights". In: *Advances in space research* 50.4 (2012), pp. 508–515.
- [32] Baris Gumusel, Levent Kavurmacioğlu, and Cengiz Camci. "Aerodynamic Drag Characteristics and Shape Design of a Radar Antenna Used for Airport Ground Traffic Control". In: *Progress in Computational Fluid Dynamics* 10 (Dec. 2010). DOI: 10.1504/PCFD.2010.030420.
- [33] Joseph Carroll. "Guidebook for analysis of tether applications". In: (Mar. 1985).
- [34] Brahim Benmokrane et al. "Creep-rupture limit for GFRP bars subjected to sustained loads". In: *Journal of composites for construction* 23.6 (2019), p. 06019001.

- [35] M. Madonia, M. Trancossi, and A. Coppola. "Quite-Rigid Airship Structure Concept and Design for Enhanced Hovering Capability". In: *SAE International Journal of Aerospace* 5 (July 2012), pp. 101–112. DOI: 10.4271/2012-01-1892.
- [36] H. Du et al. "Flight performance simulation and station-keeping endurance analysis for stratospheric super-pressure balloon in real wind field". In: *Aerospace Science and Technology* 86 (2019), pp. 1–10. DOI: 10.1016/j.ast.2019.01.001.
- [37] Huafei Du et al. "Station-keeping performance analysis for high altitude balloon with altitude control system". In: *Aerospace Science and Technology* 92 (2019), pp. 644–652. DOI: <https://doi.org/10.1016/j.ast.2019.06.035>.
- [38] S. Gudmundsson. "Chapter 15 - Aircraft Drag Analysis". In: *General Aviation Aircraft Design*. Ed. by S. Gudmundsson. Boston: Butterworth-Heinemann, 2014, pp. 661–760. ISBN: 978-0-12-397308-5. DOI: 10.1016/B978-0-12-397308-5.00015-5.
- [39] J. Förste. "Schlichting, H., Boundary-Layer Theory". In: *Zeitschrift Angewandte Mathematik und Mechanik* 60.4 (Jan. 1980), pp. 217–217. DOI: 10.1002/zamm.19800600419.
- [40] H. G. Weller et al. "A tensorial approach to computational continuum mechanics using object-oriented techniques". In: *Computers in Physics* 12.6 (1998), pp. 620–631. DOI: 10.1063/1.168744.
- [41] Sadaf Maramizonouz and Sadeq Nadimi. "Drag force acting on ellipsoidal particles with different shape characteristics". In: *Powder Technology* 412 (2022), p. 117964. ISSN: 0032-5910. DOI: 10.1016/j.powtec.2022.117964.
- [42] Gholamhossein Bagheri and Costanza Bonadonna. "On the drag of freely falling non-spherical particles". In: *Powder Technology* 301 (2016), pp. 526–544. ISSN: 0032-5910. DOI: 10.1016/j.powtec.2016.06.015.
- [43] R.C. Hibbeler. *Mechanics of Materials*. Always learning. Pearson. ISBN: 9780134319650.
- [44] Seyed Mohammad Mojtabaei, Jurgen Becque, and Iman Hajirasouliha. "Structural Size Optimization of Single and Built-Up Cold-Formed Steel Beam-Column Members". In: *Journal of Structural Engineering* 147.4 (2021), p. 04021030. DOI: 10.1061/(ASCE)ST.1943-541X.0002987.
- [45] Zhao Qin et al. "The mechanics and design of a lightweight three-dimensional graphene assembly". In: *Science Advances* 3 (Jan. 2017), e1601536. DOI: 10.1126/sciadv.1601536.
- [46] Diab W. Abueidda et al. "Mechanical properties of 3D printed polymeric Gyroid cellular structures: Experimental and finite element study". In: *Materials & Design* 165 (2019), p. 107597. ISSN: 0264-1275. DOI: 10.1016/j.matdes.2019.107597.
- [47] Yan Yan Li et al. "Metal-organic frameworks with the gyroid surface: structures and applications". In: *Dalton Trans* 50 (14 2021), pp. 4757–4764. DOI: 10.1039/D0DT04234J.
- [48] M. Pagitz and S. Pellegrino. "Buckling pressure of 'pumpkin' balloons". In: *International Journal of Solids and Structures* 44.6 (2007), pp. 6963–6986.
- [49] Kunsel Izet-Ünsalan and Deniz Ünsalan. "A low cost alternative for satellites- tethered ultra-high altitude balloons". In: *Proceedings of 5th International Conference on Recent Advances in Space Technologies - RAST2011*. 2011, pp. 13–16. DOI: 10.1109/RAST.2011.5966806.
- [50] T. Tam and A. Bhatnagar. "1 - High-performance ballistic fibers and tapes". In: *Lightweight Ballistic Composites (Second Edition)*. Ed. by Ashok Bhatnagar. Second Edition. Woodhead Publishing Series in Composites Science and Engineering. Woodhead Publishing, 2016, pp. 1–39. ISBN: 978-0-08-100406-7. DOI: 10.1016/B978-0-08-100406-7.00001-5.
- [51] George Christopher Martin. "Physical Properties of Polymers Handbook, 2nd ed". In: *Journal of the American Chemical Society* 130.3 (2008), pp. 1033–1045. DOI: 10.1021/ja0769503.
- [52] Laurence W. McKeen. "9 - Polyolefins, Polyvinyls, and Acrylics". In: *Permeability Properties of Plastics and Elastomers (Fourth Edition)*. Ed. by Laurence W. McKeen. Fourth Edition. Plastics Design Library. William Andrew Publishing, 2017, pp. 157–207. DOI: 10.1016/B978-0-323-50859-9.00009-9.

- [53] J. D Edwards and S. F. Pickering. "Permeability of rubber to gases". In: *Scientific Papers of the Bureau of Standards* 16 (1920), pp. 347–349.
- [54] O. Hoes et al. "Systematic high-resolution assessment of global hydropower potential". In: *PLOS ONE* 12 (Feb. 2017), e0171844. DOI: 10.1371/journal.pone.0171844.
- [55] K. Ma et al. "Chapter 1 - Introduction". In: *Mooring System Engineering for Offshore Structures*. Gulf Professional Publishing, 2019, pp. 1–18. ISBN: 978-0-12-818551-3. DOI: 10.1016/B978-0-12-818551-3.00001-6.
- [56] K. Ma et al. "Chapter 15 - Mooring for floating wind turbines". In: *Mooring System Engineering for Offshore Structures*. Gulf Professional Publishing, 2019, pp. 299–315. ISBN: 978-0-12-818551-3. DOI: 10.1016/B978-0-12-818551-3.00015-6.
- [57] Abdul Hai et al. "Influence of splicing parameters on retained splice strength, elongation and appearance of spliced cotton/flax blended yarn". In: *Indian Journal of Fibre and Textile Research* 38 (Mar. 2013), pp. 74–80.
- [58] B. Brandt et al. *Silicon-chemistry carbon balance*. Online. Rue Belliard 40, 1040 Brussels, Belgium, May 2021.
- [59] G. Saevarsdottir, T. Magnusson, and H. Kvande. "Reducing the Carbon Footprint: Primary Production of Aluminum and Silicon with Changing Energy Systems". In: *Journal of Sustainable Metallurgy* 7.3 (2021), pp. 848–857. DOI: <https://doi.org/10.1007/s40831-021-00429-0>.
- [60] N. Voulvoulis et al. *Examining Material Evidence: The Carbon Fingerprint*. Online Flyer. Imperial College London, London, UK, July 2020. DOI: 10.13140/RG.2.2.12793.70241.
- [61] A. Spyroudi. *Carbon footprint of offshore wind farm components*. Online Flyer. Lowestoft, Suffolk, Apr. 2021.
- [62] H. Kuiper. *Project Guide, Design Synthesis Exercise, Sustainable Energy from Pseudo Satellites*. Delft University of Technology, Nov. 2022.
- [63] TU Delft: Faculty of Aerospace Engineering. *AE3211-I. Lecture Slides and Teaching Content*. Accessible via TU Delft institution login. Sept. 2022.
- [64] DSE Group 3. *Baseline Report - Sustainable Energy from Pseudo Satellites*. Tech. rep. TU Delft, Nov. 2022.
- [65] European Environment Agency. *External costs of electricity production*. Tech. rep. Kongens Nytorv 6, 1050 København K, Denmark, 2007.
- [66] Gabriel Di Bella et al. *Natural Gas in Europe - The Potential Impact of Disruptions to Supply*. Tech. rep. 700 19th Street, N.W. Washington, D.C. 20431: International Monetary Fund, July 2022.
- [67] R. Idel. "Levelized Full System Costs of Electricity". In: *Energy* 259 (2022), p. 124905. ISSN: 0360-5442. DOI: 10.1016/j.energy.2022.124905.
- [68] Peter Gainsford. *Global average levelised cost of hydrogen production by energy source and technology, 2019 and 2050*. IEA. 9 Rue de la Fédération, 75015 Paris, France, Oct. 2022.
- [69] Kelsey A. Horowitz et al. "A Techno-Economic Analysis and Cost Reduction Roadmap for III-V Solar Cells". In: (Nov. 2018). DOI: 10.2172/1484349.
- [70] IEA. *Nuclear Power in a Clean Energy System*. Tech. rep. License: CC BY 4.0. URL: <https://www.iea.org/reports/nuclear-power-in-a-clean-energy-system>.
- [71] Lazard. *Lazard's levelized cost of energy analysis*. Version 14. Oct. 2020.